A comprehensive review on the progress of lead zirconate-based antiferroelectric materials

Xihong Hao[a,b], Jiwei Zhai[a,]*, Ling Bing Kong[c,]* and Zhengkui Xu[d]

[a]*Functional Materials Research Laboratory, Tongji University, Shanghai 200092, P. R. China*

[b]*School of Materials and Metallurgy, Inner Mongolia University of Science and Technology, Baotou 014010, P. R. China*

[c]*School of Materials Science and Engineering, Nanyang Technological University, 50 Nanyang Avenue, Singapore 639798*

[d]*Department of Physics and Materials Science, City University of Hong Kong, Hong Kong*

Abstract

Lead zirconate ($PbZrO_3$ or PZ)-based antiferroelectric (AFE) materials, as a group of important electronic materials, have attracted increasing attention for their potential applications in high energy storage capacitors, micro-actuators, pyroelectric security sensors, cooling devices, and pulsed power generators and so on, because of their novel external electric field-induced phase switching behavior between AFE state and ferroelectric (FE) state. The performances of AFE materials are strongly dependent on the phase transformation process, which are mainly determined by the constitutions and the external field. For AFE thin/thick films, the electrical properties are also strongly dependent on their thickness, crystal orientation and the characteristics of electrode materials. Accordingly, various strategies have been employed to tailor the phase transformation behavior of AFE materials in order to improve their performances. Due to their relatively poor electrical strength (low breakdown fields), most PZ-based orthorhombic AFE ceramics are broken down before a critical switching field can be applied. As a consequence, the electric-field-induced transition between AFE and FE phase of only those AFE bulk ceramics, with compositions within tetragonal region near the AFE/FE morphotropic phase boundary (MPB), can be realized experimentally at room temperature. AFE materials with such compositions include $(Pb,A)ZrO_3$ (A=Ba, Sr), $(Pb_{1-3/2x}La_x)(Zr_{1-y}Ti_y)O_3$ (PLZT x/(1-y)/y), $(Pb_{0.97}La_{0.02})(Zr,Sn,Ti)O_3$ (PLZST) and $Pb_{0.99}(Zr,Sn,Ti)_{0.98}Nb_{0.02}O_3$ (PNZST). As compared to bulk ceramics, AFE thin and thick films always display better electric-field endurance ability. Consequently, room temperature electric-field-induced AFE-FE phase transition could be observed in the AFE thin/thick films with orthorhombic structures. Moreover, AFE films are more easily integrated with

silicon technologies. Therefore, AFE thin/thick films have been a subject of numerous researches. This review serves to summarize the recent progress of PZ-based AFE materials, focusing on the external field (electric field, hydrostatic pressure and temperature) dependences of the AFE-FE phase transition, with a specific attention to the performances of AFE films for various potential applications, such as high energy storage, electric field induced strains, pyroelectric effect and electrocaloric effect.

Keywords: Antiferroelectric, ferroelectric, lead zirconate, ceramics, thin films, structure, phase transformation, dielectric constant, dielectric loss, polarization, ferroelectric fatigue, energy storage, electric field induced strain, pyroelectric effect, electocalaric effect

*Corresponding authors: apzhai@tongji.edu.cn (JWZ), elbkong@ntu.edu.sg (LBK)

Nomenclature

AFE	antiferroelectric
FE	ferroelectric
AFEs	antiferroelectrics
FEs	ferroelectrics
PE	paraelectric
MPB	morphotropic phase boundary
DC	direct current
PZ	lead zirconate $PbZrO_3$ (=PZO)
PZT	lead zirconate titanate $Pb(Zr_{1-y}Ti_y)O_3$
PLZT	lead lanthanum zirconate titanate $(Pb_{1-3/2x}La_x)(Zr_{1-y}Ti_y)O_3$
PLZST	lead lanthanum zirconate stannate titanate $(Pb,La)(Zr,Sn,Ti)O_3$
PNZST	lead niobium zirconate stannate titanate $Pb(Zr,Sn,Ti)NbO_3$
E_F	the forward phase switching field from antiferroelectric to ferroelectric
E_A	the backward switching field from ferroelectric to antiferroelectric
T_o	Curie-Weiss temperature
a_{Rh}	lattice parameter of ferroelectric rhombohedral phase
a_{Tet}	lattice parameter of antiferroelectric tetragonal primitive
MSS	molten salt synthesis
HPS	hot pressing sintering
SPS	spark plasma sintering
CSD	chemical solution deposition
HTO	hydrothermal oxidation
PLD	pulsed laser deposition
IBAD	ion beam assisted deposition
EDS	Energy-dispersive spectroscopy
XRD	X-ray diffraction
SEM	scanning electron microscopy
AFE_o	Orthorhombic antiferroelectric
AFE_T	tetragonal antiferroelectric
ΔG	Gibbs free energy
T_{A-F}	the transition temperature from antiferroelectric to ferroelectric phase
T_{F-P}	the transition temperature from ferroelectric to paraelectric phase
T_{F-A}	the transition temperature from ferroelectric to antiferroelectric phase
T_{A-P}	the transition temperature from antiferroelectric to paraelectric phase
ω_T	the soft-mode frequency
FE_R	rhombohedral ferroelectric
FE_T	tetragonal ferroelectric
RFE	relaxor ferroelectric
$FE_{R(LT)}$	low temperature rhombohedral ferroelectric
$FE_{R(HT)}$	high temperature rhombohedral ferroelectric
PT	lead titanate $PbTiO_3$ (=PTO)
LDs	linear dielectrics
EC	electrocaloric effect

1. Introduction

1.1. Antiferroelectrics

To understand the definition of antiferroelectrics (AFEs), it is necessary to mention ferroelectrics (FEs), because they have a close relationship in terms of depolarization process. In FE materials, the adjacent diploes in one domain share the same polarization orientation, and orientation of the diploes can be aligned by an external DC electric field [1]. Therefore, materials that can be defined as FEs must have two characteristics: (i) the presence of spontaneous polarization and (ii) the reversibility of the polarization by external electric field. For illustration, Fig. 1 shows a diagram of polarization process of FEs. Based on these facts, it can be concluded that polarization in polycrystalline FE materials can be increased by the application of external DC electric-fields, which thus behave in a similar way to single crystal FEs at saturated polarization state. As a result, the electric-field dependence of polarization (P-E) of FEs is a single hysteresis loop, as shown in Fig. 2.

Differently, in AFE materials, the adjacent diploes are aligned in opposite orientation. In this case, a sufficiently high DC electric-field is required to align the polarization orientation of diploes so as to realize an FE state. This is called electric-field-induced phase switching. The phase switching behavior indicates that the difference in free energy between AFE and FE phase is small. Therefore, AFEs materials are those that have spontaneous polarizations with adjacent diploes being opposite, which can be aligned by a sufficiently high DC electric-field [2]. Thus, similar to FEs, AFEs also possess two distinct features. On the one hand, the net macroscopic remanent polarization is zero; on the other hand, P-E curves at a sufficiently high electric field display double hysteresis loops. Fig. 3 and Fig. 4 show the polarization characteristics and a P-E loop of AFEs, respectively. The forward phase switching field (E_F) and the backward switching field (E_A) can be estimated by extrapolating the two steepest sections of the hysteresis loop and obtaining their intersections with the horizontal axis. The field-induced FE phase is not stable usually, which could be back to AFE state due to the change of electric field, temperature and/or pressure.

AFEs have several subcategories, such as perovskite group [3], pyrochlore group [3, 4], liquid crystal [5], and so on. Among these AFEs, the perovskite group is the most important one. Perovskite is usually expressed as ABO_3. A typical ABO_3 united-cell structure is shown in Fig. 5. It consists of a corner-linked network of oxygen octahedra, creating an octahedral cage (B-site) and interstices (A-site).

Up to now, it has been recognized that $PbZrO_3$, $PbHfO_3$ and $NaNbO_3$ are AFEs with perovskite structure at room temperature [6, 7]. Among them, $PbZrO_3$ has been the most extensively studied because of its better phase transition-induced properties. In $PbZrO_3$, Pb^{2+} ions occupy the A-site while Zr^{4+} ions occupy the B-site. It belongs to orthorhombic structure at room temperature, with lattice constants of a=5.78 Å, b=11.74 Å, and c=8.20 Å. Each orthorhombic unit cell contains eight primitive cells, which have a tetragonal structure with lattice constants of $a_0=b_0$=4.15 Å and c_0=4.10 Å [8].

It has been demonstrated that the AFE effect of $PbZrO_3$ is originated from the antiparallel displacement of Pb^{2+} ions in the plane perpendicular to the c axis in orthorhombic unit cell, as shown in Fig. 6 [8]. The rectangle area in the diagram represents the *a-b* plane of the unit cell. The displacement was calculated to be about 0.2 Å. Thus, the anti-polar direction of lead-based orthorhombic AFEs is along the pseudocubic <110> plane, while the polar direction of parallel dipoles is along <111> of rhombohedral structure in FEs state. In this respect, the final properties of AFE materials could be tailored through proper control of the growth orientation. For example, AFE materials along <111> direction are expected to have larger field-induced strains and smaller critical phase switching fields.

Recently, an extremely weak FE effect was observed in $PbZrO_3$ by Dai *et al* [9] and Ayyub *et al* [10]. It was confirmed by Jona and co-authors that, besides Pb^{2+} ions along the <110> direction are antiparallel shift, O^{2-} ions along the <001> direction are also antiparallel shift [11]. However, the antiparallel shift of O^{2-} ions was unbalanced in contrast to Pb^{2+} ions. Basing on this fact, it could be obtained in theory that AFE state in PZ only existed in the *a-b* plane and that FE properties should also be detectable along the <001> direction. This conclusion has been proved by the experimental results [12]. Mixtured AFE and FE phases have also been observed in PZ films [13, 14].

1.2. The history of discovery of antiferroelectrics

As compared to that of FEs, the history of AFEs is very short. Generally, it is believed that the discovery of Rochelle salt (sodium potassium tartrate tetrahydrate, $NaKC_4H_4O_6\cdot 4H_2O$) in 1665 was marked as the starting point of study on FEs [15]. However, the formal definition of AFEs was only proposed by Kittel in 1951 [16]. It was predicted that AFE state would not be piezoelectrics, as it has a center of symmetry. It is well known that a large piezoelectric effect is usually found in the FE state without a center of symmetry. In the same year, the first AFEs, $PbZrO_3$, was reported by Sawaguchi [8, 17]. In that study, electric-field-induced phase transition between AFE and FE of $PbZrO_3$ bulk

ceramics was only observed at higher temperatures (above 210^{o}C), but not at room temperature. It is because the critical field for the phase transition from AFE to FE was higher than its breakdown field. In order to decrease the critical phase transition fields of $PbZrO_3$ ceramics, Shirane used Ba^{2+} and Sr^{2+} to partically substitute Pb^{2+} [18]. It was found that Ba^{2+} doping decreased the stability of AFE phase, whereas Sr^{2+} showed a reverse effect. Thereafter, in 1960s, in order to further investigate $PbZrO_3$-based AFE ceramics and obtain stable double P-E loops at room temperature, a lot of efforts had been made to reduce the critical field by chemical substitution. The most widely used doping irons are La^{3+}, Ba^{2+}, Ca^{2+} and Sr^{2+} at A site and Sn^{4+}, Ti^{4+} and Nb^{5+} at B site [18-22].

Among various examples, $(Pb,La)(Zr,Sn,Ti)O_3$ (PLZST) and $Pb(Zr,Sn,Ti)NbO_3$ (PNZST) appeared to be the most promising AFEs. Phase diagrams of $(Pb_{0.97}La_{0.02})(Zr,Sn,Ti)O_3$ and $Pb_{0.99}(Zr,Sn,Ti)_{0.98}Nb_{0.02}O_3$ were firstly constructed by Jaffe and Berlincourt [23]. It was found that AFEs with orthorhombic and tetragonal structures could be obtained through compositional optimization. It was reported that Ti addition enhanced FE properties, while Sn doping increased AFE properties. As a result, electric-field induced phase switching between AFE and FE was realized at room temperature when the $PbZrO_3$-based AFEs had tetragonal structure. Subsequently, field-induced strains and energy storage performances of AFEs were studied. However, due to the same reason, phase transition process of $PbZrO_3$-based AFE ceramics with orthorhombic structure was still not realized at room temperature.

In 1990s, with the development of new processing techniques, thin and thick films could be fabricated easily. As compared to those of bulk ceramics, electric-field endurances of AFE films were significantly improved due to their higher density and more uniform microstructure. At the same time, the operating voltages were reduced remarkably. Subsequently, it became possible to observe electric-field-induced phase transition of $PbZrO_3$-based AFEs with orthorhombic structure by using films. For example, AFE-FE phase transition was successfully observed in $PbZrO_3$ and $(Pb_{0.95}Sr_{0.05})ZrO_3$ thin films [24-27]. The broader phase region of the AFE films has practical significance because orthorhombic phase has lager induced strains and higher energy storage density than tetragonal phase. Hence, the research on $PbZrO_3$-based AFEs has been focused on thin and thick films.

1.3. Basic properties of antiferroelectrics

1.3.1. Field and temperature dependences of dielectric properties

AFEs have high dielectric constant of 50-5000, which is lower than that of FEs. Dielectric loss tangents of AFEs are usually ranging from 0.5% to 10%. Under circular function of external DC electric-field, dielectric constant of AFEs (C-V curves) displays a double buffer-fly shape, as shown in Fig. 7. As the electric-field increasing from 0 to maximum values, dielectric constant of AFEs increases firstly, and reaches the first peak value at *A* (*A*') and then decreases gradually. The phase switching from AFE to FE state at *A* (*A*') point is finished and the corresponding electric-field is called critical forward phase field E_F. Similarly, as electric-field is decreased from maximum values to 0, dielectric constant also increases firstly and then declines. A second peak value at *B* (*B*') point is obtained in this course, which denotes the phase transformation from FE to AFE state. It is called critical backward phase field E_A.

According to Park *et al* [28], the phase switching process of AFEs could be divided into six stages, as clearly demonstrated in Fig. 8. At stage 1 (from a to b), random arranged AFE domains are re-aligned at a lower electric-field; while at stage 2 (from b to c), re-aligned AFE domains are transformed into FE state at the critical forward phase switching field. With further increasing electric field, it comes to stage 3 (from c to d), at which the polarization orientation of the induced FE domains was rearranged. At stage 4 (from d to e), piezoelectric effect in the induced FE state appears at the even higher electric-field. At stage 5 (from e to f), the induced FE is back to re-aligned FE state after the release of electric-field; At stage 6 (from f to a), the re-aligned AFE returns to the initial random arranged AFE state after annealed above its Curie temperature.

AFEs also possess similar distinct temperature-dependent characters as FEs in three aspects [16, 17]. Firstly, AFE could only be present in certain temperature range, namely, AFE properties are disappeared when temperatures are above a critical value, which also is defined as Curie temperature (T_C). Secondly, with increasing temperature, dielectric constant firstly increases and then declines, and at T_C dielectric constant reaches the maximum value. Thirdly, above T_C, the relationship of dielectric constant and temperature obeys the Curie-Weiss law:

$$\varepsilon_r(0) = \varepsilon_r(\infty) + \frac{C}{T - T_o}, \tag{1}$$

where, $\varepsilon_r(0)$ and $\varepsilon_r(\infty)$ are the low frequency dielectric constant and optical dielectric constant, respectively; C is Curie-Weiss constant and T_o is Curie-Weiss temperature.

1.3.2. AFE-FE phase switching-induced crystal structure change

One of the distinct characteristics of AFE materials is their crystal structure change due to the phase transition from AFE to FE state. At sufficiently high electric-fields, orthorhombic or tetragonal AFE phases are changed into rhombohedral FE phase. Taking tetragonal AFEs as example, Fig. 9 shows the structures of a primitive cell in AFE and FE states [29]. Clearly, the lattice parameter (a_{Rh}) of FE rhombohedral phase is slightly smaller than that (a_{Tet}) of AFE tetragonal primitive cell, while c_{Rh} is obviously larger than c_{Tet}. As a result, the overall volume of a randomly orientated polycrystalline ceramics is expanded as the phase is switched from AFE to FE state, which is accompanied by a considerable field-induced strain. It has been reported that PLZST AFE ceramics can provide a strain of as high as 0.87% [30], which is much larger than the highest value of about 0.1% obtained in FE ceramics. Generally, field-induced strains with levels of 0.3-0.5% can be easily achieved reproducibly in AFE ceramics and films [29, 31, 32].

1.3.3. Phase switching induced currents

Phase switching induced current is another important characteristic of AFE materials. Fig. 10 illustrates a representative current-field (I-E) curve of AFE films [33]. Clearly, there is a sharp increase in current during the phase transition between AFE and FE state. Four obvious peaks are observed. The abnormal increase in current is caused by the turning of the diploes. For the AFE-FE transition, all anti-parallel planed diploes in a short time are induced to re-orient along the external field direction when the applied field just reaches the threshold values, thus leading to an instantaneous huge current. Similarly, for the FE-AFE transition, the induced re-oriented diploes are back to original anti-parallel planed state immediately at an applied field just below the critical field. It is noted that the field-induced phase switching process (such as critical field) could be changed due to the variation of temperature, thus that the corresponding I-E curves could also be tailored.

1.3.4. Temperature and pressure induced FE-AFE phase switching

Generally, lead based AFE materials can be divided into two subcategories, according their stability of the induced FE state. If the induced FE state can be back to original AFE phase after the remove of applied field, it is named “hard” AFE. If the induced FE state is remained when the applied field is removed, it is called “soft” AFE. However, the induced “soft” FE state is not stable, which can return to AFE state at high temperatures and/or pressures. For instance, the AFE state can be recovered as the materials with induced FE are heated above their Curie temperatures. More interestingly,

induced FE in a material could also be back to AFE state by applying a sufficiently high pressure [34]. In this case, huge induced current and voltage are produced during the FE-AFE phase switching. Fig. 11 illustrates a charge release curve of PLZST ceramics caused by a pressure induced FE-AFE phase transition [35]. The high electrical power released in a very short duration of time makes AFE materials promising candidates for applications as explosive electrical transducers.

1.4. Scope of this review

In recent years, AFE materials have been extensively investigated and quite a number of papers have been published in the open literature. However, the state-of-the-art of AFE materials is still not available up to now [36]. As compared to bulk ceramics, AFE thin and thick films are more suitable for practical applications because of their lower operating voltages and easy integration with silicon technologies. Therefore, in this paper we will review the recent progress of AFE materials, with more attention paid to AFE films. Besides, potential applications of AFE materials will be discussed to show the significance of the materials.

2. Fabrications of PZ-based AFE ceramics and films

2.1. Fabrications of PZ-based AFE ceramics

It is well known that the final electrical properties of ceramics with given chemical compositions are mainly affected by their microstructure, such as density, uniformity and grain size, and so on. Meanwhile, the electrical performances for lead-contained materials are also strongly influenced by loss of lead during the preparation procedures. Therefore, selecting a proper fabrication method is an efficient way to optimize the properties of lead-containing ceramics. A summary of the recent development on the fabrication of PZ-based AFE ceramics is presented as follows.

2.1.1. Solid-state reaction method

Solid-state reaction route is the conventional way to prepare bulk ceramics and quite a few of papers on AFE ceramics have been reported [17, 18, 37-41]. In this method, binary oxides, such as PbO and ZrO_2, with high purity are used as raw materials. Sometimes, carbonate and nitrate are also selected as the precursors. The first step is to mix the starting materials by employing bill-milling. In order to compensate the lead loss during heat treatment, excessive lead source (usually 1%) is added. Then the milled powders were calcinated at 800-900^{o}C to form the desired perovskite phase. After that, the calcinations are re-bill-milled to obtain highly reactive powders. Thirdly, the powders are pressed with the help of organic reagents (such as PVB and PVA). Finally, the green samples are sintered at

higher temperature (1250-1350^{o}C) in a lead environment. In this way, the density of the obtained AFE ceramics is usually about 95%-98% and the grain size is about several micrometers.

Just as mentioned above, lead volatilization during annealing process has a serious effect on the properties of lead-based materials. Addition of proper excess of lead is a useful way to improve their final electric properties. The effects of PbO content, from 4 mol% deficiency to 4 mol% excess, on the sintering behavior, microstructure, and properties of PLZST [$(Pb0_{.97+x}La_{0.02})(Zr_{0.66}Sn_{0.25}Ti_{0.09})O_{3+x}$] AFE ceramics, was reported by Zhou *et al* [38, 41]. As shown in Fig. 12, the density of the ceramics was evidently dependent on the lead content and the sample with 1 mol% excessive lead had the highest density. This result could be understood with the help of the microstructures of the PLZST AFE ceramics. As shown in Fig. 13, the PbO-deficient sample underwent almost no liquid-phase sintering, where small pores with larger porosity were the consequence of solid-state sintering. On the other hand, the large pores, which were formed in the sample containing too much excess PbO, might have been caused by the non-uniform distribution of the PbO-rich liquid and its flow into fine capillaries of the matrix.

2.1.2. Wet-chemistry methods

Wet-chemistry methods have also been widely employed to fabricate lead-containing AFE ceramics. Compared to solid-state reaction method, chemical methods possess at least two advantages. On the one hand, powders synthesized from wet-chemistry process have smaller grain sizes and higher reactivity, which in turn lead to the ceramics to be sintered at lower temperatures; on the other hand, chemical constitutes of powders are homogenous at the atomic level, which could avoid the structural fluctuation of the ceramics prepared by solid-state reaction technique. There have been several reports on the synthesis of AFE powders by using wet-chemistry methods, including chemical precipitation and sol-gel technique. In chemical methods, the starting materials are often nitrate, chloride and acetate [42-45].

Xue et al synthesized AFE $Pb_{0.98}La_{0.02}(Zr_{0.66}Sn_{0.27}Ti_{0.07})O_3$ powder via an aqueous solution of lactic acid [42]. AFE ceramics with good dielectric performances were obtained by sintering the powder at 1100^{o}C. Similar AFE ceramics derived from sol-gel powder were reported after annealing at 1200^{o}C by Zhai *et al* [43]. A two-step wet chemical method was used by Chen et al to synthesize PLZST ceramics with various chemical compositions [44, 45]. It was reported that grain sizes of the AFE ceramics could be easily controlled by using different sintering temperature. Fig. 14 shows SEM

images of fractured surfaces of the $Pb_{0.98}La_{0.02}(Zr_{0.65}Sn_{0.25}Ti_{0.10})O_3$ ceramics annealed at 1000^{o}C, 1050^{o}C, 1100^{o}C, 1150^{o}C, 1200^{o}C and 1250^{o}C [45]. Clearly, with increasing sintering temperature, the grain size was increased gradually. At the same time, the fracture characteristics of the samples changed from intergranular to transgranular. Temperature dependences of dielectric constant showed that the Curie point shifted from 190.9 to 196.4 ^{o}C as the average grain size increased from 2 to 9 μm, which was related to the variation of the confined elastic strain energy of the grains. However, the maximum values of dielectric constant and the field-induced longitudinal strain were observed in the sample with an average grain size of 5 μm. This means that the final performance of AFE ceramics could be optimized by properly controlling their grain sizes.

2.1.3. High-energy ball milling method

High-energy ball milling method, as a sub-diversion of mechanical activation synthesis (MAS) route, is a technique to synthesize nano-sized powders of alloys and intermetallic compounds. It has been newly developed for low-temperature production of bulk ceramics [46]. The most signification characteristic of this technique is that the reaction from oxide mixture to a designed compound is activated by mechanical energy instead of heat energy, as in the conventional solid-state reaction process. As compared with the conventional solid-state reaction and the wet-chemistry-based process routes, the high-energy ball milling process has several advantages [47]. Firstly, it uses low-cost and widely available oxides as the starting materials and skips the calcination step at intermediate temperatures, leading to a greatly simplified process. Secondly, no heat source is required and it takes place at a temperature close the room temperature in a sealed container, thus effectively alleviating the loss of lead. Furthermore, the mechanically derived powders possess higher sinterability than those synthesized through the conventional solid-state reaction and most of the wet-chemical processes.

Fabrication of $PbZrO_3$-based AFE ceramics by using high-energy ball milling route was first reported by Kong *et al* [48]. It was found that $PbZrO_3$ particles with sizes of about 20 nm were directly synthesized by high energy milling the mixture of PbO (10 wt% excess) and ZrO_2 for 24 h with a Fristsch Pulverisette 5 planetary milling system in air at room temperature. As shown in Fig. 15, the mixture of PbO and ZrO_2 was crystallized into perovskite $PbZrO_3$ phase. By using the obtained powder, almost fully dense $PbZrO_3$ ceramic with an average grain size of about 1 μm and a relative density of about 96% was achieved after sintering at 900^{o}C. Obviously, the sintering temperature is much lower than that required by the conventional solid-state reaction process. Subsequently, AFE

ceramics with more complicated compositions, such as PLZT, PLZST and PNZST, were also fabricated by using the high-energy ball milling route [49, 50]. The results indicated that AFE ceramics sintered at 1100 ^{o}C had good electrical properties.

2.1.4. Molten salt method

Molten salt synthesis (MSS) is one of the simplest ways for obtaining complex compounds, in which oxides starting materials are reacted in the molten salt medium at moderate low temperatures [51-55]. The often used salt eutectic mixtures include NaCl-KCl, KF-KCl, KNO_3-$NaNO_3$ and Li_2SO_4-Na_2SO_4, with a mole rate at their low co-molten point. MSS has three main advantages. Firstly, the preparation temperature is fairly low and comparable with that of wet-chemistry methods. Secondly, the starting materials used in solid-state reaction method can be used in this method too and the solution of the molten salts can be used repeatedly, so the cost is low. Thirdly, the final powders could be nanosized by proper control over the reaction parameters such as temperature and time, which is helpful to decrease the sintering temperature of the ceramics. Several complex ferroelectric materials with perovskite structure, like $Ba(Zr,Ti)O_3$, $(Pb,Mg)O_3$, $(Pb,Mg)O_3$-$PbTiO_3$, and $(Ba,Sr)TiO_3$, etc., have been synthesized by MSS method. In 2006, PLZST AFE powders were prepared by using salt molten method and subsequently dense ceramics with a relative density of 98% were successfully obtained at 1150 ^{o}C [51].

2.1.5. Other methods

Besides the synthesis methods mentioned above, there are other novel sintering techniques (such as hot press sintering and spark plasma sintering) that have been used to obtain dense AFE ceramics at relatively low sintering temperatures. Hot pressing sintering (HPS) is a popular technique to enhance the densification of ceramics in order to improve their electrical properties. This method was first employed by Markowski *et al* to fabricate AFE ceramics in 1996 [37]. PLZST ceramics with a relative density of 98% were fabricated by hot isostatic pressing at 20 MPa for 2 h. The AFE ceramics prepared in this way displayed good dielectric performances. Spark plasma sintering (SPS) is a rapid consolidation processing method for the fabrication of bulk materials by using microscopic electrical discharge between particles under pressures. In this case, a powder compact could be sintered to high density at relatively low temperatures within a much short time of a few minutes, compared to the conventional sintering of several hours. Zhou *et al* [56] reported that PLZST AFE ceramics with a relative density of 99.5% could be fabricated by using SPS technique at 900^{o}C for 3 min. However,

due to small grain size of 300 nm, the PLZST ceramics processed by SPS had poor electrical properties. This problem can be readily addressed by increasing the sintering temperature.

2.2. Deposition and orientation control of PZ-based AFE film

2.2.1. Deposition methods

AFE thin/thick films are more attractive from the practical application point of view. Firstly, the growth temperature of AFE films is usually below 800^{o}C, which makes them suitable for the integration with silicon technologies. Secondly, films usually have higher densities, so that they have better external electric field endurance. Finally, the operating voltages of films are significantly lower than those required by their ceramic counterparts, due to their small thickness.

Various techniques have been developed to deposit thin (<1000 nm) and thick films (>1000 nm). Deposition techniques for AFE thin films can be divided into two groups [57, 58], namely chemical routes, including sol-gel, chemical solution deposition (CSD), chemical gas evaporation and hydrothermal oxidation (HTO), and physical routes, such as physical gas evaporation, sputtering, pulsed laser deposition (PLD) and ion beam assisted deposition (IBAD). Comparatively, limited methods have been available to fabricate thick films. The fabrication techniques of thick films include modified chemical solution deposition, spraying methods, screen print and tap casting [59-64]. Among the various methods, chemical solution deposition, PLD and sputtering are the most widely used techniques for the fabrication of lead based AFE films, especially chemical solution deposition. Deposition of AFE thin and thick films by using these three methods will be discussed in detail as follows.

2.2.1.1 CSD method

Chemical solution deposition (CSD) method has various advantages, such as simple fabrication process, cheap equipment, accurate chemical composition control and deposition of films with large areas, and thus has been widely used to deposit AFE films. Briefly, CSD technique involves four steps: (i) synthesis of the precursor solution, (ii) deposition of wet films by spin-coating or dip-coating, (iii) drying and/or pyrolysis of organics and formation of amorphous films at low-temperatures (usually 300-500^{o}C), and (iv) densification and crystallization at higher temperatures (typically 600-800^{o}C). A more detailed description on the process could be found in a recent review paper [57].

The preparation of AFE films could be traced back to 1985, when PZ thin layers were first reported by Budd *et al* [65]. However, the PZ films were more susceptible to cracking and resistant to

crystallization as compared to lead titanate (PT) or PZT layers, which prevented the investigation on electrical properties of PZ-based AFE films. Until 1992, Wang *et al* [27] fabricated PZ films with better microstructure by using acetate-based precursor, which showed an improved breakdown field and allowed the observation of electric field induced phase switching from AFE to FE state at room temperature. This result inspired the study on AFE films and a lot of works started to appear after that [66-73]. Typical works were reported by Xu *et al* [72, 74-76] and Zhai *et al* [73, 77, 78]. A general chemical-solution-deposition route with acetate-based precursor was developed, which was able to deposit high quality AFE thin and thick films with typical double P-E loops (zero remanent polarization after electric field removing and lager induced maximum polarization). This processing route has been widely used since then [71, 79, 80]. Generally, this method uses glacial acetic and distill water as solvents, and zirconium propoxide, titanium isopropoxide and acetate salt (such as lead acetate trihydrate, lanthanum acetate, and tin acetate) as source materials. Examples for the fabrication of AFE thin and thick films are given below.

Fig. 16 shows an example of preparation process of PLZST AFE thin film by using acetate-based precursor, reported by Li *et al* [81]. To synthesize the precursor solution, acetate salts were firstly dissolved in glacial acetic at 100-120^{o}C. When the mixed solution was cooled to room temperature, zirconium propoxide and titanium isopropoxide were added and mixed for 0.5-1 h. During the mixing process, distilled water was added in proper ratios (generally, twenty moles of distilled water to one mole of lead) to stabilize the solution. Finally, the solution was adjusted to desired concentrations by using glacial acetic. In order to avoid the formation of crack during the heat treatment, concentration of the solution was usually 0.2-0.4 M. Spin-coating method was used to deposit wet AFE films on different substrates (Pt/Ti/SiO_2/Si and $LaNiO_3$/SiO_2/Si). Each layer was spin coated at 2000-5000 rpm for 20-30 s, and then pyrolyzed at 400-500 °C for 10-30 min to form amorphous films. The spin coating and heat-treatment were repeated several times to obtain films with desired thickness. Finally, a capping layer was deposited by using 0.2-0.8 M PbO precursor solution prepared from lead acetate trihydrate, before the films were annealed at 600-700^{o}C for 0.5-1 h to form single phase perovskite.

Two points should be emphasized when using this method to deposit AFE thin films. Firstly, to compensate the loss of lead during annealing and prevent the formation of pyrochlore phase, 5-20 % excess of lead source was added in the precursor. Secondly, the PbO capping layer was necessary to

avoid the formation of pyrochlore phase on surface of the AFE films. It was reported by Zhai *et al* [78] that fine grained pyrochlore phase would be formed on surface of the PNZST films if no PbO layer was deposited.

Generally, lead-based FE and AFE films deposited on $Pt/Ti/SiO_2/Si$ substrates by CSD procedure need to be annealed at temperatures of above 600 ^oC in order to obtain good electrical properties. Such high growth temperature often leads to a cumulative loss of lead. Decreasing the growth temperatures would be able to overcome this problem. According to Kwok and Desu [82], the temperature of complete perovskite formation of $PbZr_{1-x}TixO_3$ thin films increased with increasing content of Zr. It was found that the activation energy of nucleation was much higher than that of growth of the perovskite phase. Therefore, in order to lower the growth temperature of lead-based AFE and FE films it is necessary to lower their nucleation temperature. Strategies to lower the nucleation temperature include utilization of seeding layers, adoption of unique heat-treatment procedure and modification of chemistry properties of the precursor solutions [83-85]. A recent study indicated that $LaNiO_3$ was a promising seed layer for the deposition of PLZST AFE thin films with good electrical properties at low temperatures (500^oC) [86, 87].

A unique feature of lead-based AFE thin films fabricated by chemical solution routes is their non-uniform surface microstructure, as shown in Fig. 17, with round light-colored phases (rosettes) on top of dark phases [88]. Energy-dispersive spectroscopy (EDS) results indicated that the rosettes phase was rich in lead and the dark phase was deficient in lead. It was proposed by Alkoy *et al* [89] that the crystallization of the rosettes phase started at numerous lead-rich nucleation sites throughout the films. The formation of the dark areas was due to the volatilization of lead during the annealing.

It is more difficult to obtain crack-free and uniform thick films by using CSD. Selection of heat treatment route is the key to the preparation of AFE thick films. Fig 18 shows a flow chart of the deposition of PLZST AFE thick films by using CSD developed by Xu *et al* [74]. Although the procedure is quite similar to that used for thin films, such as the use of 10-20% lead excess in precursor solution and a PbO capping layer, several differences can be listed. Firstly, the temperature for the synthesis of precursor solution is higher in this case. The temperature to dissolve the acetate salts in glacial acetic is 120-150^oC, and the temperature to mix zirconium propoxide and titanium isopropoxide is 70-110^oC. Higher temperatures are required due to the higher contents of the starting materials. The concentration of the precursor solution is usually 0.5-0.8 M to increase the thickness of

a single layer. The spin-coating process was carried out at 5000-8000 rpm for 30-40 s to ensure the thickness uniform of the wet layers. Secondly, the pyrolysis temperature of the wet layers is increased to 500-600^{o}C, which makes each layer be nano-sized crystals and thus diminishes the overall volume shrinkage of the thick films during the final annealing process. As a result, the formation of crack during the repeated spin-coating procedure could be avoided. Lastly, after deposition of certain number of layers (every 6 layers in this example), a PbO (0.8 M in this example) layer was covered. This cycle was repeated until desired thickness was obtained. Fig. 19 (a) and (b), respectively, show SEM images of the PNZST AFE thick films (about 5 μm) with and without the PbO layers [75]. Obviously, the sample with the PbO layers has a more uniform surface microstructure. This is because thick films need longer time for the formation of perovskite phase and thus requires more lead to compensate its loss. More detailed discussion on the effect of the PbO overcoat layers can be found in Ref. [75].

2.1.1.2. PLD method

Pulsed laser deposition (PLD) method has been employed to fabricate dielectric and FE films (such as $SrTiO_3$ and $BaTiO_3$) since 1960s [57]. Fig. 20 shows a schematic diagram of PLD system. It usually consists of a vacuum chamber equipped with a pump, a target holder and rotator, substrate heater, and other components to control the growth environment (such as partial pressure of oxygen and deposition temperature). Various lasers, such as KrF (λ=248 nm), ArF (λ=193 nm), XeCl (λ=308 nm) and Nd:YAG (λ=355 nm), have been used to deposit different thin films. PLD is a simple method to deposit thin films. An intrinsic advantage of PLD is its capability to congruently evaporate the target, thus producing films with the same chemical compositions as the targets. This is especially important for the synthesis of multi-component films. A more detailed description on PLD method and its recent development have been reviewed by Martin *et al* [57].

PLD-derived PZ AFE thin films on Si substrates were reported by Chattopadhyay *et al* for the first time in 1998 [90]. The PZ films deposited at temperatures above 500^{o}C showed a pure perovskite structure with (100)-preferred orientation. Double P-E loops were observed in the PZ films. After that, PZ-based AFE films with various chemical substitutions were fabricated by using PLD [91-93]. The effects of deposition temperature (substrates holder temperature), oxygen partial pressure and post-deposition annealing on the microstructure and electrical properties of AFE thin films have been systematically studied [92-96].

Fig. 21 shows XRD patterns of the PZ thin films reported by Bharadwaja *et al* [94]. As shown in Fig. 21 (a), phase composition of the films deposited at 550^{o}C was strongly dependent on oxygen partial pressure. The optimized oxygen pressure to form single phase PZ film was 50 mTorr. At a given oxygen pressure (50 mTorr), to deposit high quality PZ thin films, deposition temperatures should be above 550^{o}C, as demonstrated by the XRD patterns in Fig. 21 (b). PZ thin films with desired phase composition and electrical properties can also be achieved by annealing the samples deposited at low temperatures. As shown in Fig. 21 (c), the samples annealed at above 600^{o}C displayed nearly single phase perovskite structure with random orientation. It was also found that microstructure of the PZ thin films were different under different deposition conditions. For example, the PZ film deposited at 550^{o}C and oxygen partial pressures of 50 mTorr showed a columnar microstructure, whereas it became multi-grained microstructure after annealing at 650^{o}C. Similar results were also observed in PLZST AFE films reported by Yao *et al* [93, 96]. In summary, microstructure and electrical properties of AFE thin films deposited by using PLD are influenced by various deposition parameters.

2.1.1.3. Sputtering method

Sputtering technique has been widely used to deposit various thin films, including semiconductor, dielectric, insulator, magnetic, and superconductors, since early 1970s [57]. There are different types of sputtering set-ups, such as multi-ion-beam sputtering (reactive magnetron co-sputtering), radio frequency magnetron sputtering and DC magnetron sputtering. A distinguished advantage of sputtering is its capability of large-scale production. In principle, sputtering method is a typical physical deposition process, in which atoms from the targets were ejected by the bombardment of plasma and subsequently deposited on substrates to form films with desired compositions and properties. A more detailed discussion of the sputtering method can be found in Ref. [57, 97, 98].

Kanno *et al* reported PZ AFE thin films deposited by using multi-ion-beam sputtering method for the first time in 1995, where Pb and Zr were used as the targets [99]. Single phase perovskite PZ films with (100) orientation were deposited on (100)/MgO and (100)Pt/MgO substrates at 415 ^{o}C. The PZ thin films with a thickness of 177 nm showed a high dielectric constant of about 400 and typical double P-E loop at room temperature. After that, Yanakawa *et al* reported a systematic investigation on the PZ films with thicknesses of 200-500 nm on Pt(111)/TiO_2/SiO_2/Si substrates prepared by the same method [100, 101]. It was found that both phase formation temperature and crystal orientation of the PZ films were strongly dependent on the content of lead. The content of lead was controlled by the

ratio of the powers applied to the Pb and Zr targets. For example, if the powers for the Pb target and the Zr target were 10 W and 250 W, no perovskite phase was formed in the deposited films after annealing at 750^{o}C. As the power for the Pb target was increased to 18 W, the sample after annealing at 750^{o}C displayed a (111)-preferred orientation of perovskite phase. The sample exhibited typical double P-E loops with maximum polarization of 36 μC/cm^2. In addition, the films with relatively low lead content (16 W for Pb target) had to be annealed at higher temperature than those with higher lead content (22 W for Pb target) to form perovskite phase.

Very recently, highly (111)-oriented AFE PLZST [$Pb_{0.97}La_{0.02}(Sn_{0.60}Sn_{0.30}Ti_{0.10})O_3$] thin films were successfully deposited on Pt(111)/TiO_2/SiO_2/Si substrates by radio frequency magnetron sputtering, with typical substrate temperature and O_2/Ar flow ratio during sputtering of 500^{o}C and 8:37 sccm (standard-state cubic centimeter per minute), respectively [102]. In this case, PLZST ceramic was used as target. This was the first report that used ceramic target to deposit AFE thin films by using sputtering. Microstructures and electrical properties of the PLZST thin films were investigated as a function of post-annealing temperature. The films post-annealed at 700^{o}C for 30 min had a smooth surface and were crack-free. They exhibited a dense columnar microstructure with an average grain size of about 0.85 μm. As a result, these films showed excellent AFE properties, including low AFE-FE switching field, high saturation polarization, high dielectric constant and low loss tangent [102].

2.2.2. Orientation control of AFE films

The properties of phase switching materials with asymmetry structures are strongly dependent on their crystalline orientations. For instance, Pb(Zr,Ti)O_3 (PZT) thin films with (100) or (111) preferred orientations often showed higher remanent polarization than those with random orientation [103-105]. (100)-textured $BaTiO_3$ ceramics have been illustrated to show higher piezoelectric constant than the randomly oriented samples. Therefore, controlling over the growth orientation has been widely used to improve performances of FE films and ceramics [63, 106]. As for AFEs, the diploes are anti-paralleled along <110> direction in AFE state and are paralleled along <111> direction in FE state [8]. Therefore, it is expected that the properties of AFE materials with different crystal orientations (such as (100), (110) and (111)) could be significantly different. Optimizations of field-induced phase switching and related properties of AFE films by controlling crystal orientation have been extensively reported [2, 73, 107-110]. However, similar study on AFE bulk ceramics is rarely available. Therefore,

in this section, we will only summarize the results on AFE films. It has been shown that the preferred orientations of AFE films are influenced by their chemical compositions, preparation method, heat treating process, substrates and buffer layers [97, 110]. As mentioned above, (110) and (111)-preferred AFE thin films on Pt(111)/TiO_2/SiO_2/Si substrates could be readily deposited by PLD and sputtering method, through the controlling over processing parameters. For the sake of space limitation and to avoid repetition, we will only discuss the orientation dependences of AFE films deposited by CSD method.

2.2.2.1. Processing-dependent orientation

Like their FE counterpart PZT, lead-based AFE films deposited on Pt(111)/TiO_2/SiO_2/Si substrates by using CSD are easily grown with (100) or (111) orientations by properly controlling their processing parameters, such as chemical composition, precursor materials, solution preparation procedure, stock solution age, heat treatment process and films thickness, etc. Tani, *et al* [108] fabricated (100)-preferred PZ films with 2-methoxyethanol based solution. In this study, each wet layer was dried at 150^{o}C, pyrolyzed at 300^{o}C and finally annealed at 700^{o}C. Similarly, Tang *et al* [111] obtained (100)-preferred PZ films, by using pyrolysis temperature of 300^{o}C and annealing temperature of 450-650^{o}C. In a recent work, Hao *et al* [112, 113] deposited highly (100)-preferred PLZT films with thickness ranging from 500 to 2500 nm on Pt-buffered silicon substrates, with drying temperature of 300^{o}C, pyrolysis temperature of 600^{o}C and final annealing temperature of 700^{o}C. However, according to Alkoy *et al*, if each wet layer was dried at 150^{o}C and pyrolyzed at 400^{o}C and the final annealing temperature was 700^{o}C, the obtained PZ films showed (111)-preferred orientation [114]. Similarly, if each wet layer was pyrolyzed at 450^{o}C, the PZ and PLZT AFE films prepared with glacial acetic based solution were usually highly (111)-oriented [115, 116]. These results indicate that lower pyrolysis temperature is beneficial to the development of (100)-preferred orientation, while higher pyrolyzed temperature leads to the formation of (111)-preferred orientation. This observation can be understood by using the model proposed by Chen *et al* [117, 118]]. As shown in Fig. 22, at lower temperature, PbO is easily formed on Pt, which has a (100) texture and induces PZT (or PZ) films to grow along the same (100) direction. In contrast, at higher pyrolysis temperature (above 400^{o}C) with rapid heating rate, an intermediation layer ($Pt_{5-7}Pb$) with (111) orientation is formed on Pt, which facilitates the growth of PZT (or PZ) films with (111) orientation.

However, due to their complicated chemical compositions, PLZST and PNZST AFE films are

difficult to grow with a preferred orientation. For example, as reported by Xu *et al* and Zhai *et al*, PLZST and PNZST AFE thin and thick films [29, 79, 88], which were prepared with similar process of the PZ and PLZT films motioned above, often displayed a random orientation.

2.2.2.2. Substrate and buffer layer dependent orientation

Use of substrates or buffer layers with preferred orientation is more effective to fabricate textured thin films. For instance, by using single crystal substrates (such as $SrTiO_3$, $LaAlO_3$, MgO and Nb: $SrTiO_3$), textured FE thin films PZT, $(Ba,Sr)TiO_3$ (BST), $Ba(Zr,Ti)O_3$ (BZT) and $Ba(Ti,Sn)O_3$ (BTS) have been successfully deposited by various methods [119-123]. Oxide buffer layers for the growth of textured FE films, according to their crystal structures, can be divided into two groups. One is compound oxide with ABO_3 crystal structure, such as $LaNiO_3$, $(Ba,Pb)ZrO_3$, $(La,Sr)MnO_3$ and $(La,Ca)MnO_3$ [124-127]. Because they are all good conductors, they also serve as bottom electrodes. These compounds have the same crystal structure of perovskite as FEs, so that they can be used as substrates to eptitaxially grow FE thin films at relatively low temperatures. Another group is simple oxide, such as TiO_2, ZrO_2, PbO and CeO_2 [128-131].

In 1993, single phase PZ thin films with (100) orientation were prepared, for the first time, on $SrTiO_3$ single-crystal substrates by a metalorganic chemical vapor deposition (MOCVD) method, using $Pb(thd)_4$ and $Zr(thd)_4$ as precursors [132]. However, because there was no bottom electrode, phase transition behavior of the PZ films was not studied. Recently, (100)-oriented PLZST AFE thin films were prepared on Nb:$SrTiO_3$ single-crystal substrates by CSD method. Phase switching process of the PLZST thin film was studied by measuring its P-E loop and C-V curve. It was shown that AFE and FE phases were co-existed in it [14].

$LaNiO_3$ was the only ABO_3 structured buffer layer used to deposit AFE thin films with preferred orientations [110, 113, 114]. It has been found that (100)-oriented $LaNiO_3$ layers on $Pt(111)/TiO_2/SiO_2/Si$ and SiO_2/Si substrates could be easily prepared by using sputtering method [115]. By using CSD method, $LaNiO_3$ layers with either (100) or (110)-preferred orientations could be fabricated by properly controlling the annealing parameters [87, 136, 137]. Generally, if each wet layer was directly annealed at high temperature (700^oC) by using rapid thermal annealing (RTA), the $LaNiO_3$ layer preferred to show (100)-orientation. In contrast, the films, fabricated through low temperature ($400\text{-}500^oC$) pyrolysis and high temperature (700^oC) annealing, were more likely to have (110)-preferred orientation. The orientations of the PZ, PLZT, PNZST and PLZST films would be the

same as the orientations of the $LaNiO_3$ buffer layers when CSD method was used [77, 86, 110, 133]. As a consequence, phase switching behavior of the AFE thin films was highly orientation-dependent.

PZ-based AFE thin films were also deposited on different simple oxide layers. It was reported by Tani *et al* [108] that a 10-nm-thick TiO_2 buffer layer could make PZ films grow along (111) plane. However, Cakare *et al* [67] found that PZ films on TiO_2 buffered Pt displayed a random orientation. Similar results were also demonstrated by PLZT and PLZST AFE films on TiO_2, ZrO_2, and CeO_2 buffered substrates [33, 115, 138]. These results indicate that the growth mechanisms of AFE thin films on simple oxide layers are more complicated and that simple oxides are not good buffer layers to facilitate the growth of AFE thin films with preferred orientation.

3. Phase transition theory of AFEs

AFEs are typical structural phase transition materials, whose phase switching process is always accompanied by structural transition. In terms of structure, there are two types of AFEs: orthorhombic AFE (AFE_O) and tetragonal AFE (AFE_T). Due to their different phase structures, temperature dependent phase transitions of the two AFEs are quite different. With increasing temperature, AFE_O usually experiences a phase switching from AFE to FE and then to PE [17, 139]. AFE_T goes through a phase transition from FE to AFE and then to PE, as the temperature is increased [140, 141].

It is believed that the practical applications of AFEs materials are closely related to their phase switching behavior. Therefore, it is important to understand the intrinsic nature of phase transition process of AFEs. There have been reports on the phase transition mechanism of AFEs, as a function of temperature, DC bias and hydrostatic pressure [6, 28, 30, 142-144]. Up to now, phenomenological theory [18, 145] and soft mode theory [146] have been successfully employed to illustrate the phase switching process, from the views of macroscopic thermodynamic and microscopic lattice dynamics, respectively.

3.1. Phenomenological theory

The thermodynamic theory of FE phase transition is an important constituent part of the phenomenological theories of FEs, which was originally introduced by Muller [147]. Based on the Landau theory of second order phase transitions, the first phenomenological model for FEs was developed by Devonshire for $BaTiO_3$ in 1949, which is so called Landau-Devonshire (L-D) theory and has been a milestone in the development of transition theories [148]. L-D theory is a universal theory to explain the phase switching process of FEs, which interprets the phase switching process by

examining the difference in free energy between the two phases involved. From the L-D theory, Gibbs free energy (ΔG) of FEs can be written as an expansion of the polarization (P) as [149]:

$$\Delta G = \frac{1}{2}\alpha P^2 + \frac{1}{4}\xi P^4 + \frac{1}{6}\zeta P^6, \quad (2)$$

where α, ξ and ζ are the phenomenological coefficients.

Following the L-D theory, the thermodynamic theory for AFEs was first considered by Kittel in 1951 [16]. It was assumed that AFEs contained two equivalent lattices, which could be polarized independently and there was an interaction between them. By denoting P_a and P_b as the polarizations of the two lattices, the free energy of AFEs can be expressed as:

$$\Delta G = f(P_a^2 + P_b^2) + gP_aP_b + h(P_a^4 + P_b^4), \quad (3)$$

where *f*, *g* and *h* are the phenomenological coefficients. Obviously, if P_a is equal to $-P_b$, the net polarization is zero and the material is in AFE state. Whether the AFE state has a lower free energy than the FE state depends on the values of the phenomenological coefficients, especially the coefficient of *g*.

Based on Kittel's results, Whatmore and Glazer developed a one-dimensional free energy function to model the displacement of Pb^{2+} ion in lead zirconate [150], and Uchino *et al* [151] added stress terms in the free energy function to determine the hydrostatic electrostrictive coefficient. Subsequently, the further development by Cross *et al* [142] enabled the theory to calculate the free energy and dielectric properties of FE, AFE and PE phases of AFEs under different conditions. A complete free energy function for AFEs with orthorhombic structure has been developed, which illustrates the temperature-dependent free energy distribution of FE, AFE and PE phases. With these developments, a general feature of free energy of AFEs with orthorhombic and tetragonal structures with respect to different phases could be obtained.

As shown in Fig. 23 (a), for orthorhombic AFEs (such as PZ), the free energy ΔG of AFE_O phase is lowest, followed by FE phase and then PE phase at low temperatures. In this case, AFE_O phase is stable. Because of the smaller difference in free energy ΔG between AFE phase and FE phase, the AFE_O phase could be induced to FE state by a DC bias. As the temperature is increased, the energy difference is decreased, so that the critical switching field from AFE to FE phase is declined. Above temperature $T_{A\text{-}F}$, which is the phase transition temperature from AFE_O to FE_T, the free energy ΔG of FE phase is lowest as compared to AFE and PE, therefore the FE phase is stable. As the temperature is

beyond T_{F-P}, the free energy ΔG of PE phase shows the smallest value, as compared to AFE and FE phases, thus the material stays in PE state. Here, the temperature T_{F-P} is Curie point, which is the phase switching temperature from FE to PE.

However, the temperature-dependent phase transition process of tetragonal AFEs is different. As shown in Fig. 23 (b), at low temperatures FE phase is stable because of its lowest free energy ΔG. In the temperature range from T_{F-A} to T_{A-P}, the free energy ΔG of AFE phase is the smallest one, so the material stays in AFE state. T_{F-A} represents the phase switching temperature from FE to AFE. Above T_{A-P}, which also is Curie point and the phase transition temperature from AFE to PE, PE phase is stable duo to its lowest free energy ΔG.

3.2. Soft mode theory

The emergence of soft mode theory has a profound significance to fundamentally understand the phase transition in solids from the view of lattice vibration. Lattice softening was first used by Raman and Nedungadi in 1940 to study the phase switching between α and β quartz [152]. The concept of "soft mode" for phase transition in FEs was proposed by Cochran [153] and Anderson [154] independently in 1959, confirmed by Baker *et al* [155] and Cowley [156] in1963, and further developed by Samara *et al* [157] in AFEs in 1975. This theory successfully connected FE and AFE phase in terms of lattice vibration for the first time, which revealed the nature of structural phase transitions in FEs and AFEs. According to the soft mode theory, it is believed that the phase transition in certain AFEs or FEs is the result of instability in one of the normal vibration modes of the lattice. The instability leads to a decrease in vibration frequency, which approaches to zero as the temperature approaches the phase transition temperature. In other words, the lattice literally softens with respect to the mode. It has been recognized that FE transition is the soft mode instabilities at Brillouin Zone center, whereas AFE transition is the soft mode instabilities at Brillouin Zone boundary. Since a conprehansive review on the development of the soft mode theory of FEs and AFEs is beyond the scope of this work, more detailed information can be found in related references [158-160].

Based on the soft mode theory, the transverse optical soft-mode frequency (ω_T) for FE transformation can be expressed as [146]

$$\omega_T^{\,2} = \frac{1}{\mu}[(SRF) - (LRF) + \gamma T], \qquad (4)$$

where μ is the reduced mass, *SRF* is the short-range forces from Brillouin boundary soft mode or short

wavelength phonon mode, *LRF* is the long-range Coulombic forces from Brillouin center soft mode or long wavelength phonon mode, γ is a temperature coefficient of the same order of magnitude as the volume coefficient of expansion, and T is the temperature. [(SRF) – (*LRF*) + γT] is the summation of all interaction for the soft phonon mode and represents the effective force constant of the soft-mode. FE transition is driven by a distorting force form long-range forces in the crystal lattice. Therefore, the cancellation of the short-range forces by long-range forces leads to a decrease in the soft-mode frequency, and eventually the soft mode condenses out and results in FE phase transition at a certain temperature.

Different from FEs, AFE phase transition is driven by the distorting forces from short-range interactions. Thus, the soft-mode frequency (ω_T) for AFE phase switching could be expressed as [146]

$$\omega_T^{\,2} = \frac{1}{\mu}[(LRF) - (SRF) + \gamma T]. \qquad (5)$$

According to Eq. (3), AFE phase transition could be realized by the cancellation of the long-range Coulomic forces by the short-rang interactions. Eqs. (4) and (5) indicate that the occurrence of the phase transition at a specific condition depends on the balance of competing forces between the long-range and the short-range force. Therefore, the short-range interactions are the restoring forces of AFE transformation, and the long-range interactions are the restoring forces of FE transition.

It is found that the short-range and long-range interactions between adjacent cations or anions could be affected by an external field. Moreover, an external field with spherical symmetry tends to decease the interaction distance (r) more effectively than an asymmetric field. For example, hydrostatic pressure increases the short-rang interactions ($\propto r^{-n}$, n=10) between adjacent cations or anions more rapidly than it increases the long-range Coulomb forces ($\propto r^{-m}$, m=3) [146]. Conversely, uniaxial stresses with cylindrical symmetry or electric field with a polar cylindrical symmetry, which include a shear component and a normal component, have less effect on reinforcing the short-range interactions as compared to a symmetric field. Depending on the relative orientations between the crystal and the external field, these asymmetric external fields (with a shear component) generally tend to enhance the long-range interactions. Therefore, it can be concluded that the phase transition of AFEs or FEs can also be triggered by external stresses or electric fields. Thus, the presence of uniaxial stress and/or DC bias field is able to strengthen the long-range Coulombic forces and enhance the FE

phase stability, whereas hydrostatic pressure favors to increase the short-range interactions and increases the AFE phase stability. This conclusion has been well proved by the following results on the specific phase transition behavior of AFEs, as a result of the application of external fields.

4. Phase transition characteristics of PZ-based AFEs under the function of external field

4.1. Phase transition characteristics of AFE ceramics and films with different composition

The final properties of a material are closely related to its chemical composition. This is also true to AFE materials. In this light, phase transition behavior and electrical properties of AFEs have been effectively tailored, through doping with different ions, such as La^{3+}, Ba^{2+}, Ca^{2+}, Sr^{2+} and Er^{3+} at *A* site and Sn^{4+}, Ti^{4+}, Nb^{5+}, Cr^{3+}, Ce^{4+} and Sb^{3+} at *B* site. It has been demonstrated that to a certain degree the stability of AFE phase of doped $PbZrO_3$ (PZ) could be estimated by the tolerance factor *t*, which is given by [161]

$$t = \frac{R_A + R_O}{\sqrt{2}(R_B + R_O)}, \tag{6}$$

where R_A is the radius of *A*-site cations, R_B is the radius of *B*-site cations, and R_O is the radius of *O* anion. When $t>1$, FE phase is stabilized, and when $t<1$, AFE phase is stabilized. According to this formula, the calculated *t* value for pure PZ is 0.97 [162]. Although quite a few of ions have been used to tailor the phase switching process and dielectric properties of PZ-based AFE ceramics and films, in terms of practical application, $(Pb,A)ZrO_3$ (A=Ba, Sr), $(Pb,La)(Zr,Ti)O_3$, $(Pb_{0.97}La_{0.02})(Zr,Sn,Ti)O_3$ and $Pb_{0.99}(Zr,Sn,Ti)_{0.98}Nb_{0.02}O_3$ are more promising candidates, which have thus been the most extensively reported in the open literature. Structures and phase transition behaviors of these AFE materials in forms of ceramics and films with different chemical constitutions will be discussed as follows.

4.1.1. Phase switching characteristics of PZ

It was found in 1952 that, with increasing temperature, PZ underwent a phase transition from AFE to paraelectric (PE) at 233^{o}C (Curie point) and no AFE-FE phase transition was observed from the temperature-dependent dielectric constant curve [17]. However, in 1966, when using a high-temperature X-ray diffraction (XRD) to examine PZ ceramics, Tennery [163] found that, as the temperature was increased, AFE phase was first changed into FE phase at 226^{o}C, and then was switched to PE at 236^{o}C. Subsequently, it was further proved by Scott and Samara [164] and Ujma and Handerdk [165] independently, that a stable PE phase within a temperature range of less than 15^{o}C existed below the Curie temperature in both polycrystalline and single crystal PZ materials. In 1970,

Samrar reported that the FE phase below Curie point could be excluded by using the function of hydrostatic pressure (above 0.1 MPa) [166]. The AFE-PE transition temperature could be increased by the application of hydrostatic pressure at a rate of 45 ± 3^{o} C/MPa. This result could be readily understood according to the soft mode theory. Because hydrostatic pressure favors to increase the short-range interactions and increases the AFE phase stability, the FE phase was excluded and the AFE-PE transition temperature was increased.

As mentioned in the beginning of this review, duo to the low breakdown field, field-induced phase transition from AFE to FE in pure PZ polycrystalline ceramics could not be observed at room temperature. In contrast to ceramics, PZ single crystals and films have much better electric field endurance because of their higher densities and more uniform microstructure.

Electric field-induced phase switching behavior of PZ single crystals was studied at DC electric fields of up to 1400 kV/cm by Fesenko *et al* [167]. A complete E-T phase diagram and exemplary isothermal dependence of polarization on electric fields have been developed, as shown in Fig. 24. The most interesting point of the diagram is the range between the two triple points, T_{tr1} and T_{tr2}, in which a "six-fold" hysteresis loop is observed, corresponding to the three phase transitions: AFE Pba2-phase to FE C2mm-phase (OR I and OR II, respectively), C2mm to FE R3m-phase (R I), and R3m to FE R3c-phase (R II). At temperatures above T_{tr1}, after observing a half-cycle of the "four-fold" loop, the crystal changes its orientation; so that the applied field becomes parallel to the <001> direction of OR I unit cell. With further increasing temperature, at 210^{o}C, the phase transition from OR I to R I takes place in the absence of a DC field. The temperature of this transition is not affected by DC fields of lower than 20 kV/cm. Within the range of 10^{o}C, typical FE loop is observed, and at 222^{o}C the PZ single crystal enters PE state.

Zhai *et al* [73, 77] reported a systematic study on highly (100)-oriented PZ films with thickness of 80-900 nm deposited on $LaNiO_3$(100)/Pt(111)/TiO_2/SiO_2/Si substrates by using CSD method. P-E loops indicated that a noticeable remanent polarization was detected for the PZ films thinner than 200 nm. Typical double P-E loops with a saturation polarization of about 40 $\mu C/cm^2$ and a nearly zero remanent polarization were observed for the PZ films thicker than 200 nm. Thinner films also had smaller dielectric constants. The presence of an interface layer in between the film and electrode, which was non-FE with a low dielectric constant, was responsible for the appearance of the remanent polarization and the smaller dielectric constant of the thinner films. The threshold phase transition

field obtained from the dielectric constant-electric field measurement was decreased with increasing film thickness, as shown in Fig. 25 (a), which was attributed to a combined effect of grain size, interface layer and internal stress.

No clear phase transition peak was detected for the PZ films thinner than 200 nm, a sharp dielectric peak at 226^{o}C was observed for the PZ films of 340-900 nm. Fig. 25 (b) shows temperature dependent dielectric constants of the 900-nm-thick film at various DC bias levels at 1 kHz. Obviously, the external DC fields have a strong effect on the temperature-induced phase transition of the PZ AFE films. At zero DC bias, FE phase existed over a temperature interval of about 46^{o}C, according to P-E loops as shown in Fig. 26, although no obvious dielectric peak was detected other than the Curie point. However, at DC fields, the AFE-FE switching appeared clearly. With increasing DC field, the AFE-FE transition shifted to lower temperatures. At the same time, the Curie point shifted to higher temperature and became broader with increasing DC bias, and thus the temperature range of the FE phase was enlarged. As shown in Fig. 25 (b), with increasing DC bias, the dielectric constant increased in the AFE phase region, but decreased in the FE phase region. These results further demonstrate that DC field favors to stabilize FE phase by enhancing the long-range force.

The 900-nm PZ film at room temperature was in AFE state, as evidenced by the "squared" double loop with zero remanent polarization in Fig. 26. With increasing temperature, E_F, E_A, the hysteresis widths (E_F-E_A) and the maximum polarization values all gradually decreased. At 180^{o}C, typical FE P-E loop was observable, indicating that the PZ film was in FE state.

4.1.2. Phase switching characteristics of (Pb,A)ZrO_3 (A=Ba, Sr)

The use of Ba^{2+} and Sr^{2+} to tailor phase transition properties of PZ AFEs was reported by Shirane in 1952 [18]. It was found that the effects of Ba^{2+} and Sr^{2+} were contradictory. Ba^{2+}-doping destabilized the AFE phase while Sr^{2+}-doping stabilized the AFE phase to a certain degree. Composition-dependent phase diagrams were also reported in the study. These results inspired a stong research interest in Ba^{2+} and Sr^{2+} doped PZ. There have been quite a number of reports on Ba^{2+} and Sr^{2+}-doped PZ ceramics and thin films.

Phase transition behavior of $(Pb_{1-x}Ba_x)ZrO_3$ (PBZ) ceramics with $0 \leq x \leq 0.3$ were reported by Shirane [17, 18] for the first time in 1951. At room temperature, with increasing content of Ba^{2+}, the PBZ ceramics underwent a phase transition from AFE to FE and to PE. However, no temperature-induced phase transition from AFE to FE was detected for the PBZ ceramics with $x \leq 0.05$

[139]. A complete phase diagram of PBZ was reported by Pokheral *et al* [168], as shown in Fig. 27. With $0 \leq x \leq 0.175$, the PBZ was in AFE state at room temperate. With increasing x, the AFE-FE switching temperature decreased. With $0.175 \leq x \leq 0.40$, the PBZ was in FE state. A dielectric relaxor state was observed for $x \geq 0.25$. With $0.4 \leq x \leq 1$, the PBZ was in PE state. Curie point of PBZ decreased with increasing content of Ba^{2+}.

Recently, PBZ ($0 \leq x \leq 1$) thin films with a thickness of about 500 nm were successfully deposited on $Pt(111)/TiO_2/SiO_2/Si$ substrates [116, 169]. With increasing concentration of Ba^{2+}, orientation of the PBZ films was changed from (111) to (110) gradually. At the same time, grain size of the films decreased, and the surface became more and more homogeneous and uniform. At room-temperature, state of the PBZ thin films was changed from AFE to FF and then to PE with increasing content of Ba^{2+}. The room-temperature P-E loops of the PBZ thin films with different compositions are shown in Fig 28. With x=0 and 0.05, the PBZ films exhibited typical double P-E loops, indicating their AFE nature. With x=0.10, a loop with moderate remanent polarization was observed, illustrating that AFE and FE phase co-existed in the films. As for x=0.20 and 0.30, typical FE loops were obtained. With x=0.50, a very slim P-E loop was recorded, denoting its PE nature. Evidently, the phase transition of the PBZ thin films as a function of composition is similar to that of their ceramic counterparts. Typical ferroelectric relaxor behavior was also observed in the samples with high contents of Ba^{2+}.

Comparatively, Shirane [18] found that $(Pb_{1-x}Sr_x)ZrO_3$ (PSZ) ceramics showed a different scenario of phase-composition relationship, as shown by the diagram in Fig. 29. Interestingly, no FE phase was present in PSZ and the Curie point had a maximum value of 250^{o}C at x=0.10. Besides the Curie point, there was another phase strasition point for PSZ, corresponding to the phase transition from one AFE to another AFE, which decreased with increasing content of Sr^{2+}. Similar results were also observed in PSZ films at x=0.05, with a maximum Curie point of 251^{o}C [18].

In addition to phase compositions and dielectric properties, the critical switching fields between AFE and FE of PZ AFEs were also influenced by Ba^{2+} or Sr^{2+}-doping [170]. For example, pure PZ, 5 mol% Ba^{2+} and 5 mol% Sr^{2+}-doped PZ films had the forwad thershold fields from AFE to FE of 450, 280 and 500 kV/cm, and reverse fields from FE to AFE of 260, 110 and 330 kV/cm, respectively.

4.1.3. Phase switching characteristics of $(Pb,La)(Zr,Ti)O_3$

La-modified lead zirconate tatanate [$(Pb_{1-3/2x}La_x)(Zr_{1-y}Ti_y)O_3$, PLZT x/(1-y)/y] solid solutions were developed by Haertling, initially as promising electro-optic mateirals [171]. Room temperature

phase diagram of PLZT is shown in Fig. 30. Depending compositions, various phases could be available in PLZT solid solutions. Typical phases include orthorhombic AFE (AFE_O), rhombohedral FE (FE_R), tetragonal FE (FE_T), relaxor FE (RFE) and PE. AFE_O is located in the Zr-rich side. High content of Ti favors to FE phase. PLZT can has potential applications as transducers, autuators, electro-optical switching, pyroelectric detectors, higher pulsed current generation and so on. Keeping in line with the topic of this review, we only discuss state-of-the-art of AFE_O PLZT.

(A) PLZ

For y=0, PLZT becomes PLZ. Because the radius of La^{3+} is smaller than that of Pb^{2+}, it is expected that proper content of La^{3+} could be able to stabilize the AFE state of PZ. Up to now, there are only a limited number of reports on PLZ AFE thin films. The first example of PLZ AFE thin films with a maximum La^{3+} content of 9 mol% was reported by Bharadwaja *et al* by using PLD technique [95, 172, 173]. At room temperature, PLZ underwent a phase transition from AFE to FE with increasing content of La^{3+}, which was evidenced by P-E results. It was found that the addition of 1 mol% La^{3+} reduced the Curie point by approximately 22^{o}C.

In a separate study, Parui *et al* [174] deposited PLZ thin films with La^{3+} content of up to 6 mol% by using a CSD route. Different results were observed in this case. It was found that Curie points were 230^{o}C, 215^{o}C, 194^{o}C, 265^{o}C, 245^{o}C, 235^{o}C and 250^{o}C for the samples with La^{3+}contents of 0, 1, 2, 3, 4, 5 and 6 mol%, respectively. P-E results showed that all the PLZ films were in AFE state at room temperature. Electric field induced phase transition between AFE and FE had a similar variation trend in Curie point. At 40^{o}C, forward switching fields (E_F) of the samples were 340, 220, 340, 310, 330 and 380 kV/cm, respectively. No explanation was available for such a fluctuation in the properties of the PLZ AFE thin films.

(B) PZT 95/5

Similarly, for x=0, PLZT would be PZT. Different from La^{3+}, Ti^{4+} is used to partially replace Zr^{4+}. The addition of Ti^{4+} was found to destabilize the AFE state. The room temperature morphotropic phase boundary (MPB) for AFE_O and FE_R lies at $Pb(Zr_{0.95}Ti_{0.05})O_3$ (PZT 95/5) [171]. PZT 95/5 possesses abundant phase switching behavior as a function of temperature, electric field and/or hydrostatic pressure. Therefore, PZT 95/5 AFEs have been extensively studied in recent years.

One of the early studies on temperature-dependent phase transition of PZT 95/5 ceramics was reported by Handerek and Ujma [175]. A multi-phase transition, AFE_O-FE_R-FE_T-PE, was observed at

110, 151 and 241ºC during heating process. During cooling process, the phase transition temperatures in the reverse order were 239, 141 and 24ºC, respectively. This means that the phase transitions had larger thermal hysteresis.

Owing to the relatively small difference in free energy between AFE and FE, electric field induced AFE-FE phase transition in PZT 95/5 ceramics at room temperature was easily realized and the induced FE state was stable after the removal of electric fields [176]. However, the induced FE state was not stable and returned to AFE state by hydrostatic pressure or explosive shock wave. At the same time, the stored charges would be released in a very short period of time, which was accompanied by a high voltage. As a result, PZT 95/5 ceramics have been the potential candidates for applications as high-voltage (current) power suppliers. It was reported that a maximum load voltage of about 38 kV in PZT95/5 ceramics could be achieved in 1.3 μs during the FE-AFE phase transition at a hydrostatic press of 1.4 GPa [177]. A higher load voltage of 81 kV was reported by Mock *et al* in PZT 95/5 ceramics during the FE-AFE phase transition induced by the application of 2.9 GPa [178]. Before the electrical breakdown, 74% charge was released. It was also stated that a completely hydrostatical depolarization could also be attained at a stress of 0.29 GPa, which was proved by the investigation on hydrostatic press-induced FE-AFE phase switching.

The phase transition between AFE and FE in PZT 95/5 had a volume change of about 0.4% [179]. This large volume variation had a negative effect on breakdown strength of the ceramics. Because the deteriorated dielectric breakdown strength was attributed to mechanical failures, it was proposed to use porous ceramics to buffer the shock compressions. There have been several reports on porosity-dependent phase transition of PZT 95/5 ceramics [179-182]. A systematic study on the effects of porosity, pore shape and pore size on hydrostatic pressure-induced FE-AFE phase transition of PZT 95/5 ceramics has been reported by Zeng *et al* [181, 182]. It was found that high porosity led to a low pressure and diffuses phase transition. The porous PZT 95/5 ceramics with spherical pores exhibited higher phase transition pressures than those with irregular pores. Moreover, the FE-AFE phase transition of porous PZT95/5 ceramics with poly-dispersed irregular pores was more diffusive than those of the PZT95/5 ceramics with mono-dispersed irregular pores.

(C) PLZT

Due to the co-effect of La^{3+} and Ti^{4+}, the composition/temperature range of AFE phase in PLZT solid solution could be expanded, as shown in Fig. 30 [171]. PLZT AFEs shared similar temperature

and electric field-induced phase transition to PZT 95/5. Investigations on PLZT AFEs have been mainly focused on bulk ceramics [183-186]. Extensive works on PLZT x/95/5 ceramics have been reported by Viehland *et al* [187-189]. A general conclusion was that La^{3+} doping disrupted the long-range dipolar order of FE state, so that the FE state was suppressed and the AFE phase was stabilized. PE-FE phase switching temperatures were 242, 232, 220 and 220^{o}C for the samples with x=0, 1, 2 and 3, respectively. However, for the samples with x=4-9, no distinct dielectric peaks could be observed. Instead, there was only a plateau at 220-240^{o}C.

Kong *et al* [71] studied the effect of annealing temperature on electrical properties of AFE PLZT 2/95/5 thin films. The random oriented PLZT 2/95/5 thin films with a thickness of about 700 nm were deposited on Pt-buffered silicon substrates by using a CSD method. Annealing temperatures were 550, 600, 650 and 700^{o}C. With increasing annealing temperature, average grain sizes of the samples increased from 20 to 200 nm. At the same time, the room-temperature dielectric properties and saturation polarization of the thin films were improved, while the critical phase transition fields between AFE and FE state were declined, as a result of increasing annealing temperature.

Recently, thickness-dependent phase transition of highly (100)-oriented PLZT 2/95/5 films was studied by Hao *et al* [113]. As the thickness was increased from 500 to 2500 nm, double P-E loops of the PLZT 2/95/5 films changed from "slanted" to "squared" shape gradually. However, the critical forward and backward switching fields of the films were kept almost unchanged, which were about 220 kV/cm and 95 kV/cm, respectively.

4.1.4. Phase switching characteristics of PLZST and PNZST

$(Pb_{0.97}La_{0.02})(Zr,Sn,Ti)O_3$ (PLZST) and $Pb_{0.99}(Zr,Sn,Ti)_{0.98}Nb_{0.02}O_3$ (PNZST) have been the most studied PZ-based AFEs. Phase diagrams of PLZST and PNZST were developed by Berlincourt in 1960s [23, 190]. The two groups of AFEs shared a similar variation in phase composition. As shown in Fig. 31, with increasing content of Ti, the phase composition varies in the order of AFE_O, AFE_T, $FE_{R(LT)}$ (low temperature rhombohedral ferroelectric) and $FE_{R(HT)}$ (high temperature rhombohedral ferroelectric). Compared to PZ and PLZT AFEs, these two systems possess a wider AFE region. Because the larger difference in free energy between AFE_O and the induced FE state, the critical phase switching fields are beyond their breakdown fields of the bulk ceramics. Thus, only those ceramics in the AFE_T region could exhibit room-temperature electric field-induced AFE-FE switching behavior. However, as mentioned above, due to their increased electrical breakdown strength, the electric

field-induced phase transition between AFE and FE state could be realized at room temperature in both AFE_O and AFE_T films. Thus, PLZST and PNZST were mainly studied in the form of films.

(A) PLZST

Chan *et al* [191] studied phase transition behavior of PLZST [$Pb_{0.97}La_{0.02}(Zr_{0.65}Sn_{0.22}Ti_{0.13})O_3$] ceramic AFEs in the tetragonal region. Representative P-E loops of the sample at different temperatures are shown in Fig. 32. It was found that FE state could be easily induced at low temperatures (below 90^{o}C in this case) and the induced FE state did not return to the original AFE state after the removal of electric fields. However, at higher temperatures (above 90^{o}C), the sample were of stable AFE phase and the induced FE phase returned to AFE state after the removal of electric fields. It was interestingly noticed that the forward phase switching field (E_F) kept to be nearly a constant of about 20 kV/cm while the backward field (E_A) gradually increased as the measurement temperature was increased, resulting in a decrease in hysteresis width ΔE (E_F-E_A). This observation can be explained by using the phenomenological thermodynamic theory in terms of free energy. As showed in Fig. 23 (b), for AFEs with tetragonal structure, the difference in ΔG between AFE and FE is small at low temperatures (slightly above T_{F-A}), thus AFE phase is not stable and the induced FE phase can exist as a metastable state. With increasing temperature, the difference in ΔG is increased, so that the AFE becomes more stable and double P-E loops are observable. In other words, the induced FE state at low temperatures could return to AFE state by increasing temperature. It has also been demonstrated that the FE-AFE phase transition temperature is affected by external DC fields. The FE-AFE phase transition temperature was increased proportionally to the magnitude of the DC field (lower than E_F).

Similar results were also reported by Yang *et al* [182, 183], who investigated the temperature-dependent dielectric properties of PLZST AFE ceramics with tetragonal structure as a function of DC electric field. Temperature-dependent curve of dielectric constant of the virgin sample showed only one dielectric peak, corresponding to the AFE-PE phase transformation. With increasing DC field (lower than the forward transition field E_F), the dielectric peak shifted to lower temperatures gradually, which was opposite to the trend of FEs. This result could be explained according to the soft model theory. As mentioned in section 3, DC field tends to strengthen the long-range Coulombic forces, so that the AFE state is destabilized and the temperature range of AFE state is narrowed as the DC field is increased.

PLZST AFE ceramics with various compositions near the AFE_T-FE_R MBP were studied by Markowski *et al* [37] and Pan *et al* [161]. The PLZST ceramics were prepared by using the traditional solid state reaction and their composition-dependent phase transition behavior as a function of electric-field and temperature were systematically investigated. According to their location in the phase diagram, the ceramics could be divided into two groups. In one group, the compositions of the samples were perpendicular to the AFE_T-FE_R MPB line, meaning that the ceramics had a fixed Zr content and were varied in Ti:Sn ratio. As the composition was moved into the bottom of the AFE_T region with increasing Sn^{4+} content, there were several general observations: (i) the critical phase switching fields between AFE and FE state, room-temperate dielectric constant and loss factor were increased; (ii) the temperature of the dielectric maxima, corresponding to the AFE_T-PE transition, remained constant and but became more diffusive; (iii) the FE-AFE switching was shifted to lower temperatures. In the other group, the compositions of the samples were located along the AFE_T-FE_R MPB line with fixed Ti^{4+} content and varied Zr:Sn ratio. With increasing content of Zr^{4+}, i.e., moving from left to right along the MPB line, following observations were summarized: (i) the phase switching fields between AFE and FE state tended to decrease; (ii) hysteresis width ΔE, AFE-PE transition temperature, dielectric constant, loss factor and FE-AFE switching temperature all increased. Similar results were also reported by Wang *et al* [194, 195].

Recently, composition-dependent phase transition behavior of PLZST AFE films has been systematically investigated by Xu *et al* [74] and Hao *et al* [196]. The compositions covered from AFE_T to AFE_O in the PLZST diagram. Electrical properties of the PLZST thin films studied by Hao *et al* are summarized in Table 1 [196]. Generally, composition-dependent electrical properties of the PLZST thin films are consistent with the results of the AFE_T ceramics. Namely, the AFE films with high content of Zr^{4+} and low content of Ti^{4+}, located in the bottom of the PLZST diagram and close to the point of PZ, possessed larger phase switching fields, wider hysteresis width and higher dielectric peak temperature.

Temperature-dependent dielectric constants of both $Pb_{0.97}La_{0.02}(Zr_{0.75}Sn_{0.22}Ti_{0.03})O_3$ and $Pb_{0.97}La_{0.02}(Zr_{0.75}Sn_{0.18}Ti_{0.07})O_3$ thin films, at various DC electric fields, were studied to compare the phase transition behaviors of AFEs with orthorhombic and tetragonal structures [196], as shown in Fig. 33 (a) and (b). $Pb_{0.97}La_{0.02}(Zr_{0.75}Sn_{0.22}Ti_{0.03})O_3$ was located in the AFE_O region. It had a forward switching field E_F of 221 kV/cm at room temperature. $Pb_{0.97}La_{0.02}(Zr_{0.75}Sn_{0.18}Ti_{0.07})O_3$ was located in

the AFE_T region and its room temperature E_F was 108 kV/cm. At electric fields below the forward switching field, AFE_O underwent AFE-FE-PE phase transition as the temperature is increased. The AFE-FE phase transition temperature was decreased whereas the FE-PE phase transition temperature was increased as the DC field was increased. In other words, with increasing temperature, the temperature range of FE phase could be widened by the application of DC fields. Differently, AFE_T had only one dielectric peak as the temperature is increased. At DC fields below its forward switching field, the sample underwent only AFE-PE transition and no FE phase was observed.

Thickness dependences of phase transition behavior of PLZST AFE films, deposited on Pt-buffered silicon substrates, were studied by Xu *et al* [72] and Li *et al* [81]. Xu *et al* [72] found that phase switching fields, dielectric constant and maximum polarization of the PLZST AFE films were all gradually increased as their thinness was increased from 100 nm to 1000 nm. It was suggested that the high tensile stress in the thinner films was responsible for their lower phase transition fields. Li *et al* [81] observed a similar variation trend in dielectric constant and maximum polarization with film thickness. However, the phase switching field gradually decreased as the film thickness was increased from 235 nm to 660 nm. The difference in field-thickness relationship between the two groups of authors was attributed to the presence of dead layer by Li *et al* [81].

(B) PNZST

Similar to PLZST, PNZST AFEs also have orthorhombic or tetragonal structures, as showed in Fig. 31. The investigation on bulk ceramics mainly focused on AFEs with tetragonal, while AFE_O films have also been studied. Phase transition behavior of PNZST AFEs is similar to those of their PLZST counterparts.

According to Akiyama and Fujisawa [197], PNZST AFE_T ceramics, with a composition of $Pb_{0.99}Nb_{0.02}[(Zr_{0.69}Sn_{0.31})_{0.945}Ti_{0.055}]_{0.98}O_3$, had a AFE-PE phase transition as temperature increasing, accompanied by an increased EF-AFE phase transition field. Composition-dependent phase transition behavior of PNZST AFE_T ceramics was studied by Feng *et al* [198]. At a given Zr:Sn ratio (7:3), with increasing content of Ti^{4+}, the critical phase transition field and the AFE-PE transition temperature both decreased, while dielectric constant increased. At a fixed content of Ti^{4+}, with increasing content of Sn^{4+}, the critical phase transition field between AFE and FE state and room-temperature dielectric constant both increased, while the AFE-PE transition temperature decreased. This result means that Sn^{4+} was able to stabilize the AFE state and Ti^{4+} stabilized the FE state, but both ions led to a decrease

in the AFE-PE transition temperature. For example, the induced FE phase of the sample with higher Ti^{4+} content was remained after the removal of the electric field.

The temperature dependence of phase transition process of $Pb_{0.99}Nb_{0.02}[(Zr_{0.57}Sn_{0.43})_{1-y}Ti_y]_{0.98}O_3$ (y=0.060, 0.063, 0.067, 0.069, 0.071 and 0.075) ceramics was reported by Frederik and Tan [199]. Although all samples were AFE phase at room temperature, the electric field-induced FE phase in the samples with compositions of $y \geq 0.069$ became metastable and the FE-AFE phase transition did not occur after unloading of the electric fields. With decreasing temperature, both the remanent polarization and the coercive field increased, which was consistent with those observed in normal FEs. However, an increase in temperature destabilized the FE phase. Above a certain temperature (50 ^oC for y=0.069), the induced FE phase would return to AFE phase upon removal of the electric fields and the AFE phase could be existed stably. Further increase in temperature led to an increase in critical phase switching field and a decrease in maximum polarization. A plateau region (from 170 to 120^oC for y=0.069) in the temperature-dependent dielectric constant curves on cooling process was obtained, within which a phase switching occurred from PE single-cell cubic phase (PE_{SC}) to PE multicell cubic phase (PE_{MC}) and then to AFE_T phase.

Phase transition behavior of PNZST AFE_O films with (100)-preferred orientation have been extensively studied by Zhai *et al* [133, 134]. Their properties were similar to those of pure PZ films [73, 77]. With increasing thickness, the critical phase transition field between AFE and FE state of the films gradually decreased. With increasing temperature, the AFE phase was destabilized and the critical phase transition field decreased. Similarly, there existed FE phase between AFE and PE phase in the temperature-induced phase transition process and the temperature region of FE phase could be expanded by applying electric fields.

Besides the temperature and electric field-induced phase transition, pressure-induced FE-AFE switching in PLZST and PNZST ceramics with a composition located in tetragonal region have also been studied extensively. Typical work on pressure-induced FE-AFE transition was reported by Berlincourt [34]. FE-AFE transition in $Pb_{0.995}Nb_{0.01}[(Zr_{0.7}Sn_{0.3})_{0.94}Ti_{0.6}]_{0.99}O_3$ ceramic was observed at a hydrostatic pressure of 28 MPa.

The effect of hydrostatic pressure on phase transition behavior of $Pb_{0.97}La_{0.02}(Zr_{0.64}Sn_{0.264}Ti_{0.085})O_3$ AFE_T ceramics was reported by Xu *et al* [35]. It was found that stable FE phase could be induced in the samples at 5 kV/mm and 100^oC. The induced FE phase was back to

AFE state upon the application of hydrostatic pressure. As the temperature was increased from 20 to 60 ^{o}C, the critical hydrostatic pressure decreased from 70 to 40 MPa. Moreover, for a virgin sample, as the hydrostatic pressure was increased from 0.1 to 500 MPa, the AFE-PE switching temperature gradually increased while dielectric constant of the samples was reduced. These results further demonstrated that hydrostatic pressure favored to AFE state, as predicated by the soft model theory.

Recently, Dai *et al* [144] studied the depolarization behavior of induced FE in PNZST ceramics as a function of hydrostatic pressure and external electric field. The ceramics with a composition of $Pb_{0.99}Nb_{0.02}(Z_{r0.75}Sn_{0.2}Ti_{0.05})_{0.98}O_3$ were prepared by the conventional solid state reaction process and then switched into FE state by electric poling. As shown in Fig. 34 (a), as a positive DC field was applied to the samples, the pressure for FE-AFE phase transition increased with increasing strength of electric field. At negative fields, the critical phase transition pressure decreased with increasing electric field. Positive DC field means that direction of the electric field is the same as that used to pole the ceramics, while negative field means that the polarity of the field is opposite to that of the poling field. As a result, a hydrostatic pressure-electric field phase diagram can be drawn, as shown in Fig. 34 (b). Therefore, FE-AFE switching can be controlled concurrently by hydrostatic pressure and electric field.

The effect of hydrostatic pressure on the AFE-PE phase transition of PLZST ceramics with a composition of $Pb_{0.97}La_{0.02}(Zr_{0.67}Sn_{0.23}Ti_{0.10})O_3$ was also studied by Dai *et al* [200]. The AFE-PE phase transformation temperature was increased at a rate of 0.2^{o}C/MPa, with increasing pressure. At the same time, with increasing pressure, the peak of dielectric constant (versus temperature) was decreased and broadened gradually. These experimental results also mean that the application of hydrostatic pressures stabilized the AFE phase.

4.2. Phase transition characteristics of AFE films with multilayer structures

4.2.1. Phase switching characteristics of oxide layer buffered AFE films

Oxide buffer layers were used to control the orientations of AFE films, thus leading to possible studies on orientation-dependent phase transition behavior of the AFE films. As mentioned in section 2, according to their structure and conductivity, oxide buffer layers can be divided into two classes: (i) conductive layers with ABO_3 structure, such as $LaNiO_3$ (LNO) and $(La,Sr)MnO_3$; (ii) insulating layers with MO_2 structure, such as TiO_2, ZrO_2 and CeO_2.

An extensive investigation on (100)-textured PZ, PNZST and PLZST films deposited on

different substrates was reported by Zhai *et al* [2, 43, 73, 78]. It was found that the PNZST films on $Pt/TiO_2/SiO_2/Si$ substrates were (110)-oriented, whereas they had (100)-preferred orientation when deposited on $LNO(100)/Pt/TiO_2/SiO_2/Si$ substrates. The (100)-orientated PNZST films have a columnar-like grain microstructure, with dielectric constant and saturation polarization being increased and dielectric loss tangent being reduced, as compared to the (110)-oriented films.

The difference in orientation also resulted in a difference in phase transition fields of the AFE films with same composition and thickness. Hao *et al* [86] studied phase transition behaviors of the LNO-buffered PLZST and PLZT thick films with (110)-preferred orientation, which was along the anti-parallel direction of AFEs. It was found that the (110)-oriented PLZST thin films had higher dielectric constant, lower dielectric loss tangent, increased saturation polarization, declined remanent polarization and enhanced phase switching fields, as compared to the (111)-orientated AFEs films without LNO buffer layer. In a separate study, Hao *et al* [110] deposited PLZT AFE thick films (2500 nm) with (110) and (100) orientations on $LNO(110)/Pt/TiO_2/SiO_2/Si$ and $Pt/TiO_2/SiO_2/Si$ substrates, respectively, by using a CSD method. As shown in Fig. 35, the PLZT thick films with (110) orientation had a more homogeneous microstructure, larger saturation polarization, higher dielectric constant and much smaller phase transition field comparatively.

Similar to those observed in FE thin films, electrical properties of AFE films have also been improved by using insulating layers. Typical work was reported by Hao *et al* [33], where PLZST thin films were deposited on $Pt/TiO_2/SiO_2/Si$ substrates with a thin buffer layer of TiO_2, ZrO_2 and CeO_2. It was found that although (111)-preferred orientation of the AFE films was suppressed due to the insertion of the buffer layers, the AFE films with ZrO_2 and CeO_2 buffer layers showed a more homogeneous microstructure as compared to those directly deposited on the $Pt/TiO_2/SiO_2/Si$ substrates. As a result, both the dielectric and electrical properties of the PLZST AFE thin films were improved due the presence of the buffer layers.

4.2.2. Phase transition characteristics of AFE films with superlattice structure

In recent years, artificial perovskite oxide superlattices, which are composed of combinations of two or more oxide layers, such as FE layer, ferromagnetic layer, and superconducting layer, etc., have been widely studied. Because large lattice distortion can be introduced in the in-plane direction by the layer stacking, various unusual physical properties have been created, such as enhanced dielectric properties in $BaTiO_3/SrTiO_3$ and $(Pb,La)TiO_3/PbTiO_3$ superlattices, elevated magnetoresistance in

$Pr_{0.85}Ca_{0.15}MnO_3/Ba_{0.64}Sr_{0.4}TiO_3$ superlattices, and artificial ferroelectricity in $SrZrO_3/SrTiO_3$ superlattices [201,202]. This subsection was aimed to summarize the progress in artificial superlattices involving a layer of AFEs.

An earlier work on superlattices with AFE layer, (100)-textured $PbZrO_3/PbTiO_3$ (PZO/PTO), was reported by Kanno *et al* [203]. The $[(PZO)_n/(PTO)_n]_m$ superlattice structures were prepared on Pt(100)MgO substrates by using a multi-ion-beam sputtering method. In the formula, *n* is the number of unit cell (or thickness of individual layer) and *m* is the total number of the $[(PZO)_n/(PTO)_n]$ layers. It was found that the decrease in the number of unit cell (*n*) led to an enhancement in dielectric constant and remanent polarization. Similar results were also obtained in the same superlattices by Choi *et al* [204]. In this case, the $PbZrO_3/PbTiO_3$ superlattices were fabricated on $La_{0.5}Sr_{0.5}CoO_3$(100)/MgO substrates by using PLD method. However, no AFE behavior was observed in both cases.

Pintilie *et al* [205] deposited $PbZrO_3/Pb(Zr_{0.8}Ti_{0.2})O_3$ (PZO/PZT) superlattices on $SrRuO_3$(100)/$SrTiO_3$ substrates by using PLD method. A clear interface between the two different layers was observed by using TEM [205].They also found that the thickness of individual layers had a strong effect on dielectric properties and phase transition behavior of the superlattice structures. There was a critical thickness of individual layers, which was 9-10 nm. The sample with the critical thickness of individual layer had a maximized dielectric constant. Meanwhile, a thickness-induced AFE-FE transition was also observed in the sample with the critical thickness. The shape of room-temperature capacitance-voltage (C-V) curves of the PZO/PZT superlattices with a total thickness of 100 nm had a close relationship with the values of *m* (=1, 2, 4 and 6). The samples with *m*=1, 2 and 4 (50, 25 and 12.5 nm of individual layers) demonstrated an obvious double butterfly shape, indicating their AFE nature of these structure. The critical electric field for AFE-FE switching decreased with decreasing thickness of the individual layer. The sample with *m*=6 (9 nm of individual layers) possessed typical FE behavior. These results were also confirmed by their P-E loops and current-voltage curves. In a recent study, Bao *et al* [201] prepared $PbZrO_3/Pb(Zr_{0.4}Ti_{0.6})O_3$ superlattices with a individual layer of 9-10 nm and total thickness of 200 nm. P-E loops also indicated that no AFE phase was observed in this multi-layered structure.

Besides AFE/FE superlattices, on AFE/PE artificial multi-layer structures have also been reported. For example, a multi-layer structure of PZO/BZO, consisting of AFE $PbZrO_3$ and PE

$BaZrO_3$, was fabricated on $LaNiO_3$(100)/Pt/Ti/SiO_2/Si substrates at 475°C by radio-frequency magnetron sputtering [206]. The PZO/BZO superlattices had an average composition of $(Pb_{0.75}Ba_{0.25})ZrO_3$ (PBZ). The thicknesses of each layer of PZO and BZO were varied, with ratios of PZO to BZO of 1.5 nm/0.5 nm, 3 nm/1 nm, 6 nm/2 nm and 12 nm/4 nm. The total thickness of the films was about 120 nm. It was found that the decrease in stacking periodicity increased the mean *c*-axis parameter of the superlattices and thus led to an enhancement in dielectric and ferroelectric properties. A linear increase in remanent polarization P_r and coercive field E_C with incresasing electric field was observed in the superlattice films, which was not observed in the PBZ solid-solution films. This "linear" ferroelectricity was independent of measuring temperature up to 100 °C. The retention of ferroelectric property was also greatly improved in the superlattice films, either at room temperature or at 100 °C. The superlattice films showed a dielectric property insensitive to temperature, which was entirely different from that of the PBZ films. Moreover, leakage current was significantly suppressed in the superlattice films due to the presence of the wide-bandgap sublayer of BZO.

5. Important potential applications of AFEs

The phase transition process of AFE materials is always accompanied by a remarkable and sharp change in polarization and volume, as a result of the application of electric field, temperature, or hydrostatic pressure. Therefore, AFE materials have potential applications in high-energy capacitors, high-strain actuators, IR pyroelectric detectors, cooling devices and pulsed voltage/current suppliers, and so on. Pulsed voltage/current during the phase transition from the induced FE to AFE has been discussed in section 4. In this section, four types of potential applications of AFE materials related to their remanent characteristics, i. e., high-energy storage, field-induced strain, pyroelectric and electrocaloric effect, will be summarized.

5.1. High-energy storage performance

AFEs, as a subcategory of dielectrics like linear dielectrics (LDs) and FEs, can be used in electric energy storage capacitors. Energy storage capacities of the three kinds of dielectric materials can be evaluated from their P-E loops, as shown in Fig. 36. The energy stored per unit volume of a dielectric, *J*, can be given by [207]:

$$J = \int_0^{D_{\max}} EdD , \qquad (7)$$

where E is the applied electric field and $D_{\max}$ is the electric displacement (D) at the highest applied

field (E_{max}). For the dielectrics with high relative dielectric constant, D can be replaced by the polarization (P). Accordingly, the above formula can be written as [207]:

$$J = \int_0^{P_{max}} EdP = \int_0^{E_{max}} PdE\,, \tag{8}$$

Evidently, based on Eq. (8), the J value of the dielectrics can be easily obtained by numerical integration of the area between the polarization axis and the curves of *P-E* loops. As shown in Fig. 36, when the electric field is increased from zero to the maximum E_{max}, the polarization is also increased to its maximum P_{max}, and the electrical energy is stored in the capacitor as J_{store}, illustrated by the green and red area. During the discharge process from E_{max} to zero, the recoverable electrical energy with a density J_{reco} is then released, represented by the green area in the figure. This means that part of the stored energy (the red area enclosed by the loops) is dissipated during the depolarization process because of the hysteresis loss. Based on these results, the energy storage efficiency η can be defined as:

$$\eta = \frac{J_{reco}}{J_{store}} \times 100\%. \tag{9}$$

Since the permittivity is defined as dP/dE, Eq. (8) can be expressed as:

$$J = \int_0^{E_{max}} \varepsilon_0 \varepsilon_r E dE. \tag{10}$$

Thus, for linear dielectric materials, whose permittivity is independent on external electric field, Eq. (10) can be simply expressed as:

$$J = \int_0^{E_{max}} PdE = \frac{1}{2}\varepsilon_0 \varepsilon_r E^2. \tag{11}$$

This result indicates that the energy storage density for linear dielectric materials is directly proportional to the relative permittivity of the dielectrics and the square of the applied electric field.

Obviously, according to Eqs (8)-(11), in order to improve the energy storage density and efficiency, large difference between maximum polarization and remanent polarization and high

breakdown field are desired. It can be seen from Fig. 36 that, for high-density energy storage applications, AFEs are superior to FEs, because their much more stored charges can be released due to the absence of any remanent polarization. AFEs are also superior to LDs because of their higher dielectric constant and larger polarization.

Although Jaffe stated in 1962 that AFEs might be a promising candidate for high energy storage [20], it was until 1971 that a moderate energy density of 2.1 J/cm^3 was achieved by using PZ AFE thick films with a small amount of low-softening-point glass [207]. The poor energy storage performance of AFEs ceramics has been attributed mainly to their relatively low breakdown fields, due to their inhomogeneous microstructures. As a result, little attention has been paid to the energy storage properties of AFE ceramics.

Recently, with the rapid development of microelectronic devices towards miniaturization, lightweight and integration, dielectric films with high energy storage density have attracted increasing attention, because of their higher critical breakdown field. An improved energy storage density, with a value of 7-8 J/ cm^3, was reported in AFE thin and thick films on Pt-buffered silicon substrates by Xu *et al* [74]. Thereafter, Parui reported that an even higher room-temperature recoverable energy density of 14.9 J/cm^3 could be possible by using a 700 nm 5 mol% La-doped PZ film at 600 kV/cm [208]. These results inspired the interest in the applications of AFE films as energy storage devices.

More recently, a similar result was reported by Hao *et al* [26]. They found that a recoverable energy density J_{reco} of 14.5 J/cm^3 could be achieved by using a 500-nm 5 mol% Sr-doped PZ thin film at 900 kV/cm at room temperature. At the same time, a higher energy efficiency η of 78% was realized in this film correspondingly. An enhanced fatigue endurance and stable temperature-dependent energy storage performance were also observed in the Sr-doped PZ films. The authors also found that lead content had an essential influence on the energy storage density of the AFE films [209]. For example, J_{reco} value of the 400-nm-thick $Pb_{0.97}La_{0.02}(Zr_{0.97}T_{i0.03})TiO_3$ films at 1200 kV/cm could be remarkably increased from 3.3 to 11.7 J/cm^3 by using 20 mol% excess lead. More interestingly, dense and uniform PLZT AFE films (1000 nm) deposited on $LaNiO_3$-buffered Ni foil substrates by using a CSD method exhibited an excellent breakdown endurance of above 3500 kV/cm and an extremely high J_{reco} of 53 J/cm^3 [210, 211]

Composition dependence of energy storage behaviors of PLZST AFE thin films with orthorhombic structure was first studied by Mirshekarloo *et al* [212]. The room temperature maximum

value of J_{reco} was 13.7 J/cm^3 in $Pb_{0.97}La_{0.02}(Zr_{0.75}Sn_{0.20}Ti_{0.05})O_5$ films. In fact, AFE films with orthorhombic or tetragonal structures could be readily obtained by chemical composition controlling. It is well known that crystal structure has a strong influence on phase transition process, dielectric properties and strains of AFEs. Thus, it is reasonably believed that the energy storage performance of AFEs is also affected by their structure. Recently, 1.8-μm-$(Pb_{0.97}La_{0.02})(Zr_{0.95-x}Sn_xTi_{0.05})O_3$ AFE thin films with orthorhombic (x=0.05 and 0.25) and tetragonal (x=0.40) structures were deposited on Pt-buffered Si substrates by using a CSD route by Hao *et al* [213]. It was found that the films with tetragonal structure with higher tin contents displayed higher dielectric constant and improved critical electric breakdown field, and thus higher recoverable energy storage density. Specifically, the AFE thin films with x=0.40 possessed a huge J_{reco} of 56 J/cm^3, as shown in the Fig. 37.

Besides high energy storage density, AFE materials also possess high charge releasing speed (the FE-AFE switching speed), which is an important parameter required by practical applications. It was reported by Pan *et al* [30] that the FE-AFE switching time of PLZST ceramics first gradually increased with increasing applied electric field and then kept to be a constant of 1-2 μs. Moreover, the samples with larger FE-AFE switching field E_A had a higher switching speed. Therefore, the switching speed was related to the stability of the induced FE phase. It was believed that the stability of the induced FE phase increased with increasing applied electric field and thus the energy barrier for the recovery of the AFE phase is increased. As a result, the switching time also increased. When the applied field was high enough to complete the AFE-FE transition, a further increase in the applied field would not increase the stability of the induced FE phase and thus the switching time leveled off. A very high charge releasing speed was observed in PLZST ceramics by Zhang *et al* recently [214]. It has been found that more than 80% stored electric charge could be released in just 65 ns for the PLZST ceramics with a composition of $Pb_{0.925}La_{0.05}(Zr_{0.42}Sn_{0.40}Ti_{0.18})O_3$. Furthermore, the AFE ceramic capacitors could withstand 2000 times of change-discharge cycling without significant degradation in performance at 35 kV/cm.

There are other reports on the FE-AFE phase switching speeds of AFE thin film [215-217]. For instance, a systematic investigation on electric field, temperature and thickness dependences of FE-AFE switching process of pure PZ films was reported by Bharadwaja *et al* [215]. They found that 60% of the stored energy in the 550-nm-thick PZ films could be released in less than 7 ns at room temperature and 200 kV/cm. As the applied field was further increased, the switching time showed an

almost negligible variation, but the amount of the released charge was increased. Increase in temperature led to reduced switching time (6 ns), but the amount of released charge decreased. At a given applied field of 200 kV/cm, the maximum amount of released charge increased with increasing thickness, but the switching time was not affected.

5.2. Field-induced strains

Electric field-induced strains in AFEs and FEs are generally attributed to the following four types of electricmechanical effects: (i) electrostriction, (ii) piezoelectricity, (iii) ferroelectricity, and (iv) induced phase changes [20, 218]. Electrostrictive materials are mainly relaxore FEs (such as PLZT and lead magnesium niobate or PMN), with large nonlinear electromechanical responses and minimum hysteresis. The electrostrictive strain originates from the alignment of micro-polar domains and is always positive, regardless of the direction of the applied electric field. Differently, the field-induced piezoelectric strain is linear, which can be either positive or negative, depending on the direction of the applied field. As for FEs, the field-induced strain is due to the domain switching, so that it shows well-known butterfly loops. However, the field-induced strain between AFE and FE state exhibits an abrupt increase at forward field and a sharp decrease at backward field. Namely, the field-induced strain in AFEs possesses an "on"/"off" characteristic. More importantly, the strain levels achieved in AFEs can be up to 1%. Strain level of 0.3-0.6% can be easily obtained with AFE ceramics and films, which are much higher than those (0.1%) achievable in other three types of electricmechanical materials. Therefore, AFEs are more desirable for applications in large-strain and high-force actuators.

AFE phase is stable under certain conditions. Phase transitions from AFE to FE or PE can be triggered by electric field or heating. The transitions from AFE to either PE or FE are always accompanied a rapid increase in specific volume (V), because $V_{FE}>V_{PE}>V_{AFE}$. Generally, c/a ratio of the primitive unit cell of AFEs is less than 1 and a_{FE} is lager than c_{AFE}, but smaller than a_{AFE}. As a result, when an electric field E is applied along c-direction of an AFE single crystal, it should expand along the E-direction (longitudinal strain), but shrink in directions normal to the field (transverse strain). Because the ratio of a_{FE}/c_{AFE} is larger than the ratio of a_{AFE}/a_{FE}, there is an increase in the overall volume [23, 28]. However, the scenario for polycrystalline ceramics is more complicated due to the randomly oriented grains. Typical field-induced longitudinal, transverse and volume strain of the PLZST ceramics with a composition of $Pb_{0.98}La_{0.02}(Zr_{0.66}Ti_{0.10}Sn_{0.24})_{0.995}O_3$ were reported by Pan *et al*

[28, 219], as shown in Fig. 38. Different from AFE single crystal, AFE ceramics experienced not only longitudinal but also transverse expansions during the AFE-FE phase switching. Due to the inverse piezoelectric effect of the induced FE, above the threshold of the AFE-FE switching, further increase in the field would result in an additional strain in the longitudinal direction, which was accompanied by a compressive deformation along the transverse directions. Accordingly, the longitudinal strain always increased with increasing electric field, whereas the transverse strain was maximized at a certain electric field, as shown in Fig. 38.

A comprehensive study on the primitive cell volumes of $FE_{R(LT)}$, $FE_{R(HT)}$, AFE_T, AFE_O, and PE phases was reported by Berlincouet [23]. The primitive unit cell volume has an order of AFE_O<AFE_T<PE<$FE_{R(LT)}$<$FE_{R(HT)}$. The specific volume difference between AFE_O and $FE_{R(HT)}$ is as high as 0.96%.

An earlier work on electric field-induced strain in AFEs was reported by Pan *et al* [30]. The AFE ceramics were PLZST with compositions located in the AFE_T region. Longitudinal field-induced strain varied in the range of 0.18%-0.87% depending on composition. It was found that larger strains were observed in the samples with compositions close to the AFE_T-FE_R MPB. The maximum longitudinal strain of 0.87%, corresponding 0.95% increase in volume, was obtained in $Pb_{0.97}La_{0.02}(Zr_{0.66}Ti_{0.11}Sn_{0.23})O_3$. Moreover, according to temperature-dependent induced strain, maximum strain was always achieved near the AFE-FE transition temperature, where AFE_T and FE_R co-existed. Therefore, like piezoelectric effect in FEs, AFEs with compositions near MPB also have optimized induced strains. This conclusion has been supported by widely available experimental data in the open literature [37], where a maximum longitudinal strain of 0.3%-0.4% can be readily achieved.

Akiyama and Fujisawa [197] studied the composition dependent field-induced strains of PNZST AFE_T ceramics. They found that, at E=80 kV/cm, longitudinal strain was gradually increased with increasing Zr/Sn ratio. The maximum strain observed in the PNZST ceramics was 0.44%. Recently, longitudinal and transverse strains of $Pb_{0.99}Nb_{0.02}[(Zr_{0.57}Sn_{0.43})_{1-y}Ti_y]_{0.98}O_3$ (y=0.060, 0.063, 0.067, 0.069, 0.071 and 0.075) ceramics were reported by Frederick *et al* [192].The samples with y≤0.067 were all stable AFE at room temperature. They showed similar longitudinal strain of about 0.3%, but their transverse strain was decreased from 0.09% to 0.01% with increasing value of y. For the samples with y≥0.069, the induced FE could not be back to AFE after the removal of the electric field. Thus,

their field-induced strains behaved like FEs, with a longitudinal strain of less than 0.1%.

Because large strain actuators are usually placed under prestressed conditions to maintain their integrity for practical applications, it is important to study the effect of prestress on field-induced strains of AFE materials. The effects of prestress on the field-induced strain of AFE PLZST ceramics, $Pb_{0.98}La_{0.02}(Sn_{0.33}Zr_{0.55}Ti_{0.12})_{0.995}O_3$ (labeled as B1) and $Pb_{0.98}La_{0.02}(Sn_{0.24}Zr_{0.66}Ti_{0.10})_{0.995}O_3$ (labeled as A2), were reported by Pan *et al* [219]. Without a prestress, A2 and B1 had the maximum induced longitudinal strain of about 0.27% and 0.24%, respectively. Once a small prestress (3 MPa) was applied, the longitudinal strains of the two samples were decreased by 50%. However, with further increasing stress, the two samples responded differently. The longitudinal strain of A2 continued to decrease with stressing, whereas that of B1 started to increase instead. This difference was well explained by considering the characteristics of the induced FEs ("soft" or 'hard"), as well as the geometry and clamping effect of the samples. However, in a separate study by Essig *et al* [220], a different prestress-dependent induced strain was observed in PLZST and PNZST AFE ceramics. In the temperature range of 20-85^{o}C, the longitudinal strain was increased gradually with increasing stress, which was not explained by the authors. These contradictory results mean that the mechanism of the prestress-dependent induced strains in AFEs could be complicated and further works are necessary to arrive at conclusive understandings.

There have also been reports on electric field-induced strains of AFE films. (111)-oriented PZ films with a longitudinal strain of 0.7% were reported by Tani *et al* [106]. The PZ films were deposited on Pt-buffered silicon substrates by a CSD method. Similarly, a maximum longitudinal strain of 6.4-6.8% was reported in 500-nm-thick (111)-oriented PZ films by Maiwa and Ichinose [31]. The field-induced in PLZST and PNZST thick films were studied by Xu *et al* [29]. It was reported that 5-μm-thick $Pb_{0.99}Nb_{0.02}(Zr_{0.85}Sn_{0.13}Ti_{0.02})O_3$ and $Pb_{0.97}La_{0.02}(Zr_{0.65}Sn_{0.31}Ti_{0.04})O_3$ films with the same orthorhombic structure showed a maximum longitudinal strain of 0.48% and 0.38%, respectively. Interestingly, Sengupta *et al* [218] found that the induced strains of AFE materials are also affected by the operating frequency. In this study, a (111)-preferred $Pb_{0.99}Nb_{0.02}[(Zr_{0.58}Sn_{0.42})_{0.96}Ti_{0.04}]_{0.98}O_3$ thin film with a thickness of 1200 nm was used, which was deposited on Pt(111)/TiO_2/SiO_2/Si substrates by a CSD method. As the measurement frequency was increased from 10 Hz to 10 kHz, the maximum longitudinal strain of the film gradually decreased from 0.16% to 0.09%. Similar result was observed in (100)-oriented $Pb_{0.97}La_{0.2}(Zr_{0.95}Zr_{0.05})O_3$ thin film with a thickness of about 1670 nm [113]. As the

frequency was increased from 100 Hz to 1 kHz, the maximum longitudinal strain of the film was declined from 0.4% to 0.33%. However, P-E loops of the thin film measured at different frequencies were almost the same. These results implied that the response of the volume change during the AFE-FE switching was slower as compared to the response of polarization switching.

Composition dependence of field-induced strains of AFE films was reported by Mirshekarloo *et al* in a recent study [210]. The studied AFE films were orthorhombic $(Pb_{0.97}La_{0.02})(Zr_{1-x-y}Sn_xTi_y)O_3$ with a thickness of 800-900 nm deposited on Pt-buffered substrates by a CSD process. It was found that the longitudinal strains of the films increased with increasing content of Zr^{4+}. Specifically, the $(Pb_{0.97}La_{0.02})(Zr_{0.90}Sn_{0.05}Ti_{0.05})O_3$ thin film had a maximum strain of 0.49%.

Because the anti-polar direction of AFEs is along the pesudocubic <110> direction while the polar of FE phase is along <111> direction, it is expected the orientation of AFE films should have a strong effect on their induced strains [109, 110]. An example was demonstrated by $(Pb_{0.97}La_{0.02})(Zr_{0.95}Ti_{0.05})O_3$ AFE thick films [110]. The films on $Pt(111)/TiO_2/SiO_2/Si$ substrates were (100)-oriented while those on $LaNiO_3(110)$/Si substrates were (110)-oriented. Both films were 2500 nm in thickness and deposited by using a CSD method. As demonstrated in Fig. 39 (a), the maximum strain of the (110)-oriented film was 0.55%, whereas that of the (100)-oriented film was 0.31%. A remarkable enhancement in strain, by about 77%, was obtained if a film with (110) orientation was used instead of the one with (100) orientation. Also, the AFE-FE switching field of the (110)-oriented thick film (200 kV/cm) was much lower than that (256 kV/cm) of the (100)-oriented film.

Another example was demonstrated by using highly (100) and (111)-oriented $Pb_{0.97}La_{0.02}(Zr_{0.85}Sn_{0.13}Ti_{0.02})O_3$ AFE thin films [109]. The (100) and (111)-oriented films with a thickness of about 700 nm were fabricated on $LaNiO_3(100)/Pt(111)/TiO_2/SiO_2/Si$ and $Pt(111)/TiO_2/SiO_2/Si$ substrates, respectively. The (111)-oriented AFE film had smaller phase switching field and higher saturated polarization than the (100)-preferred one. Moreover, the (111)-oriented AFE film had higher electric-field induced strain (0.79%) than the (100)-orientated sample (0.48%), as shown in Fig. 39 (b). Therefore, controlling the preferred orientation is an affective way to optimize the field-induced strain performances of AFE materials.

5.3. Pyroelectric effect

Pyroelectric effect of a material refers to its ability of to generate a temporary voltage (or current) when it is heated or cooled. The temperature variation alters the positions of the atoms slightly within

the crystal structure, so that the polarization of the material is changed. As a result, a voltage across the material is created. Because of the temperature-dependent polarization, AFE and FE materials usually possess good pyroelectric responses than other materials. Two parameters, pyroelectric coefficient *p* [$p=(Dd/dT)_E=(dP_s/dT)E+\varepsilon_0(d\varepsilon_r/Dt)_E E$] and pyroelectric figure of merit *FOM* ($FOM = p/C_v\sqrt{\varepsilon_0\varepsilon_r \tan\delta}$), are usually used to evaluate the performances of pyroelectric materials [221]. In the formulas, D is the dielectric displacement, T is temperature, P_s is spontaneous polarization, E is applied electric field, ε_0 is the dielectric constant of free space, ε_r is relative dielectric constant of the material, C_v is heat capacity, and tanδ is dielectric loss of the material. According to Byer and Roundy [222], pyroelectric coefficient can be deduced from the collected current in the material and is given by:

$$p = \frac{I}{AdT/dt}, \tag{12}$$

where I is the collected current flowing through the pyroelectrics-based capacitor, A is the electrode area and dT/dt is the rate of temperature variation.

Generally, there are two types of pyroelectrics [221]. Type one is the conventional pyroelectrics that are poled materials and operated in the temperature range without phase transition and below the Curie temperature, so that the pyroelectric response is reversible and stable. Type two is the phase-switching pyroelectrics that are operated near the phase transition temperature and a DC bias is usually employed to stabilize the pyroelectric effect. Pyroelectric effect in various FE materials, such as $Pb(Zr,Ti)O_3$ (PZT), $(Ba,Sr)TiO_3$ (BST), $Ba(Zr,Ti)O_3$ (BZT), $Pb(Sc,Ta)O_3$ (PST) and $PbMg_{1/3}Nb_{2/3}O_3$-$PbTiO_3$ (PMN-PT), and so on, has been widely investigated [223-226]. Due to their abundant types of phase transition (such as AFE-FE, FE-AFE, FE-PE and AFE-PE), lead-based AFE materials have been shown to possess more interesting pyroelectric responses. Typical works on pyroelectric properties of AFE materials will be summarized below.

Pyroelectric effect of AFEs was first found in PZ single crystal by Ujma and Handerek [227], when they attempted to demonstrate the presence of FE phase in PZ just below its Curie temperature. It was found that strong pyroelectric currents in the vicinity of T_F (phase transition tempearure between AFE and FE phase) and T_P (phase transition tempearure between FE and PE phase) could be detected during both heating and cooling processes. However, there was a heat hysteresis in the two processes.

Subsequently, pyroelectric effect was also observed in $Pb(Zr_{0.95}Ti_{0.05})O_3$ and Nb-doped $Pb(Zr_{0.92}Ti_{0.08})O_3$ AFE ceramics [228, 229]. With increasing temperature, $Pb(Zr_{0.95}Ti_{0.05})O_3$ ceramics underwent a series of phase switching, A_O-$F_{R(LT)}$, $F_{R(LT)}$-$F_{R(HT)}$ and $F_{R(HT)}$-PE, at 88, 160, and 243 ^oC, and large pyroelectric current densities in the order of 10^{-8} A/cm^2 were detected in the vicinity of the phase transition temperature. During the cooling process, reverse phase transitions occurred with a certain degree of delay, indicating the presences of thermal hysteresis of the phase transition. Similar phase switching sequence was also observed in Nb-doped $Pb(Zr_{0.92}Ti_{0.08})O_3$ ceramics. Moreover, it was found that, as the content of Nb_2O_5 was increased from 0.2% to 1.5%, the $F_{R(LT)}$-$F_{R(HT)}$ switching temperature was increased while the $F_{R(HT)}$-PE switching temperature was decreased, and at the same time, the pyroelectric current peaks became diffused and lowered.

Another example of pyroelectric effect of AFEs was reported by Yang *et al* [230]. The AFE material was PLZST ceramics with a composition of $Pb_{0.97}La_{0.02}(Zr_{0.75}Sn_{0.09}Ti_{0.16})O_3$ located in the AFE_T region. It had a forward switching field of 4 kV/mm. Below 15^{o}C, the induced FE state was retained after removal of the DC field. Fig. 40 shows temperature dependences of pyroelectric properties, due to the phase transition from induced FE to AFE, at various applied DC fields. It can be seen that the magnitude and peak temperature of the pyroelectric current were tunable within a wide temperature range from 5 to 100^{o}C. The peak temperature was increased at a rate of 38^{o}C/kV·mm^{-1} as the applied fields were less than 3 kV/mm. The pyroelectric coefficient reached the order of 10^{-7}-10^{-6} C/cm^2·K, with a peak width of 45^{o}C at ambient temperature. At high applied field, for instance, E=3 kV/cm, the induced FE phase was stabilized and FE-AFE switching was prevented.

Xu *et al* [231] investigated the pyroelectric effects of AFE_O PNZST $[Pb_{0.99}Nb_{0.02}(Zr_{0.85}Sn_{0.13}Ti_{0.02})_{0.98}O_3]$ and AFE_T PLZST $[Pb_{0.97}La_{0.02}(Zr_{0.75}Sn_{0.16}Ti_{0.09})O_3]$ thin films. Both samples with (100)-preferred orientation were deposited on $LaNiO_3$(100)/Pt/SiO_2/Si substrates by using a CSD process. Similar to bulk ceramics, the induced FE phase in PLZST films could only be stable at low temperatures and high DC electric fields. In other words, the transition temperature from the induced FE to AFE could be tuned by DC field, resulting in a tunable pyroelectric effect. In contrast, AFE phase of PNZST films was stable at low temperatures and its induced FE phase was stable at high temperature. As a result, the forward switching field was decreased as the temperature was increased. Accordingly, pyroelectric current due to the AFE-FE phase switching could also be tuned by DC field in a wide range of temperature. It was found that the peak pyroelectric coefficient in

an order of 10^{-7} C/cm^2·K was shifted from 20 to 100^{o}C as the DC voltage was decreased from 14 to 7.5 V.

Composition dependent pyroelectric properties of $(Pb_{0.87}La_{0.02}Ba_{0.1})(Zr_{0.7}Sn_{0.3-x}Ti_x)O_3$ (PLBZST, x=0.06, 0.07, 0.08, and0.09) ceramics were investigated by Zhang *et al* [232]. P-E loops measured at 50^{o}C indicated that the PLBZST ceramics experienced a phase transition from AFE to FE with increasing content of Ti^{4+} (*x*). At the same time, as x was increased from 0.06 to 0.09, the AFE-PE transition temperature was decreased from 68 to 53^{o}C and the peak value of dielectric constant was increased from 5200 to 13500. At a given electric field of 5 kV/cm, the peak pyroelectric coefficient due to the AFE-PE phase switching was increased from 0.2 to 6.5 μC/cm^2·K with increasing *x*.

The authors characterized the pyroelectric effects of the PLBZST ceramics with x=0.09 at various DC fields. Temperature dependent dielectric constant showed that Curie point decreased as the electric field was increased from 0 to 6 kV/cm and then increased gradually as the field was further increased from 7 to 8.5 kV/cm. This result indicated that, with increasing temperature, AFE-PE switching occurred in the PLBZST ceramic with x=0.09 if the applied fields were less than 6 kV/cm, while FE-PE transition occurred in it at electric fields of above 7 kV/cm. Large pyroelectric coefficients were detected during both the AFE-PE and FE-PE switching processes. Moreover, the maximum pyroelectric coefficient of 0.84 μC/cm^2·K was observed at 8.5 kV/cm.

Pyroelectric responses of PLBZST $[(Pb_{0.87}La_{0.02}Ba_{0.1})(Zr_{0.7}Sn_{0.24}Ti_{0.06})O_3]$ ceramics with various excess PbO (0%, 3%, 6%, and 9% in weight) were investigated by Zhang *et al* [221]. Compared to those without excess content of PbO, PLBZST ceramics with excess PbO exhibited higher AFE-PE transition temperatures, increased dielectric constant and lower dielectric loss tangent. As the excess content of PbO was increased from 0 to 9 wt%, pyroelectric coefficient of the PLBZST ceramics was increased from 0.16 μC/cm^2·K to 0.4 μC/cm^2·K, and their figure of merit was increased from 40×10^{-5} Pa$^{-0.5}$ to 140×10^{-5} Pa$^{-0.5}$, at DC field of 4 kV/cm, at temperatures near the AFE-PE switching points.

It should be noted that the magnitude of poled field also has a strong effect on pyroelectric coefficient, as reported by Chan *et al* [91] and Zhang *et al* [234]. The PLZST ceramics studied by Zhang *et al* [234] were $Pb_{0.955}La_{0.03}(Zr_{0.42}Sn_{0.40}Ti_{0.18})O_3$ and $Pb_{0.97}La_{0.02}(Zr_{0.42}Sn_{0.40}Ti_{0.18})O_3$. It was found that the unpoled sample had no pyroelectric effect, since there was no induced FE in it. Significant pyroelectric effects were observed in the poled samples. The pyroelectric coefficient was gradually increased with increasing DC field. More importantly, the peak temperature of pyroelectric

coefficient was DC field-independent. However, $Pb_{0.955}La_{0.03}(Zr_{0.42}Sn_{0.40}Ti_{0.18})O_3$ ceramics had a large thermal hysteresis of about 30 ^oC, which is undesirable for their practical applications. The authors found that the thermal hysteresis was closely related to the content of La^{3+}. By reducing the content of La^{3+}, they prepared $Pb_{0.97}La_{0.02}(Zr_{0.42}Sn_{0.40}Ti_{0.18})O_3$. The ceramics had a much smaller thermal hysteresis of less than 1.5°C and a larger pyroelectric coefficient of 25 $\times 10^{-8}$ $C/cm^2 \cdot K$, in a temperature range from 105 to 135°C.

5.4. Electrocaloric effect

Electrocaloric (EC) effect, the reverse course of pyroelectric effect, is the change in temperature of a material upon the application or removal of an electric field under adiabatic conditions [235, 236]. The mechanism of EC effect can be explained by using a conceptual macro-scale model. When an electric field is applied to an EC material, the material becomes more polar-ordered, reducing the entropy associated with polarization. If this process occurs under reversible adiabatic conditions, the total entropy of the material remains constant. The remaining components of the entropy (hence the temperature) must then increase to compensate for the decrease in the polarization entropy. The converse is true if the material becomes less polar-ordered upon removal of the electric field. The material must then cool down to compensate for the increase in the polarization entropy. Evidently, the principle of EC cooling follows that of vapor-compression systems and goes through the same stages of the reverse of Carnot cycle. The main difference is that the working medium is solid materials for EC and that all the processes must be separated in time. Compared to the traditional cooling technology, EC cooling has the advantages of greenhouse gases free and the solid-state structure, so it is a very promising technique for the next generation of cooling devices.

According to the Maxwell relation $\left(\frac{\partial D}{\partial T}\right)_E = \left(\frac{\partial S}{\partial E}\right)_T$, the reversible adiabatic temperature change (ΔT) and the isothermal entropy change (ΔS) in a material at an applied electric-field E can be expressed as [237]:

$$\Delta T = -\frac{1}{\rho C}\int_{E_1}^{E_2} T\left[\frac{\partial D}{\partial T}\right]_E dE, \tag{13}$$

$$\Delta S = -\int_{E_1}^{E_2}\left[\frac{\partial D}{\partial T}\right]_E dE, \tag{14}$$

where ρ is the mass density, C is the molar heat capacity, T is the operating temperature, P is the

maximum polarization at applied field E; and E_1 and E_2 are the initial and final applied field, respectively. Clearly, $\left(\frac{\partial D}{\partial T}\right)_E$ is the pyroelectric coefficient, as defined above. Eq. (13) and (14) indicate that, in order to obtain larger ΔT and ΔS, the materials should have a high pyroelectric coefficient.

Because of their good pyroelectric properties, FEs and AFEs have been acknowledged to be the promising EC materials. The use of FEs and AFEs as EC materials for solid-state cooling has been proposed since 1960s [236]. Significant achievements have been made in these EC materials, such as $Pb(Zr,Ti)O_3$, $BaTiO_3$, $(Pb,Sr)TiO_3$ and $(Pb,Mg)NbO_3$-$PbTiO_3$ thin films and single crystals, as well as poly vinylidene fluoride (PVDF)-based FE polymers. In line with the topic of the review, only EC effects of AFEs are discussed. More detailed information on EC materials could be found in recent reviews [237, 239].

As mentioned above, high pyroelectric coefficient is desired to achieve large temperature change in polar materials. Moreover, significant pyroelectric effect is usually observed during phase transition processes, such as FE-PE switching. Because AFEs possess more types of phase transition than their FE counterparts, AFEs have higher pyroelectric coefficients.

The first work on the EC effect in AFEs was reported by Thacher *et al* [236] in 1968, in which a peak temperature reduction, ΔT=1.6^{o}C, was realized in $Pb(Zr_{0.455}Sn_{0.455}Ti_{0.09})O_3$ ceramics during the PE-AFE phase transition at an applied electric field of 30 kV/cm and about 50^{o}C. In 1981, a higher value of ΔT=2.6^{o}C at E=30 kV/cm (corresponding to 750 V) was observed in $Pb_{0.99}Nb_{0.02}(Zr_{0.75}Sn_{0.20}Ti_{0.05})_{0.98}O_3$ ceramics during the AFE-PE phase transition by Tullte and Payne [240]. However, the poor cooling efficiency and the high operating voltages have hindered AFE ceramics for practical applications.

Fortunately, it was recognized by Mischenko *et al* [241] that the EC effect achieved in bulk ceramics was limited by their low electric breakdown strength and it is not their intrinsic material properties. As mentioned before, thin films have higher dielectric strength than their ceramic counterparts. Using thin films for EC applications could be a practical strategy. Major advances have been made in EC effects with AFE thin films. In 2006, a record high EC effect was reported in 350-nm-thick $PbZr_{0.95}T_{0.05}O_3$ film deposited on Pt-buffered silicon substrates by using a CSD method [241]. As shown in Fig. 41, with increasing ΔE (ΔE=E_2-E_1), EC effect was greatly improved. A giant

EC effect of ΔT=12^{o}C at ΔE=480 kV/cm (corresponding 12 V) was obtained in the thin films near its Curie temperature of 220 ^{o}C. This result greatly propelled the study on EC effect in FE and AFE films. Another example was reported by Parui and Krupanidhi [242], where a 700 nm pure PZ film had an EC effect of ΔT=12^{o}C (at ΔE=600 kV/cm) at 235^{o}C. Subsequently, a moderate temperature reduction of ΔT=8.5^{o}C (at ΔE=754 kV/cm) at 220^{o}C was reported in $Pb_{0.97}La_{0.02}(Zr_{0.95}Ti_{0.05})O_3$ thin films by Hao *et at* [243]. Evidently, the peak value of EC effect is usually near the Curie temperature of AFEs, which is too high to meet the requirement of near room-temperature cooling.

A very encouraging result was reported by Peng *et al* recently [244]. Near room temperature EC effect was observed in 320-nm $Pb_{0.98}Ba_{0.20}ZrO_3$ thin films deposited on Pt-buffered silicon substrates, as shown in Fig. 42. It had a giant temperature change ΔT=45.3^{o}C (at E=598 kV/cm) at 17^{o}C. Moreover, it is also found that peak of EC effect is quite broad, showing potential applications of such AFE thin films.

6. Fatigue behavior and mechanism of AFE materials

Like FEs, AFEs also have polarization fatigue under repetitive electrical stress. Polarization fatigue usually results in a reduction in saturation polarization, strain and dielectric constant and an increase in remanent polarization, dielectric loss tangent and leakage current [245-247]. It has become a main hindrance for the applications of FEs and AFEs. Over the last decades, in order to improve their fatigue endurance, fatigue behavior of FEs has been extensively investigated and numerous models have been proposed to explain the fatigue mechanism. Fatigue behavior and mechanism of FEs have been thoroughly reviewed by Lou [248]. Generally, fatigue behavior of FEs has both intrinsic and extrinsic contributions. Intrinsic contributors include material composition and sample microstructure, while extrinsic contributors include surface condition, type of electrodes, operating temperature, and strength and type of driving fields. Although fatigue effect of FE materials has been extensively studied, a general conclusion is still not available to date and contradictory results are often found in the open literature.

Compared to that of FEs, fatigue behavior of AFE materials is much less investigated. Similarly, the mechanism of fatigue of AFEs has also not been fully understood. For the completeness of this review, a brief summary on the progress on the study of fatigue behavior of AFEs is presented in two aspects: origination of fatigue and strategies to improve the fatigue performance.

6.1. Origination of fatigue in AFE materials

Although it is generally believed that AFE materials undergo a similar fatigue processes as FEs do, the fatigue of AFEs is usually much less severe than that of their FE counterparts, if same measurement conditions are adopted. For instance, for the PNZST AFE and FE thin films deposited on Pt-buffered silicon substrates with similar composition, the AFE films showed less polarization fatigue than the FE films after 10^9 cycling [249]. The better fatigue endurance of the AFEs was attributed to the presence of the 180^o domains, which have smaller stress during switching as compared to the 90^o domains in FEs.

According to their locations and forms, the fatigue contributors of AFEs can be generally divided into three classes. The first one is called domain-wall pinning effect, which is caused by ionic defects and trapped charges [248, 250]. Typical trapped charge is injected charge, which prohibits domain nucleation and switching, thus producing screening electric field. Wang *et al* [251, 252] proposed that, if the domain wall pinning is dominant in a capacitor, a higher driving field would improve the fatigue behavior of the capacitor. This is because larger electric field enables the domain switching and depinning easier.

The second type is called micro-cracking effect (mechanic model), which is caused by the repetitive larger strain and the cluster growth of point defects during the cycling. Evident microcracks were observed in fatigued AFE bulk ceramic by Zhou *et al* [246]. It was suggested that the presence of microcracks reduced the local effective fields for polarization switching or yielded conductive corrosion pathways in the materials, leading to the appearance of fatigue [248, 253].

The third one is called “dead” layer effect. It is believed that an interface layer between the electrodes and the AFE/FE film is usually present, which grows as a consequence of cycling, due to the accumulation of oxygen vacancies. Although the microscopic nature of the “dead” layer is still not verified, the explanation by using the “dead” layer model is quite straight-forward. As the thickness of interface layer is increased, the field applied to the materials will be decreased and eventually is not strong enough to switch the domains, which in turn leads to a suppression of polarization as the cycling number is increased. Obviously, if micro-cracking effect and/or “dead” layer effect are dominant in AFEs, higher deriving field will result in more severe fatigue.

6.2. Strategies s to improve fatigue endurance of AFE films

According to the above discussion, one can improve the fatigue endurance by decreasing the domain-wall pinning, reducing the microcracks and eliminating the “dead” layer. However, reports on

strategies to improve the fatigue endurance of AFE materials are quite limited.

Zhai *et al* [240] found that the fatigue endurance of PNZST AFE thin films on Pt(111)/TiO_2/SiO_2/Si substrates could be greatly enhanced by the using of $LaNiO_3$ buffer layers. It was believed that the oxide buffer layer acted as a sink of oxygen vacancies, which effectively prevented the growth of the "dead layer".

A detailed investigation on fatigue behavior of doped PZ films was reported by Hao *et al* [26, 163]. As shown in Fig. 43, the reductions of saturation polarization after 10^8 cycling are 49%, 12% and 28% for pure PZ, 5 mol% Sr^{2+}-dpoed and Ba^{2+}-doped PZ films, respectively. The enhanced fatigue endurance of doped PZ films was contributed to the decrease of oxygen vacancy density and the suppression of its mobility by the Ba^{2+} and Sr^{2+} doping, which in turn reduced the domain-wall pinning effect. The decrease of oxygen vacancy density and the suppressed mobility were ascribed to the stronger bonding energy of the Sr-O bond (426 kJ/mol) and the Ba-O bond (562 kJ/mol) than that of the Pb-O bond (382 kJ/mol). Also, because of the stronger bonding energy of Ba-O than that of Sr-O, Ba^{2+}-doped PZ AFE thin films showed the best fatigue endurance among the three samples.

7. Concluding remarks

Great achievements have been made in the preparation, understanding of phase-transition mechanism and fatigue effect in the PZ-based AFE materials. Moreover, compared with bulk ceramics, AFE materials in film form are attracting increasing attention due to their higher breakdown fields, lower growth temperatures and easier integration with silicon technologies. Therefore, it is believed that the research activities in this area will continuously focus on AFE films in the near further.

Various methods and techniques have been developed to fabricate AFE ceramics and deposit AFE thin and thick films. For AFE ceramics, new synthetic strategies, such as wet-chemical synthesis, molten salt processing and high-energy mechanochemical technique, reserve further development to synthesize precursor powders with high sinterability and desired performances of cost-effective final products. It is also possible to develop AFEs with new compositions for better electrical properties. For AFE films, controlling over their orientations with desired electrical properties for given applications will be main subject of research.

The phase transition process of AFE materials is always accompanied by a remarkable and sharp change in polarization and volume, as a result of the application of electric field, temperature or hydrostatic pressure. Therefore, AFEs have potential applications in high-energy capacitors,

high-strain actuators, IR pyroelectric detectors, cooling devices and pulse voltage/current suppliers, which has revived this family of materials, noting the heavy investment in energy-oriented research worldwide. However, there is still long way to go before they can be used for practical applications. Taking EC effect as an example, although large EC value has been observed in AFE thin films, the cooling efficiency must be limited, due to the low overall heat capacity of thin films. Thus, the cooling performance observed currently could not meet the requirement of cooling for micro-electron devices that are working near room temperature. As a result, it is highly desirable to develop AFE thick films with sufficiently high EC effect near room temperature.

Like FEs, AFEs also experienced polarization fatigue under repetitive electrical stress. Although the progress on study on fatigue behavior of FEs can be used to understand that of AFEs, more efforts should be made to further clarify the fatigue mechanism of AFEs, so as to establish strategies to improve the fatigue resistance of AFE materials.

Acknowledgements

This work was supported by the National Natural Science Foundation of China under grant No. 51002071, Start-up grant of Nanyang Technological University (2012) and AcRF Tier 1 (RG 44/12), MOE, Singapore.

References

[1] G. H. Haertling, "Ferroelectric ceramics: history and technology", *J. Am. Ceram. Soc.* 82 , 797-818 (1999).

[2] J. W. Zhai, X. Li and H. Chen, "Effect of orientation on the ferroelectric-antiferroelectric behavior of sol-gel deposited (Pb,Nb)(Zr,Sn,Ti)O_3 thin films", *Thin Solid Films* 446, 200-204 (2004).

[3] E. C. Subbarao, "Ferroelectric and antiferroelectric materials", *Ferroelectrics* 5, 267-280 (1973).

[4] D. Bernard, J. Pannetier and J. Lucas, "Ferroelectric and antiferroelectric materials with pyrochlore structure", *Ferroelectrics* 21, 429-431 (1978).

[5] I. Nishiyama, "Antiferroelectric liquid crystals", *Adv. Mater.* 6 (12), 966-970 (1994).

[6] G. A. Samara, "pressure and temperature dependence of the dielectric properties and phase transition of the antiferroelectric perovskites: $PbZrO_3$ and $PbHfO_3$", *Phys. Rev. B* 1 (9), 3777-3786 (1970).

[7] O. A. Zhelnova and O. E. Fesenko, "Phase transitions and twinning in $NaNbO_3$ crystals", *Ferroelectrics* 75, 465-476 (1987).

[8] E. Sawaguchi, H. Maniwa and S. Hoshino, "Antiferroelectric structure of lead zirconate", *Phys. Rev.* 83 (5), 1078 (1951).

[9] X. H. Dai, J. F. Li and D. Viehland, "Weak ferroelectric in antiferroelectric lead zirconate", *Phys. Rev. B* 51 (5), 2651-2655 (1995).

[10] P. Ayyub, S. Chattopadhyay, R. Pinto and M. S. Multani, "Ferroelectric behavior in thin films of antiferroelectric materials", *Phys. Rev. B* 57 (10), R5559-R5562 (1998).

[11] F. Jona, G. Shirane, F. Mazzi and R. Pepinsky, "X-ray and neutron diffraction study of antiferroelectric lead zirconate, $PbZrO_3$", *Phys. Rev.* 105 (3), 849-856 (1957).

[12] T. Asada and Y. Koyama, "Coexistence of ferroelectricity and antiferroelectricity in lead zirconate titanate", *Phys. Rev. B* 70, 104105-1-5 (2004).

[13] L. Pintilie, K. Boldyreva, M. Alexe and D. Hesse, "Coexistence of ferroelectricity and antiferroelectricity in epitaxial $PbZrO_3$ films with different orientations", *J. Appl. Phys.* 103, 024101-1-5 (2008).

[14] X. H. Hao, J. W. Zhai, Z. X. Yue and J. B. Xu, "Phase transformation properties of highly (100)-oriented PLZST 2/85/12/13 antiferroelectric thin films deposited on Nb-$SrTiO_3$

single-crystal substrates", *J. Am. Ceram. Soc.* 94 (9), 2816-2818 (2011).

[15] T. Mitsui, "Theory of the ferroelectric effect in Rochelle salt", *Phys. Rev.* 111 (5), 1259-1267 (1958).

[16] C. Kittel, "Theory of antiferroelectric crystal", *Phys. Rev.* 82 (5), 729-732 (1951).

[17] G. Shirane, E. Sawaguchi and Y. Takaui, "Dielectric properties of lead zirconate", *Phys. Rev.* 84 (3), 476-481 (1951).

[18] G. Shirane, "Ferroelectricity and antiferroelectricity in ceramic $PbZrO_3$ containing Ba or Sr", *Phys. Rev.* 86 (2), 219-227 (1952).

[19] I. J. Frjtz and J. D. Keck, "Pressure-temperature phase diagrams for several modified lead zirconate ceramics", *J. Phys. Solids* 39, 1163-1167 (1978).

[20] B. Jaffe, "Antiferroelectric ceramics with field-enforced transition: a new nonlinear circuit element", *Proc. IRE* 1264-1267 (1961).

[21] D. Berlincourt, H. H. A. Krueger and B. Jaffe, "Stability of phases in modified lead zirconate with variation in pressure, electric field, temperature and composition", *J. Phys. Chem. Solids* 25, 659-674 (1964).

[22] C. E. Land, "Bistable optical information storage using antiferroelectric-phase lead lanthanum zirconate titanate ceramics", *J. Am. Ceram. Soc.* 71 (11), 905-908 (1988).

[23] D. Berlincourt, "Transducers using forced transition between ferroelectric and antiferroelectric state", *IEEE Trans. Sonics Ultrason.* 13, 116-125 (1966).

[24] J. F. Li, D. D. Viehland, T. Tani, C. D. E. Lakeman and D. A. Payne, "Piezoelectric properties of sol-gel-derived ferroelectric and antiferroelectric thin layer", *J. Appl. Phys.* 75 (1), 442-448 (1994).

[25] I. Kanno, S. Hayashi, M. Kitagawa, R. Takayama and T. Hirao, "Antiferroelectric $PbZrO_3$ thin films prepared by multi-ion-beam sputtering", *Appl. Phys. Lett.* 66 (2), 125-147 (1995).

[26] X. H. Hao, J. W. Zhai and X. Yao, "Improved energy storage performance and fatigue endurance of Sr-doped $PbZrO_3$ antiferroelectric thin films", *J. Am. Ceram. Soc.* 92 (5), 1133-1135 (2009).

[27] F. Wang, W. K. Li and G. H. Haertling, "Transverse electro-optic effect of antiferroelectric lead zirconate thin films", *Opt. Lett.* 17 (16), 1122-1124 (1992).

[28] S. E. Park, M. J. Pan, K. Markowski, S. Yoshikawa and L. E. Cross, "Electric field phase transition of antiferroelectric lead lanthanum zirconate titanate stannate ceramics", *J. Appl. Phys.*

82 (4), 1798-1803 (1997).

[29] B. M. Xu, Y. H. Ye and L. E. Cross, "Dielectric properties and field-induced phase switching of lead zirconate tatanate stannate antiferroelectric thick films on silicon substrates", *J. Appl. Phys.* 87 (5), 2507-2515 (2000).

[30] W. Y. Pan, C. Q. Dam, Q. M. Zhang and L. E. Cross, "Large displacement transducers based on electric field forced phase transitions in the tetragonal $(Pb_{0.97}La_{0.02}(Ti,Zr,Sn)O_3$ family of ceramics", *J. Appl. Phys.* 66 (12), 6014-6023 (1989).

[31] H. Maiwa and N. Ichinose, "Electric and electromechanical properties of $PbZrO_3$ thin films prepared by chemical solution deposition", *Jpn. J. Appl. Phys.* 40, 5507-5510 (2001).

[32] D. Forst, J. F. Li and Z. K. Xu, "Incommensurately modulated polar structure in antiferroelectric tin-modified lead zirconate titanate: II, dependence of structure-property relations on Tin content", *J. Am. Ceram. Soc.* 81 (9), 2225-2236 (1998).

[33] X. H. Hao, J. W. Zhai, Z. X. Yue, J. Zhou, J. Yang and S. L. An, "Effects of oxide buffer layers on the microstructure and electrical properties of PLZST 2/87/10/3 antiferroelectric thin films", *J. Cryst. Growth* 314, 151-156 (2011).

[34] D. Berlincourt, H. Jaffe, H. H. A. Krueger and B. Jaffe, "Release of electrical energy in $PbNb(Zr,Ti,Sn)O_3$ by temperature- and by pressure-enforced phase transitions", *Appl. Phys. Lett.* 3 (5), 90-92 (1963).

[35] Z. Xu, Y. J. Feng, S. G. Zheng, A. Jin, F. L. Wang and X. Yao, "Phase transition and dielectric properties of La-doped $Pb(Zr,Sn,Ti)O_3$ antiferroelectric ceramics under hydrostatic pressure and temperature", *J. Appl. Phys.* 92 (5), 2663-2667 (2002).

[36] H. B. Liu and B. Dkhil, "A brief review on the model antiferroelectric $PbZrO_3$ perovskite-like material"**,** *Z. Kristallogr.* 226, 163-170 (2011).

[37] K. Markowski, S. E. Park, S. Yoshikawa and L. E. Cross, "Effect of compositional variations in lead lanthanum zirconate stannate titanate system on electrical properties", *J. Am. Ceram. Soc.* 79 (12), 3297-3304 (1996).

[38] L. J. Zhou, D. C. Lupascu, A. Zimmermann and Y. Zhang, "Discontinuous switching in antiferroelectric ceramics monitored by acoustic emissions", *J. Appl. Phys.* 97, 124106-1-8 (2005).

[39] W. M. Zhang, W. Huebner, S. E. Sampayan and M. L. Krogh, "Polarization switching of and

electron emission from lead lanthanum zirconate titanate ceramics", *J. Am. Ceram. Soc.* 82 (3), 591-599 (1999).

[40] V. J. Tennery, "High-temperature phase transitions in $PbZrO_3$", *J. Am. Ceram. Soc.* 49 (9), 483-486 (1966).

[41] L. J. Zhou, A. Zimmermann, Y. P. Zeng and F. Alainger, "Effects of PbO content on the sintering behavior, microstructure, and properties of La-doped PZST antiferroelectric ceramics", *J. Mater. Sci. Mater. Electron.* 15, 145-151 (2004).

[42] L. H. Xue, Q. Li, Y. Y. Zhang, R. Liu and X. H. Zhen, "Synthesis, sintering and characterization of PLZST perovskite prepared by a lactate precursor route", *J. Eur. Ceram. Soc.* 26, 323-329 (2006).

[43] J. W. Zhai and H. Chen, "Crystallization kinetics and dielectric properties in sol-gel derived $(Pb,La)(Zr,Sn,Ti)O_3$ ceramics", *J. Appl. Phys.* 94 (1), 589-593 (2003).

[44] M. Chen, X. Yao and L. Y. Zhang, "Preparation of $(Pb,La)(Zr,Sn,Ti)O_3$ antiferroelectric ceramics using colloidal processing and the field induced strain properties", *J. Eur. Ceram. Soc.* 21, 1159-1164 (2001).

[45] M. Chen, X. Yao and L. Y. Zhang, "Grain size dependence of dielectric and field-induced strain properties of chemical prepared $(Pb,La)(Zr,Sn,Ti)O_3$ antiferroelectric ceramics", *Ceram. Intern.* 28, 201-207 (2002).

[46] L. Zhang, Z. Xu, Y. J. Feng, Y. Y. Hu and X. Yao, "Synthesis, sintering and characterization of PNZST ceramics from high-energy ball milling process", *Ceram. Intern.* 34, 709-713 (2008).

[47] L. B. Kong, T. S. Zhang, J. Ma and F. Boey, "Process in synthesis of ferroelectric ceramics materials via high-energy mechanochemical technique", *Prog. Mater. Sci.* 53, 207-323 (2008).

[48] L. B. Kong, J. Ma, W. Zhu and O. K. Tan, "Preparation of antiferroelectric lead zirconate ceramics from high-energy ball milling process", *Mater. Lett.* 49, 96-101 (2001).

[49] L. B. Kong, J. Ma, T. S. Zhang, W. Zhu and O. K. Tan, "Preparation of antiferroelectric lead zirconate titanate stannate ceramics by high-energy ball milling process", *J. Mater. Sci. Mater. Electron.* 13, 89-94 (2002).

[50] L. B. Kong, J. Ma, W. Zhu and O. K. Tan, "Preparation and characterization of PLZT ceramics using high-energy ball milling", *J. Alloys Comp.* 322, 290-297 (2001).

[51] S. X. Zhao, Q. Li, L. Wang and Y. L. Zhang, "Molten salt synthesis of lead lanthanum zirconate

titanate stannate powders and ceramics", *Mater. Lett.* 60, 425-430 (2006).

[52] S. X. Zhao, Q. Li, F. B. Song, C. H. Li and D. Z. Shen, "Molten salts synthesis of relaxor ferroelectrics PMN-PT powders", *Key Eng. Mater.* 336-338, 10-13 (2007).

[53] K. H. Yoon, Y. S. Cho and D. H. Kang, "Molten salt synthesis of lead-based relaxors", *J. Mater. Sci.* 33, 2977-2984 (1998).

[54] C. L. Mao, G. S. Wang, X. L. Dong, Z. Y. Zhou and Y. Y. Zhang, "Low temperature synthesis of $Ba_{0.70}Sr_{0.30}TiO_3$ powders by the molten-salt method", *Mater. Chem. Phys.* 106, 164-167 (2007).

[55] E. M. Sabolsky, L. Maldonado, M. M. Seabaugh and L. Swartz, "Textured-Ba(Zr,Ti)O_3 piezoelectric ceramics fabricated by templated grain growth (TGG)", *J. Electroceram.* 25, 77-84 (2010).

[56] L. J. Zhou, Z. Zhao, A. Zimmermann, F. Aldinger and M. Nygren, "Preparation and properties of lead zirconate stannate titanate sintered by spark plasma sintering", *J. Am. Ceram. Soc.* 87 (4), 606-611 (2004).

[57] L. W. Martin, Y. H. Chu and R. Tamesh, "Advances in the growth and characterization of magnetic, ferroelectric, and multiferroic oxide thin films", *Mater. Sci. Eng. R* 68, 89-133 (2010).

[58] R. W. Schwartz, "Chemical solution deposition of perovskite thin films", *Chem. Mater.* 9, 2325-2340 (1997).

[59] H. D. Chen, K. R. Udayakumar, C. J. Gaskey, L. E. Cross, J. J. Bernstein and L. C. Niles, "Fabrication and electrical properties of lead zirconate titanate thick films", *J. Am. Ceram. Soc.* 79 (8), 2189-2192 (1996).

[60] L. Y. Wang, K. Yao and W. Ren, "Piezoelectric $K_{0.5}Na_{0.5}NbO_3$ thick films derived from polyvinylpyrrolidone-modified chemical solution deposition", *Appl. Phys. Lett.* 93, 092903-1-3 (2008).

[61] J. Lu, J. Chu, Y. Yang and W. H. Huang, "Fabrication of thick Pb(Zr,Ti)O_3 films by modified sol-gel methods for application in MEMS", *J. Micromechatron.* 2, 159-171 (2004).

[62] M. H. Zhang, H. Wang, F. Xiang and X. Yao, "Low-temperature sintering $(Ba_{0.6}Sr_{0.4})TiO_3$ thick films prepared by screen printing", *Intern. J. Appl. Ceram. Technol.* 6, 257-263 (2009).

[63] F. Fu, J. W. Zhai, Z. K. Xu, B. Shen and X. Yao, "Fabrication of grain orientation $BaTiO_3$ thick films by template grain growth method", *Solid State Comm.* 151, 120-122 (2011).

[64] P. Ctibor, H. Ageorges, V. Stengl, N. Murafa, I. Pis, T. Zahoranova, V. Nehasil and Z. Pala,

"Structure and properties of plasma sprayed $BaTiO_3$ coatings: spray parameters versus strucuture and photocatalytic activity", *Ceram. Intern.* 37, 2561-2567 (2011).

[65] K. D. Budd, S. K. Dey and D. A. Payne, "Sol-Gel Processing of $PbTiO_3$, $PbZrO_3$, PZT and PLZT Thin- Films," *British Ceram. Soc. Proc.* 36, 107-121 (1985).

[66] Y. Akiyama, S. Kimura and I. Fujimura, "Development of (Pb,Nb)(Zr,Sn,Ti)O_3 films using a sol-gel process and resulting antiferroelectric properties", *Jpn. J. Appl. Phys.* 32, 4154-4157 (1993).

[67] L. Cakare, M. Kosec and B. Malic, "Sol-gel processing of $PbZrO_3$ thin films", *J. Sol-Gel Sci. Techn.* 19, 603-606 (2000).

[68] K. K. Li, F. Wang and G. H. Haertling, "Antiferroelectric lead zirconate thin films derived from acetate precursors", *J. Mater. Sci.* 30, 1386-1890 (1995).

[69] H. Maiwa and N. Ichinose, "Electrical and electromechanical properties of $PbZrO_3$ thin films prepared by chemical solution deposition", *Jpn. J. Appl. Phys.* 40, 5507-5510 (2001).

[70] X. G. Tang, J. Wang, X. X. Wang and H. L. W. Chan, "Electrical properties of highly (111)-oriented lead zirconate thin films" *Solid State Comm.* 130, 373-377 (2004).

[71] L. B. Kong and J. Ma, "Preparation and characterization of antiferroelectric PLZT 2/95/5 thin films via a sol-gel process", *Mater. Lett.* 56, 30-37 (2002).

[72] B. M. Xu, Y. H. Ye, Q. M. Wang and L. E. Cross, "Dependence of electrical properties on film thickness in lanthanum-doped lead zirconate titanate stannate antiferroelectric thin films", *J. Appl. Phys.* 85 (7), 3753-3758 (1999).

[73] J. W. Zhai, Y. Yao. X. Li, T. F. Hung, Z. K. Xu, H. Chen, E. V. Colla and T. B. Wu, "Dielectric properties of oriented $PbZrO_3$ thin films grown by sol-gel process", *J. Appl. Phys.* 92 (7), 3990-3994 (2002).

[74] B. M. Xu, Y. H. Ye, Q. M. Wang, N. G. Pai and L. E. Cross, "Effect of compositional variations electrical properties in phase switching (Pb,La)(Zr,Ti,Sn)O_3 thin and thick films", *J. Mater. Sci.* 35, 6027-6033 (2000).

[75] B. M. Xu, L. E. Cross and D. Ravichandran, "Synthesis of lead zirconate titanate stannate antiferroelectric thick films by sol-gel processing", *J. Am. Ceram. Soc.* 82 (2), 306-312 (1999).

[76] B. M. Xu, L. E. Cross and J. J. Bernstein, "Ferroelectric and antiferroelectric films for microelectromechanical systems applications", *Thin Solid Films* 377-378, 712-718 (2000).

[77] J. W. Zhai and H. Chen, “Direct current field and temperature dependent behaviors of antiferroelectric to ferroelectric switching in highly (100)-oriented $PbZrO_3$ thin films”, *Appl. Phys. Lett.* 82 (16), 2673-2675 (2003).

[78] J. W. Zhai, X. Li, X. Yao and H. Chen, “Growth and characterization of PNZST thin films”, *Mater. Sci. Eng.* B 99, 230-233 (2003).

[79] W. G. Qu and X. L. Tan, “Texture control and ferroelectric properties of $Pb(Nb,Zr,Sn,Ti)O_3$ thin films prepared by chemical solution method”, *Thin Solid Films* 496, 383-388 (2006).

[80] X. H. Hao, J. W. Zhai and X. Yao, “Preparation of highly (111)-oriented $(Pb,La)(Zr,Sn,Ti)O_3$ (PLZST) antiferroelectric thin films by modified sol-gel process using a navel thin source, dibutyloxide of tin”, *J. Sol-Gel Sci. Techn.* 42, 365-368 (2007).

[81] X. Li, J. W. Zhai and H. Chen, “$(Pb,La)(Zr,Sn,Ti)O_3$ antiferroelectric thin films grown on $LaNiO_3$-buffered and Pt-buffered silicon substrates by sol-gel processing”, *J. Appl. Phys.* 97, 024102-1-7 (2005).

[82] C. K. Kwok and S. B. Desu, “Low temperature perovskite formation of lead zirconate titanate thin films by a seeding process”, *J. Mater. Res.* 8 (2), 339-344 (1993).

[83] H. Suzuki, T. Koizumi, Y. Kondo and S. Kaneko, “Low-temperature processing of $Pb(Zr_{0.53}Ti_{0.47})O_3$ thin films from stable precursor sol”, *J. Eur. Ceram. Soc.* 19, 1397-1401 (1999).

[84] Y. J. Song, Y. F. Zhu and S. B. Desu, “Low temperature fabrication and properties of sol-gel derived (111) oriented $Pb(Zr_{1-x}Ti_x)O_3$ thin films” *Appl. Phys. Lett.* 72 (21), 2686-2688 (1998).

[85] J. Perez, P. M. Vilarinho and A. L. Kholkin, “High-quality $PbZr_{0.52}Ti_{0.48}O_3$ films prepared by modified sol-gel route at low temperature”, *Thin Solid Films* 449, 20-24 (2004).

[86] X. H. Hao and J. W. Zhai, “Low-temperature growth of (110)-preferred $Pb_{0.97}La_{0.02}(Zr_{0.88}Sn_{0.10}Ti_{0.02})O_3$ antiferroelectric thin films on $LaNiO_3$/Si substrate”, *J. Cryst. Growth* 310, 1137-1141 (2008).

[87] X. H. Hao, J. W. Zhai and X. Yao, “Metal-organic chemical liquid deposited (110)-preferred $LaNiO_3$ buffer layer for $Pb_{0.97}La_{0.02}(Zr_{0.88}Sn_{0.10}Ti_{0.02})O_3$ antiferroelectric films”, *Ceram. Intern.* 34, 1007-1010 (2008).

[88] X. H. Hao, J. W. Zhai, X. J. Chou and X. Yao, “The electrical properties and phase transformation of PLZST 2/85/13/2 antiferroelectric thin films on different bottom electrode”,

Solid State Comm. 142, 498-503 (2007).

[89] E. M. Alkoy, S. Alkoy and T. Shiosaki, "Effects of Ce, Cr and Er doping and annealing conditions on the microstructure and electrical properties of $PbZrO_3$ thin films prepared by sol-gel process", *Jpn. J. Appl. Phys.* 44, 6654-6660 (2005).

[90] S. Chattopadhyay, P. Ayyub, V. R. Palkar, M. S. Multani, S. P. Pai, S. C. Purandare and R. Pinto, "Dielectric properties of oriented thin films of $PbZrO_3$ on Si produced by pulsed laser ablation", *J. Appl. Phys.* 83 (12), 7808-7812 (1998).

[91] I. W. Kim, D. S. Lee, S. H. Kang and C. W. Ahn, "Antiferroelectric characteristics and low frequency dielectric dispersion of $Pb_{1.075}La_{0.025}(Zr_{0.95}Ti_{0.05})O_3$ thin films", *Thin Solid Films* 441, 115-120 (2003).

[92] S. S. N. Bharaswaja and S. B. Krupanidhi, "Antiferroelectric lead zirconate thin films by pulsed laser ablation", *Mater. Sci. Eng. B* 64, 54-59 (1999).

[93] Y. B. Yao, J. W. Zhai and H. Chen, "Dielectric properties of lead lanthanum zirconate titanate antiferroelectric thin films prepared by pulsed laser deposition", *J. Appl. Phys.* 95 (11), 6341-6346 (2004).

[94] S. S. N. Bharaswaja and S. B. Krupanidhi, "Dielectric and dc electrical studies of antiferroelectric lead zirconate thin films", *Mater. Sci. Eng. B* 78, 1-10 (2000).

[95] S. S. N. Bharaswaja, A. Laha, S. Halder and S. B. Krupanidhi, "Reversible and irreversible switching processes in pure and lanthanum modified lead zirconate thin films", *Mater. Sci. Eng. B* 94, 218-222 (2002).

[96] Y. B. Yao, S. G. Lu, H. Chen, J. W. Zhai and K. H. Wong, "Role of oxygen pressure during pulsed laser deposition on the electrical and dielectric properties of antiferroelectric lanthanum-doped lead zirconate stannate titanate thin films", *J. Appl. Phys.* 96 (1), 569-574 (2004).

[97] J. Schwarzkopf and R. Fornari, "Epitaxial growth of ferroelectric oxide films", *Prog. Cryst. Growth Charact. Mater.* 52, 159-212 (2006).

[98] P. J. Kelly and R. D. Arnell, "Magnetron sputtering: a review of recent developments and applications", *Vacuum* 56, 159-172 (2000).

[99] I. Kanno, S. Hayashi, M. Kitagawa, R. Takayama and T. Hirao, "Antiferroelectric $PbZrO_3$ thin films prepared by multi-ion-beam sputtering", *Appl. Phys. Lett.* 66 (2), 145-147 (1995).

[100] K. Yamakawa, S. Trolier-Mckinstry, J. P. Dougherty and S. B. Krupanidhi, “Reactive magnetron co-sputtered antiferroelectric lead zirconate thin films”, *Appl. Phys. Lett.* 67 (14), 2014-2016 (1995).

[101] K. Yamakawa, K. W. Gachigi, S. Trolier-Mckinstry and J. P. Dougherty, “Structure and electrical properties of antiferroelectric lead zirconate thin films prepared by reactive magnetron co-sputtering”, *J. Mater. Sci.* 32, 5169-5176 (1997).

[102] Z. K. Xu and W. H. Chan, “Preparation and electrical properties of high (111) oriented antiferroelectric PLZST films by radio frequency magnetron sputtering”, *Acta Mater.* 55, 3923-3928 (2007).

[103] W. S. Kim, J. K. Yang and H. H. Park, “Influence of preferred orientation of lead zirconate titanate thin films on the ferroelectric properties”, *Appl. Surf. Sci.* 169-170, 549-552 (2001).

[104] T. Oikawa, M. Aratani, H. Funakubo, K. Saito and M. Mizuhira, “Composition and orientation dependence of electrical properties of epitaxial $Pb(Zr_xTi_{1-x})O_3$ thin films grown using metalorganic chemical vapor deposition”, *J. Appl. Phys.* 95, 3111-3115 (2004).

[105] R. Ramesh, T. Sands and V. G. Keramidas, “Effect of crystallographic orientation on ferroelectric properties of $PbZr_{0.2}Ti_{0.8}O_3$ thin films”, *Appl. Phys. Lett.* 63, 731-733 (1993).

[106] X. Y. Ding, B. Shen, J. W. Zhai, Z. K. Xu, F. Fu, J. J. Zhang and X. Yao, “Preparation and piezoelectric properties of (h00)-oriented $BaTiO_3$ ceramics by tap casting”, *Ferroelectrics* 401 (1), 30-35 (2010).

[107] E. M. Alkoy, S. Alkoy and T. Shiosaki, “Investigation of the electrical properties of [111] oriented $PbZrO_3$ thin films obtained by sol-gel process”, *Jpn J. Appl. Phys.* 45 (5), 4137-4142 (2006).

[108] T. Tani, J. F. Li, D. Viehland and D. A. Payne, “Antiferroelectric-ferroelectric switching and induced strains for sol-gel derived lead zirconate thin layers”, *J. Appl. Phys.* 75 (6), 3017-3023 (1994).

[109] X. H. Hao, J. W. Zhai, F. Shang, J. Zhou and S. L. An, “Orientation-dependent phase switching process and strains of $Pb_{0.97}La_{0.02}(Zr_{0.85}Sn_{0.13}Ti_{0.02})O_3$ antiferroelectric thin films”, *J. Appl. Phys.* 107, 116101-1-3 (2010).

[110] X. H. Hao, J. W. Zhai, J. C. Yang, H. P. Ren and X. W. Song, “Improved field-induced strains and fatigue endurance of PLZT antiferroelectric thick films by orientation control”, *Phys. Stat.*

Sol. RRL 3, 248-250 (2009).

[111] X. G. Tang, A. L. Ding and W. G. Luo, "Surface morphology and chemical states of highly oriented $PbZrO_3$ thin films prepared by a sol-gel process", *Appl. Surf. Sci.* 174, 148-154 (2001).

[112] X. H. Hao, J. W. Zhai, X. W. Song, J. C. Yang and H. P. Ren, "Fabrication and characterization of sol-gel derived (100)-textured $(Pb_{0.97}La_{0.02})(Zr_{0.95}Ti_{0.05})O_3$ thin films", *J. Am. Ceram. Soc.* 92 (2), 3081-3083 (2009).

[113] X. H. Hao, J. W. Zhai, F. Zhou, X. W. Song and S. L. An, "Thickness and frequency dependence of electric-field-induced stains of sol-gel derived $(Pb_{0.97}La_{0.02})(Zr_{0.95}Ti_{0.05})O_3$ antiferroelectric films", *J. Sol-Gel Sci. Techn.* 53, 366-371 (2010).

[114] E. M. Alkoy, S. Alkoy and T. Shiosaki, "Microstructure and crystallographic orientation dependence of electrical properties in lead zirconate thin films prepared by sol-gel process", *Jpn. J. Appl. Phys.* 44 (12), 8606-8612 (2005).

[115] X. H. Hao, J. W. Zhai and X. Yao, "Electrical properties of $Pb_{0.97}La_{0.02}(Zr_{0.95}Ti_{0.05})O_3$ antiferroelectric thin films on TiO_2 buffer layer", *Mater. Res. Bull.* 43, 1038-1045 (2008).

[116] X. H. Hao, J. W. Zhai and X. Yao, "A comprehensive investigation on the phase transformation behavior and electrical properties of $(Pb_{1-x}Ba_x)ZrO_3$ ($0 \leq x \leq 0.5$) thin films", *J. Appl. Phys.* 104, 124101-1-7 (2008).

[117] S. Y. Chen and I. W. Chen, "Temperature-time texture transition of $Pb(Zr_{1-x}Ti_x)O_3$ thin films: I, role of Pb-rich intermediate phase", *J. Am. Ceram. Soc.* 77 (9), 2332-2336 (1994).

[118] S. Y. Chen and I. W. Chen, "Temperature-time texture transition of $Pb(Zr_{1-x}Ti_x)O_3$ thin films: II, heat treatment and compositional effects", *J. Am. Ceram. Soc.* 77 (9), 2337-2344 (1994).

[119] M. Y. Liao, K. Nakajima, M. Imura and Y. Koide, "Improved ferroelectric properties of $Pb(Zr_{0.52},Ti_{0.48})O_3$ thin film on single crystal diamond using CaF_2 layer", *Appl. Phys. Lett.* 96, 012910-1-3 (2010).

[120] T. Oikawa, M. Aratani, H. Funakubo, K. Saito and M. Mizuhira, "Composition dependence of structural and optical properties of $Ba(Zr_x,Ti_{1-x})O_3$ thin films grown on MgO substrates by pulsed laser deposition" *Thin Solid Films* 519 (19), 6313-6318 (2011).

[121] S. N. Song, J. W. Zhai, L. N. Gao and X. Yao, "Orientation-dependent dielectric properties of $Ba(Sn_{0.15}Ti_{0.85})O_3$ thin films prepared by sol-gel method", *J. Phys. Chem. Solids* 70 (8), 1213-1217 (2009).

[122] S. Y. Wang, B. L. Cheng, Can Wang, S. Y. Dai, H. B. Lu, Y. L. Zhou, Z. H. Chen and G. Z. Yang, "Reduction of leakage current by Co doping in Pt/$Ba_{0.5}Sr_{0.5}TiO_3$/Nb-$SrTiO_3$ capacitor", *Appl. Phys. Lett.* 84, 4116-4118 (2004).

[123] J. Miao, J. Yuan, H. Wu, S. B. Yang, B. Xu, L. X. Cao and B. R. Zhao, "Crystal orientation dependence of the dielectric properties for epitaxial $BaZr_{0.15}Ti_{0.85}O_3$ thin films", *Appl. Phys. Lett.* 90, 022903-1-3 (2007).

[124] S. N. Song, J. W. Zhai and X. Yao, "Enhanced dielectric properties of LSCO-buffered $Ba(Sn_{0.05}Ti_{0.95})O_3$ thin films prepared by sol-gel processing", *J. Sol-Gel Sci. Techn.* 44, 75-79 (2007).

[125] J. W. Zhai, X. Yao, L. Y. Zhang, B. Shen and H. Chen, "Orientation control and dielectric properties of sol-gel deposited $Ba(Ti,Zr)O_3$ thin films", *J. Cryst. Growth* 262, 341-347 (2004).

[126] L. J. Wu and J. M. Wu, "Thickness-dependent dielectric properties of nanoscale Pt/$(Pb,Ba)ZrO_3$/$BaPbO_3$ capacitors", *J. Cryst. Growth* 308, 424-429 (2007).

[127] F. Chen, Q. Z. Liu, H. F. Wang, F. H. Zhang and W. B. Wu, "Polarization switching and fatigue in $Pb(Zr_{0.52}Ti_{0.48})O_3$ films sandwiched by oxide electrodes with different carrier types", *Appl. Phys. Lett.* 90, 192907-1-3 (2007).

[128] L. N. Gao, J. W. Zhai, S. N. Song, X. H. Hao and X. Yao, "Effects of CeO_2 buffer layer thickness on the orientation and dielectric properties of $Ba(Zr_{0.20}Ti_{0.80})O_3$ thin films", *J. Cryst. Growth* 311, 299-303 (2009).

[129] W. Gong, J. F. Li, X. C. Chu, Z. L. Gui and L. T. Li, "Preparation and characterization of sol-gel derived (100)-textured $Pb(Zr,Ti)O_3$ thin films: PbO seeding role in the formation of preferential orientation", *Acta Mater.* 52 (9), 2787-2793 (2004).

[130] Z. Chen, C. T. Yang, B. Li and B. C. Yang, "Investigation on the effects of PbO content and seeding layer of TiO_2 and ZrO_2 on the orientation and microstructure of $Pb(Zr_{0.52}Ti_{0.84})O_3$ ferroelectric films grown by reverse dip-coating method of sol-gel", *Mater. Lett.* 60, 1559-1564 (2006).

[131] S. Bhaskar, S. B. Majumder, P. S. Dobal, S. B. Krupanidhi and R. S. Katiyar, "Dielectric and ferroelectric response of sol-gel derived $Pb_{0.85}La_{0.15}TiO_3$ ferroelectric thin films on different bottom electrodes", *Thin Solid Films* 406, 30-39 (2002).

[132] G. R. Bai, H. L. M. Chang, D. J. Lam and Y. Gao, "Preparation and structure of $PbZrO_3$ epitaxial films by metalorganic chemical vapor deposition", *Appl. Phys. Lett.* 62, 1754-1756 (1993).

[133] J. W. Zhai Jiwei, M. H. Cheung, Z. K. Xu, X. Li, H. Chen, E. V. Colla and T. B. Wu, "Dielectric and ferroelectric properties of highly orientated $(Pb,Nb)(Zr,Sn,Ti)O_3$ thin films grown by a sol-gel process", *Appl. Phys. Lett.* 81 (19), 3621-3623 (2002).

[134] J. W. Zhai, H. Chen, E. V. Colla and T. B. Wu, "Direct current field adjustable ferroelectric behavior in $(Pb,Nb)(Zr,Sn,Ti)O_3$ antiferroelectric thin films", *J. Phys: Condens. Matt.* 15, 963-969 (2003).

[135] N. Wakiya, T. Azuma, K. Shinozaki and N. Mizutani, "Low-temperature epitaxial growth of conductive $LaNiO_3$ thin films by RF magnetron sputtering", *Thin Solid Films* 410, 114-120 (2002).

[136] D. H. Bao, X. Yao, N. Wakiya, K. Shiozaki and N. Mizutani, "Preparation of conductive $LaNiO_3$ films electrodes by a simple chemical solution deposition technique for integrated ferroelectric thin films", *J. Phys. D: Appl. Phys.* 36, 1217-1221 (2003).

[137] G. S. Wang, Q. Zhao, X. J. Meng, J. H. Chu and D. Remiens, "Preparation of highly (100)-oriented $LaNiO_3$ nanocrystalline films by metalorganic chemical liquid deposition", *J. Cryst. Growth* 277, 450456 (2005).

[138] X. H. Hao, J. W. Zhai, J. B. Xu and X. Yao, "Preparation of PLZT antiferroelectric thin films on ZrO_2 buffered substrates", *Ferroelctrics* 357, 253-258 (2007).

[139] K. H. Yoon, S. C. Hwang and D. H. Kang, "Dielectric and field-induced strain behaviour of $(Pb_{1-x}Ba_x)ZrO_3$ ceramics", *J. Mater. Sci.* 32, 17-21 (1997).

[140] V. M. Ishchuk, S. V. Matveev and V. L. Sobolev, "Two-phase (ferroelectric and antiferroelectric) nuclei and diffuse phase transition in the vicinity of the ferroelectric - antiferroelectric - paraelectric triple point", *Appl. Phys. Lett.* 79, 2949-2951 (2001).

[141] P. Liu and X. Yao, "Dielectric properties and phase transitions of $(Pb_{0.87}La_{0.02}Ba_{0.1})(Zr_{0.6}Sn_{0.4-x}Ti_x)O_3$ ceramics with compositions near AFE/RFE phase boundary", *Solid State Comm.* 132, 809-813 (2004).

[142] M. J. Haun, T. J. Harvin, M. T. Lanagan, Z. Q. Zhuang, S. J. Jang and L. E. Cross, "Thermodynamic theory of $PbZrO_3$", *J. Appl. Phys.* 65, 3173-3180 (1989).

[143] D. Forst, J. F. Li and Z. K. Xu, "Incommensurately modulated polar structures in antiferroelectric tin-modified lead zirconate titanate: II, dependence of structure-properties relations on tin content", *J. Am. Ceram. Soc.* 81, 2225-2236 (1998).

[144] Z. H. Dai, Z. Xu and X. Yao, "Effect of dc bias on pressure-induced depolarization of Pb(Nb,Zr,Sn,Ti)O_3 ceramics", *Appl. Phys. Lett.* 92, 072904-1-3 (2008).

[145] P. Yang and D. A. Payne, "Thermal stability of field-forced and field-assisted antiferroelectric-ferroelectric phase transitions in Pb(Zr,Sn,Ti)O_3", *J. Appl. Phys.* 71, 1361-1367 (1992).

[146] P. Yang and D. A. Payne, "The effect of external field symmetry on the antiferroelectric-ferroelectric phase transformation", *J Appl. Phys.* 80, 4001-4005 (1996).

[147] L. E. Cross and R. E. Newnham, "History of ferroelectrics", *High-Technology Ceramics-Past, Present, and Future* Volume III, 289-305 (1987).

[148] A. F. Devonshire, "XCVI. Theory of barium titanate", *Philos. Mag.* 40, 1040-1050 (1949).

[149] A. F. Devonshire, "Theory of ferroelectrics", *Adv. Phys.* 3, 85-130 (1954).

[150] R. W. Whatmore and A. M. Glazer, "Structure phase transitions in lead zirconate", *J. Phys. C: Solid State Phys.* 12, 1505-1519 (1979).

[151] K. Uchino, L. E. Cross, R. E. Newnham and S. Nomura, "Electrostrictive effects in antiferroelectric perovskites", *J. Appl. Phys.* 52, 1455-1459 (1981).

[152] C. V. Raman and T. M. K. Nedungadi, "The α-β transformation of quartz", ***Nature*** 145, 147-147 (1940).

[153] W Cochran, "Crystal stability and the theory of ferroelectricity", *Phys. Rev. Lett.* 3, 412-414 (1959).

[154] P. W. Anderson, "Ording and antiferromagnetism in ferrites", *Phys. Rev.* 102, 1008-1013 (1956).

[155] A. S. Baker, Jr. and M. Tinkham, "Far-infrared ferroelectric vibration mode in $SrTiO_3$", *Phys. Rev*. 125, 1527-1530 (1962).

[156] R. A. Cowley, "Lattice dynamics and phase transitions of strontium titanate", *Phys. Rev.* 134 (4A), A981-A997 (1964).

[157] G. A. Samara, T. Sakudo and K. Yoshimitsu, "Important generalization concerning the role of competing forces in displacive phase transitions ", *Phys. Rev. Lett.* 35, 1767-1769 (1975).

[158] R. Blinc, “The soft mode concept and the history of ferroelectricity”, *Ferroelectric* 74, 301-303 (1987).

[159] W Cochran, “Crystal stability and the theory of ferroelectricity”, *Adv. Phys.* 9, 387-423 (1960).

[160] A. W. Hewat, “Soft modes and structure, spontaneous polarization and Curie constant of perovskite ferroelectrics: tetragonal potassium niobate”, *J. Phys. C: Solid State Phys.* 6, 1074-1084 (1973).

[161] M. J. Pan, K. A. Markowski, S. E. Park, S. Yoshikawa and L. E. Cross, “Antiferroelectric-to-ferroelectric phase switching PLSnZT ceramics. I. Structure, compositional modification and electrical properties”, *Appl. Ferroelectrics, 1996. ISAF'96., Proc. Tenth IEEE Intern.Symp.* 1, 267-270 (1996).

[162] P. Baettig, C. F. Schelle, R. Lesar, U. V. Waghare and N. A. Spaldin, “Theoretical prediction of new high-performance lead-free piezoelectric”, *Chem. Mater.* 17 (6), 1376-1380 (2005).

[163] V. J. Tennery, “Hight-temperature phase transitions in $PbZrO_3$”, *J. Am. Ceram. Soc.* 49, 483-486 (1966).

[164] B. A. Scott and G. Burns, “Crystal growth and observation of the ferroelectric phase of $PbZrO_3$”, *J. Am. Ceram. Soc.* 55, 331-333 (1972).

[165] Z. Ujma and J. Handerdk, “Phase transitions and spontaneous polarization in $PbZrO_3$”, *Phys. Stat. Sol. (a)* 28, 489-496 (1975).

[166] G. A. Samara, “Pressure and temperature dependence of the dielectric properties and phase transitions of the antiferroelectric perovskites: $PbZrO_3$ and $PbHfO_3$”, *Phys. Rev. B* 1, 3777-3786 (1970).

[167] O. E. Fesenko, R. V. Kolesova and Y. G. Sindeev, “The structural phase transitions in lead zirconate in superhigh electric fields”, *Ferroelectrics* 20, 177-178 (1978).

[168] B. P. Pokharel and D. Pandey, “Dielectric studies of phase transitions in $(Pb_{1-x}Ba_x)ZrO_3$”, *J. Appl. Phys.* 88, 5364-5373 (2000).

[169] X. H. Hao and J. W. Zhai, “Dielectric properties of $Pb_{1-x}Ba_xZrO_3$ thin films with higher barium content”, *Key Eng. Mater.* 421-422, 119-122 (2010).

[170] X. H. Hao, J. W. Zhai, J. Zhou, Z. X. Yue, J. C. Yang, W. G. Zhao and S. L. An, "Structure and electrical properties of $PbZrO_3$ antiferroelectric thin films doped with barium and strontium”, *J. Alloys Comp.* 509, 271-275 (2011).

[171] G. H. Haertling and C. E. Land, "Hot-pressed (Pb,La)(Zr,Ti)O_3 ferroelectric ceramics for electrooptic applications", *J. Am. Ceram. Soc.* 54, 1-11 (1971).

[172] S. S. N. Bharadwaja and S. B. Krupanidhi, "Study of La-modified antiferroelectric $PbZrO_3$ thin films", *Thin Solid Films* 423, 88-96 (2003).

[173] S. S. N. Bharadwaja, S. Saha, S. Bhattacharyya and S. B. Krupanidhi, "Dielectric properties of La-modified antiferroelectric $PbZrO_3$ thin films", *Mater. Sci. Eng. B* 88, 22-25 (2002).

[174] J. Parui and S. B. Krupanidhi, "Effect of La modification on antiferroelectric and dielectric phase transition in sol-gel grown $PbZrO_3$ thin films", *Solid State Comm.* 150, 1755-1759 (2010).

[175] J. Handerek and Z. Ujma, "Phase transitions in PZT-95/5 ceramics studied by dielectric and pyroelectric measurements: unusual properties in vicinity of the antiferroelectric-ferroelectric phase transition", *J. Phys.: Condense Matt.* 7, 1721-1728 (1995).

[176]B. A. Tuttle, J. E. Smay, J. Ceasarano III, J. A. Voigt, T. W. Scofied, W. R. Olson and J. A. Lewis, "Robocast $Pb(Zr_{0.95}Ti_{0.05})O_3$ ceramics monoliths and composites", *J. Am. Ceram. Soc.* 84 (4), 872-874 (2001).

[177] P. C. Lysne and C. M. Percival, "Electric energy generation by shock compression of ferroelectric ceramics: normal-mode response of PZT 95/5", *J. Appl. Phys.* 46, 1519-1525 (1975).

[178] W. Mock, Jr. and W. H. Holt, "Pulse charging of nanofarad capacitors from the shock depoling of PZT 56/66 and PZT 95/5 ferroelectric ceramics", *J. Appl. Phys.* 49, 5846-5854 (1978).

[179] B. A. Tuttle, P. Yang, J. H. Gieske, J. A. Voigt, T. W. Scofield, D. H. Zeuch and W. R. Olson, "Pressure-induced phase transition of controlled-porosity $Pb(Zr_{0.95}Ti_{0.05})O_3$ ceramics", *J. Am. Ceram. Soc.* 84 (6), 1260-1264 (2001).

[180] D. A. Hall, J. D. S. Evans, S. J. Covey-Crump, R. F. Holloway, E. C. Oliver, T. Mori and P. J. Withers, "Effects of superimposed electric field and porosity on the hydrostatic pressure-induced rhombohedral to orthorhombic martensitic phase transformation in PLZ 95/5 ceramics", *Acta Mater.* 58, 6584-6591 (2010).

[181] T. Zeng, X. L. Dong, C. L. Mao, Z. Y. Zhou and H. Yang, "Effects of pore shape and porosity on the properties of porous PZT 95/5 ceramics", *J. Eur. Ceram. Soc.* 27, 2025-2029 (2007).

[182] T. Zeng. X. L. Dong, H. L. He, X. F. Chen and C. H. Yao, "Pressure-induced ferroelectric to antiferroelectric phase transformation in porous PZT 95/5 ceramics", *Phys. Stat. Sol. (a)* 204,

1216-1220 (2007).

[183] Z. Ujma, J. Handerek, M. Pawalczyk, H. Hassan, G. E. Kugel and C. Carabatos-Nedelec, "The antiferroelectric-ferroelectric-paraelectric phase sequence in lead-lanthanum zirconate-titanate ceramics with 8% Ti content", *J. Phys.: Condens. Matt.* 6, 6843-6856 (1994).

[184] Z. Ujma, J. Handerek, H. Hassan, G. E. Kugel and M. Pawalczyk, "Phase transitions in lead-lanthanum zirconate-titanate ceramics with Zr/Ti ratio of 92/8 and a La content of up to 1 at.%", *J. Phys.: Condens. Matt.* 7, 895-906 (1995).

[185] Z. Xu, X. Dai, J. F. Li and D. Viehland, "Coexistence of incommensurate antiferroelectric and relaxorlike ferroelectric orderings in high Zr-content La-modified lead zirconate titanate ceramics", *Appl. Phys. Lett.* 68, 1628-1630 (1996).

[186] A. Pelaiz-Barranco and D. A. Hall, "Influence of composition and pressure on the electric field-induced antiferroelectric to ferroelectric phase transition in lanthanum modified lead zirconate titanate ceramics", *IEEE Tran. Uleras. Ferroelect. Freq. Contr*. 56, 1785-1791 (2009).

[187] X. Dai and D. Vihland, "Effects of lanthanum modification on the antiferroelectric-ferroelectric stability of high zirconate-content lead zirconate titanate", *J. Appl. Phys.* 76 (6), 3701-3709 (1994).

[188] Z. Xu, X. Dai and D. Vihland, Impurity-induced incommensuration in antiferroelectric La-modified lead zirconate titanate", *Phys. Rev. B* 51 (1), 6261-6271 (1995).

[189] D. Viehland, X. H. Dai, J. F. Li and Z. Xu, "Effects of quenched disorder on La-modified zirconate titanate: long- and short-range ordered structurally incommensurate phases, and glassy polar clusters", *J. Appl. Phys.* 84 (1), 458-471 (1998).

[190] W. Y. Pan, Q. M. Zhang, A. Bhalla and L. E. Cross, "Field-forced antiferroelectric-to-ferroelectric switching in modified lead zirconate titanate stannate ceramics", *J. Am. Ceram. Soc.* 72 (4), 571-578 (1989).

[191] W. H. Chan, Z. K. Xu, J. W. Zhai, E. V. Colla and H. Chen, "Phase stability and pyroelectricity of antiferroelectric PLZST oxide", *J. Electroceram.* 21, 145-148 (2008).

[192] T. Q. Yang, X. Yao and L. Y. Zhang, "Effects of compositional variations on antiferroelectric-ferroelectric phase transition of PLZST ceramics", *J. Inorg. Mater*. (in Chinese) 15 (5), 807-814 (2000).

[193] T. Q. Yang, P. Liu, Y. L. Zhang and X. Yao, "Dielectric properties of PZST antiferroelectric ceramics", *Piezoelect. Acoustoopt.* (in Chinese) 22, 299-301 (2000).

[194] L. Wang, Q. Li, L. H. Xue and Y. L. Zhang, "Effect of Zr:Ti ratio in the lead lanthanum zirconate stannate titanate ceramics on the microstructure and electric properties", *J. Phys. Chem. Solids* 68, 2008-2013 (2007).

[195] L. Wang, Q. Li, L. H. Xue and X. M. Liang, "Effect of Ti^{4+}:Sn^{4+} ratio on the phase transition and electric properties of PLZST antiferroelectric ceramics", *J. Mater. Sci.* 42, 7397-7401 (2007).

[196] X. H. Hao and J. W. Zhai, "Composition-dependent electrical properties of (Pb,La)(Zr,Sn,Ti)O_3 antiferroelectric thin films grown on platinum-buffered silicon substrates", *J. Phys. D: Appl. Phys.*, 40, 7447-7453 (2007).

[197] Y. Akiyama and E. Fujisawa, "Field-induced antiferroelectric-to-ferroelectric phase transition of lead niobium zirconate titanate stannate ceramics", *Jpn. J. Appl. Phys.* 36, 5997-6000 (1997).

[198] Y. J. Feng, Z. Xu and X. Yao, "Effect of Sn doping on the phase transition behaviors of antiferroelectric lead zirconate titanate", *Mater. Sci. Eng. B* 99, 499-501 (2003).

[199] J. Frederick and X. L. Tan, "Strains and polarization during antiferroelectric-ferroelectric phase switching in $Pb_{0.99}Nb_{0.02}[(Zr_{0.57}Sn_{0.43})_{1-y}Ti_7]_{0.98}O_3$ ceramics", *J. Am. Ceram. Soc.* 94 (4), 1149-1155 (2011).

[200] Z. H. Dai, X. Yao, Z. Xu, Y. J. Feng and J. Wang, "Phase transition and dielectric properties of PbLa(Zr,Sn,Ti)O_3 antiferroelectric ceramics under hydrostatic pressure", *J. Electroceram.* 21, 596-600 (2008).

[201] D. H. Bao, R. Scholz, Z. Alexe and D. Hesse, "Growth, microstructure, and ferroelectric of $Pb(Zr_{0.04}Ti_{0.60})O_3/PbZrO_3$ superlattices prepared on $SrTiO_3$(100) substrates by pulsed laser deposition", *J. Appl. Phys.* 101, 054118-1-7 (2007).

[202] T. Harigai, S. M. Nam, H. Kakemoto, S. Wada, K. Saito and T. Tsurumi, "Structure and dielectric properties of perovskite-type artificial superlattices", *Thin Solid Films* 509, 13-17 (2006).

[203] I. Kanno, S. Hayashi, R. Takayama and T. Hirao, "Superlattices of $PbZrO_3$ and $PbTiO_3$ prepared by multi-ion-beam sputtering", *Appl. Phys. Lett.* 68, 328-330 (1996).

[204] T. Choi and J. Lee, "Enhancement of dielectric and ferroelectric properties of $PbZrO_3/PbTiO_3$ artificial supperlattices", *J. Kor. Phys. Soc.* 46, 116-119 (2005).

[205] L. Pintilie, K. Boldyreva, M. Alexe and D. Hesse, "Capacitance tuning in antiferroelectric-ferroelectric $PbZrO_3$-$Pb(Zr_{0.8}Ti_{0.2})O_3$ epitaxial multilayers", *New J. Phys.* 10, 013003-1-12 (2008).

[206] C. L. Hung, Y. L. Chueh, T. B. Wu and L. J. Chou, "Characteristics of constrained ferroelectric in $PbZrO_3$/$BaZrO_3$ superlattice films", *J. Appl. Phys.* 97, 034105-1-6 (2005).

[207] I. Burn and D.M. Smyth, "Energy storage in ceramic dielectrics", *J. Mater. Sci.* 7, 339-343 (1972).

[208] J. Parui and S. B. Krupanidhi, "Enhancement of charge and energy storage in sol-gel pure and La-modified $PbZrO_3$ thin films", *Appl. Phys. Lett.* 92, 192901-1-3 (2008).

[209] X. H. Hao, J. Zhou and S. L. An, "Effects of PbO content on the dielectric properties and energy storage performance of $(Pb_{0.97}La_{0.02})(Zr_{0.97}Ti_{0.03})O_3$ antiferroelectric thin films", *J. Am. Ceram. Soc.* 94, 1647-1650 (2011).

[210] B. H. Ma, D. K. Kwon, M. Narayanan and U. Balachandran, "Fabrication of antiferroelectric PLZT films on metal foils", *Mater. Res. Bull.* 44, 11-14 (2009).

[211] B. H. Ma, D. K. Kwon, M. Narayanan and U. Balachandran, "Dielectric properties and energy storage capability of antiferroelectric $Pb_{0.92}La_{0.08}Zr_{0.95}Ti_{0.05}O_3$ film-on-foil capacitors", *J. Mater. Res.* 24, 2993-2996 (2009).

[212] M. S. Mirshekarloo, Kui Yao and T. Sritharan, "Large strain and high storage density in orthorhombic perovskite $(Pb_{0.97}La_{0.02})(Zr_{1-x-y}Sn_xTi_y)O_3$ antiferroelectric thin films", *Appl. Phys. Lett.* 97, 142902-1-3 (2010).

[213] X. H. Hao, Y. Wang, L. Zhang, L. W. Zhang and S. L. An, "Composition-dependent dielectric and energy-storage properties in $(Pb,La)(Zr,Sn,Ti)O_3$ antiferroelectric thick films", *Appl. Phys. Lett.* 102, 163903-1-4 (2013).

[214] H. L. Zhang, X. F. Chen, F. Cao, G. H. Wang and X. L. Dong, "Charge-discharge properties of an antiferroelectric ceramics capacitor under different electric fields", *J. Am. Ceram. Soc.* 93, 4015-4017 (2010).

[215] S. S. N. Bharadwaja and S. B. Krupanidhi, "Backward switching phenomenon form field forced ferroelectric to antiferroelectric phases in antiferroelectric $PbZrO_3$ thin films", *J. Appl. Phys.* 89, 4541-4547 (2001).

[216] B. M. Xu, P. Moses, N. G. Pai and L. E. Cross, "Charge release of lanthanum-doped zirconate

titanate stannate antiferroelectric thin films", Appl. Phys. Lett. 72, 593-595 (1998).

[217] K. G. Brooks, J. Chen, K. R. Udayakumar and L. E. Cross, "Electric field forced phase switching in La-modified lead zirconate titanate stannate thin films", *J. Appl. Phys.* 75 (3), 1699-1704 (1994).

[218] S. S. Sengupta, D. Roberts and J. F. Li, "Field-induced phase switching and electrical deiven strains in sol-gel derived antiferroelectric (Pb,Nb)(Zr,Sn,Ti)O_3 thin films", *J. Appl. Phys.* 78 (2), 1171-1177 (1995).

[219] M. J. Pan, S. E. Park, K. A. Markowski, S. Yoshikawa and L. E. Cross, "Antiferroelectric-to-ferroelectric phase switching PLSnZT ceramics II. The effect of pre-stress conditions on the strain behavior", *Appl. Ferroelect., 1996. ISAF'96, Proc. Tenth IEEE Intern. Symp.* 2, 759-762 (1996).

[220] O. Essig, P. Wang, M. Hartweg, P. Janker, H. Nafe and F. Aldinger, "Uniaxial stress and temperature dependence of field induced strains in aftiferroelectric lead zirconate titanate stannate ceramics", *J. Eur. Ceram. Soc.* 19, 1223-1228 (1999).

[221] Q. F. Zhang, S. L. Jiang, Y. K. Zeng, M. Y. Fan, G. Z. Zhang, Y. Y. Zhang, Y. Yu, J. Wang and J. G. He, "Large electric-induced pyroelectric properties in $(Pb_{0.87}La_{0.02}Ba_{0.1})(Zr_{0.7}Sn_{0.24}Ti_{0.06})O_3$ antiferroelectric ceramics with excess PbO", *J. Appl. Phys.* 109, 124111-1-6 (2011).

[222] R. L. Byer and C. B. Roundy, "Pyroelectric coefficient direct measurement technique and application to a nsec response time detector", *Ferroelectrics* 3, 333-338 (1972).

[223] R. W. Whatmore, "Pyroelectric devices and materials", Rep. Prog. Phys. 49, 1335-1386 (1986).

[224] A. Sharma, Z. G. Ban, S. P. Alpay and J. V. Mantese, "Pyroelectric response of ferroelectric thin films", *J. Appl. Phys.* 95, 3618-3625 (2004).

[225] Y. X. Tang, X. Y. Zhao, X. Q. Feng, W. Q. Jin and H. S. Luo, "Pyroelectric properties of [111]-oriented $Pb(Mg_{1/3}Nb_{2/3})O_3$-$PbTiO_3$ crystal", *Appl. Phys. Lett.* 86, 082901-1-3 (2005).

[226] C. Bjormander, K. Sreenivas, A. M. Grishin and K. V. Rao, "Pyroelectric $PbSc_{0.5}Ta_{0.5}O_3/Y_1Ba_2Cu_3O_{7-x}$ thin-films heterostructures", *Appl. Phys. Lett.* 67, 58-60 (1995).

[227] Z. Ujma and J. Handerek, "The pyroelectric effect in single crystal and ceramic $PbZrO_3$", *Ferroelectrics* 33, 37-42 (1981).

[228] J. Handerek and Z. Ujma, "Phase transitions in PZT-95/5 ceramics studied by dielectric and pyroelectric measurements: unusual properties in the vicinity of the

antiferroelectric-ferroelectric phase transitions", *J. Phys.: Condens. Matt.* 7, 1721-1728 (1995).

[229] Z. Ujma, L. Szymczak, J. Handerek, K. Szot and H. J. Penkalla, "Dielectric and pyroelectric properties of Nb-doped $Pb(Zr_{0.92}Ti_{0.08})O_3$ ceramics", *J. Eur. Ceram. Soc.* 20, 1003-1010 (2000).

[230] T. Q. Yang, P. Liu, Z. Xu, L. Y. Zhang and X. Yao, "Tunable pyroelectricity in La-modified PZST antiferroelectric ceramics", *Ferroelectrics* 230, 181-186 (1999).

[231] Z. K. Xu, J. W. Zhai, W. H. Chan and H. Chen, "Phase transformation and electric field tunable pyroelectric behavior of $Pb(Nb,Zr,Sn,Ti)O_3$ and $(Pb,La)(Zr,Sn,Ti)O_3$ antiferroelectric thin films", *Appl. Phys. Lett.* 88, 132908-1-3 (2006).

[232] Q. F. Zhang, S. L. Jiang, Y. K. Zeng, M. Y. Fan, Q. P. Wang, G. Z. Zhang, Y. Y. Zhang, Y. Yu and J. Wang, "Large pyroelectric response in $(Pb_{0.87}La_{0.02}Ba_{0.1})(Zr_{0.7}Sn_{0.3-x}Ti_x)O_3$ antiferroelectric ceramics under DC bias field", *Appl. Phys. A* 103, 1159-1163 (2011).

[234] H. L. Zhang, X. F. Chen, F. Cao, G. S. Wang, X. L. Dong, Y. Gu and Y. S. Liu, "Reversible pyroelectric response in $Pb_{0.955}La_{0.03}(Zr_{0.42}Sn_{0.40}Ti_{0.18})O_3$ ceramics near its phase transition", *Appl. Phys. Lett.* 94, 252902-1-3 (2009).

[235] Y. Sungtaek Ju, "Solid-state refrigeration based on the electrocaloric effect for electrics cooling", *J. Electron. Pack.* 132, 041004-1-6 (2010).

[236] J. F. Scott, "Electrocaloric materials", *Annu. Rev. Mater. Res.* 41, 1-12 (2011).

[237] M. Valant, "Electrocaloric materials for further solid-state refrigeration technologies", *Prog. Mater. Sci.* 57, 980-1009 (2012).

[238] X. Y. Li, S.-G. Lu, X.-Z.Chen, H. M. Gu, X.-S. Qian and Q. M. Zhang, "Pyroelectric and electrocaloric materials", *J. Mater. Chem. C* 1, 22-37 (2013).

[239] P. D. Thacher, "Electrocaloric effects in some ferroelectric and antiferroelectric $Pb(Zr,Ti)O_3$ compounds", *J. Appl. Phys.* 39, 1996-2002 (1968).

[240] B. A. Tuttle and D. A. Payne, "The effects of microstructure on the electrocaloric properties of $Pb(Zr,Sn,Ti)O_3$ ceramics", *Ferroelectrics* 37, 603-606 (1981).

[241] A. S. Mischenko, Q. Zhang, J. F. Scott, R. W. Whatmore and N. D. Mathur, "Giant electrocaloric effect in thin-film $PbZr_{0.95}Ti_{0.05}O_3$", *Science* 311, 1270-1271 (2006).

[242] J. Parui and S. B. Krupanidhi, "Electroaloric effect in antiferroelectric $PbZrO_3$ thin films", *Phys. Stat. Sol. RRL* 2, 230-232 (2008).

[243] X. H. Hao, Z. X. Yue, J. B. Xu, S. L. An and C.-W. Nan, "Energy storage performance and

electrocaloric effect in (100)-preferred $Pb_{0.97}La_{0.02}(Zr_{0.95}Ti_{0.05})O_3$ antiferroelectric thick films", *J. Appl. Phys.* 110, 064109-1-5 (2011).

[244] B. L. Peng, H. Q. Fan and Q. Zhang, "A giant electrocaloric effect in nanoscale antiferroelectric and ferroelectric phase coexisting in relaxor $Pb_{0.8}Ba_{0.2}ZrO_3$ thin films at room temperature", *Adv. Funct. Mater*. 23, 2987-2992 (2013).

[245] J. H. Jang and K. H. Yoon, "Effect of antiferroelectric buffer on electric fatigue and leakage in ferroelectric Pb(Zr,Sn,Ti)NbO_3 thin films", *Thin Solid Films* 401, 67-72 (2001).

[246] L. J. Zhou, G. Rixecker, A. Zimmermann and F. Aldinger, "Electric fatigue in antiferroelectric $Pb_{0.97}La_{0.02}(Zr_{0.55}Sn_{0.33}Ti_{0.12})O_3$ ceramics induced by bipolar cycling", *J. Eur. Ceram. Soc*. 26, 883-889 (2006).

[247] X. J. Lou and J. Wang, "Unipolar and bipolar fatigue in antiferroelectric lead zirconate thin films and evidences for switching-induced charge injection inducing fatigue", *Appl. Phys. Lett.* 96, 102906-1-3 (2010).

[248] X. J. Lou, "Polarization fatigue in ferroelectric thin films and related materials", *J. Appl. Phys.* 105, 024101-1-24 (2009).

[249] J. H. Jang and K. H. Yoon, "Electric fatigue in sol-gel prepared Pb(Zr,Sn,Ti)NbO_3 thin films", *Appl. Phys. Lett.* 73, 1823-1825 (1998).

[250] X. J. Lou, "Why do antiferroelectrics show higher fatigue resistance than ferroelectrics under bipolar electric cycling?", *Appl. Phys. Lett.* 94, 072901-1-3 (2009).

[251] Y. Wang, K. F. Wang, C. Zhu, T. Wei, J. S Zhu and J. M. Liu, "Fatigue suppression of ferroelectric $Pb_{1-x}Ba_x(Zr_{0.52}Ti_{0.48})O_3$ thin films prepared by sol-gel", *J. Appl. Phys.* 101, 046104-1-3 (2007).

[252] Y. Wang, Q. Y. Shao and J. M Liu, "Enhanced fatigue-endurance of ferroelectric $Pb_{1-x}Sr_x(Zr_{0.52}Ti_{0.48})O_3$ thin films prepared by sol-gel method", *Appl. Phys. Lett.* 88, 122902-1-3 (2006).

[253] J. W. Zhai and H. Chen, "Electric fatigue in Pb(Nb,Zr,Sn,Ti)O_3 thin films grown by a sol-gel process", *Appl. Phys. Lett.* 83, 978-980 (2003).

Figure and Table Captions

Elsevier.

Fig. 18. Diagram of preparation of PLZST AFE thick films by chemical solution deposition method. Reproduced with permission from [74], Copyright 2000, Springer.

Fig. 19. SEM images of the PNZST thick films with 30 layers of PNZST spin coating (a) without PbO cover layer, (b) with a PbO cover layer every 6 layers of PNZST spin coating. Reproduced with permission from [75], Copyright 1999, John Wiley & Sons.

Fig. 20. Schematic diagram of a standard pulsed laser deposition system. Reproduced with permission from [57], Copyright 2010, Elsevier.

Fig. 21. (a) Effect of oxygen partial pressure on in-situ crystallization of the PZ films. The substrate temperature was 550^{o}C. (b) Effect of substrate temperature on crystallization of the PZ films. The oxygen partial pressure during deposition was 50 mTorr. (c) Effect of post-deposition annealing temperature on crystallization of the PZ films. The films were deposited at 300^{o}C with an oxygen partial pressure of 50 mTorr. Reproduced with permission from [94], Copyright 2000, Elsevier.

Fig. 22. Schematic structures of the PZT films and substrate with (a) (111) and (b) (100) texture. Reproduced with permission from [117], Copyright 1994, John Wiley & Sons.

Fig. 23. Free energies of PE, FE and AFE in AFEs with orthorhombic structure (a) and tetragonal structure (b).

Fig. 24. E-T phase diagram and exemplary isothermal dependence of polarization on the electric field. In the phase-stability regions of the diagram, the directions of anti-polarization, polarization and applied fields are indicated by referring to a formula unit cell.

Fig. 25. Thickness dependence of AFE-FE phase switching fields of the PZ films (a) and temperature-dependent dielectric constant at various DC bias fields for the 900 nm thin films at 100 kHz (b). Reproduced with permission from [77], Copyright 2003, American Institute of Physics.

Fig. 26. P-E hysteresis loops of the 900-nm $PbZrO_3$ thin films measured at different temperatures and 1 kHz. Reproduced with permission from [77], Copyright 2003, American Institute of Physics.

Fig. 27. Phase diagram of the $(Pb_{1-x}Ba_x)ZrO_3$ system. Reproduced with permission from [168], Copyright 2000, American Institute of Physics.

Fig. 28. P-E loops of the $(Pb_{1-x}Ba_x)ZrO_3$ films with x=0, 0.05, 0.10, 0.20, 0.40 and 0.50. Reproduced with permission from [116], Copyright 2008, American Institute of Physics.

Fig. 29. Phase diagram of the $(Pb,Sr)ZrO_3$ system. Reproduced with permission from [18], Copyright 1952, American Physical Society.

Fig. 30. Room temperature phase diagram of PLZT solution.

Fig. 31. Phase diagrams of $(Pb_{0.99})(Zr,Sn,T)_{0.98}Nb_{0.02}O_3$ and $(Pb_{0.97}La_{0.02})(Zr,Sn,Ti)O_3$ system. Reproduced with permission from [190], Copyright 1989, John Wiley & Sons.

Fig. 32. Two consecutive hysteresis loops of $Pb_{0.97}La_{0.02}(Zr_{0.65}Sn_{0.22}Ti_{0.13})O_3$ taken at 1 kHz and different temperatures: (a) 20°C, (b) 60°C, (c) 85°C, (d) 100°C, (e) 135°C and (f) 200°C. Loop 1 means virgin sample and Loop 2 means second run. Reproduced with permission from [191], Copyright 2008, Spinger.

Fig. 33. Temperature-dependent dielectric constant of $Pb_{0.97}La_{0.02}(Zr_{0.75}Sn_{0.22}Ti_{0.03})O_3$ (a) and $Pb_{0.97}La_{0.02}(Zr_{0.75}Sn_{0.18}Ti_{0.07})O_3$ (b) at various DC electric fields. Reproduced with permission from [196], Copyright 2007, Institute of Physics.

Fig. 34. (a) Hydrostatic pressure dependence of discharge voltage curves at various external DC voltages. (b) Hydrostatic pressure-electric field phase diagram for the polarized $Pb_{0.99}Nb_{0.02}(Zr_{0.75}Sn_{0.2}Ti_{0.05})_{0.98}O_3$ ceramics. Reproduced with permission from [144], Copyright 2008, American Institute of Physics.

Fig. 35. (a) XRD patterns of the PLZT thick films with and without the LNO buffer layer. The insert is XRD pattern of the LNO layer. (b) SEM images of the PLZT thick films with and without the LNO buffer layer. (c) P-E loops of the PLZT thick films with and without the LNO buffer layer. The insert is their temperature-dependent dielectric constant curves. Reproduced with permission from [110], Copyright 2009, John Wiley & Sons.

Fig. 36. Diagram of hysteresis and energy storage density for (a) linear dielectrics, (b) FEs, and (c) AFEs. The green area in the first quadrant is the recoverable energy density J_{reco} and the red area is the energy loss J_{loss}. Reproduced with permission from [207], Copyright 1972, Springer.

Fig. 37. Electric-field dependence of recoverable energy-storage density of $(Pb_{0.97}La_{0.02})(Zr_{0.95-x}Sn_xTi_{0.05})O_3$ films with x=0.05, 0.25 and 0.40. Reproduced with permission from [213], Copyright 2013, American Physical Society.

Fig. 38. Longitudinal, transverse and volume strain of the PLZST ceramics as a function of *E* field at 0.2 Hz [8], Copyright 1951, American Physical Society.

Fig. 39. (a) Longitudinal strains of the (100) and (110)-oriented $Pb_{0.97}La_{0.02}(Zr_{0.95}Ti_{0.05})O_3$ AFE thick films (about 2500 nm) deposited on $Pt(111)/TiO_2/SiO_2/Si$ and $LaNiO_3(110)/Si$ substrates, respectively. Reproduced with permission from [110], Copyright 2009, Wiley Blackwell. (b) Longitudinal strains of the (111) and (100)-oriented $Pb_{0.97}La_{0.02}(Zr_{0.85}Sn_{0.13}Ti_{0.02})O_3$ AFE thin films (about 700 nm) deposited on $Pt(111)/TiO_2/SiO_2/Si$ and $LaNiO_3(100)/Pt(111)/TiO_2/SiO_2/Si$ substrates, respectively. Reproduced with permission from [109], Copyright 2010, American Institute of Physics.

Fig. 40. Temperature dependence of pyroelectric current and pyroelectric coefficient of the $Pb_{0.97}La_{0.02}(Zr_{0.75}Sn_{0.09}Ti_{0.16})O_3$ AFE ceramics under various applied DC electric fields. Produced with permission from [230], Copyright 1999, Tayler and Francis Group.

Fig. 41. Electrocaloric temperature changes (ΔT) of the $PbZr_{0.95}Ti_{0.05}O_3$ thin films due to applied ΔE. The inset shows P(T) at selected applied fields *E*. The lines represent fourth-order polynomial fits to the data extracted from the upper branches of 19 hysteresis loops at $E>0$. Reproduced with permission from [241], Copyright 2006, AAAS.

Fig. 42. Electrocaloric temperature changes (ΔT) of the $Pb_{0.80}Ba_{0.20}ZrO_3$ thin films due to applied ΔE. Reproduced with permission from [244], Copyright 2013, John Wiley & Sons.

Fig. 43. Fatigue performance of pure and 5 mol% Sr^{2+} and Ba^{2+}-doped PZ films measured at room temperate and 600 kV/cm. Reproduced with permission from [170], Copyright 2011, Elsevier.

Table 1. Electrical properties of the PLZST AFE thin films with different compositions. Reproduced with permission from [196], Copyright 2007, Institute of Physics.

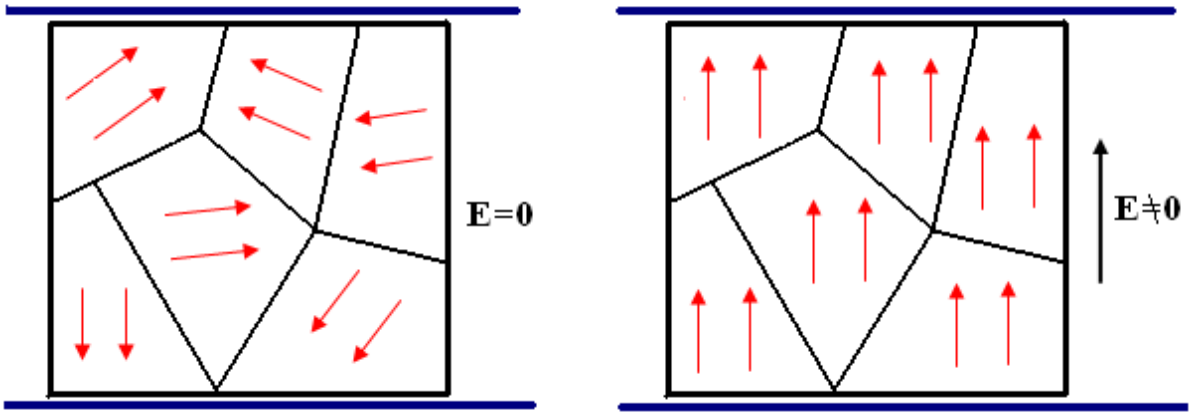

Before polarized

After polarized

Fig. 1

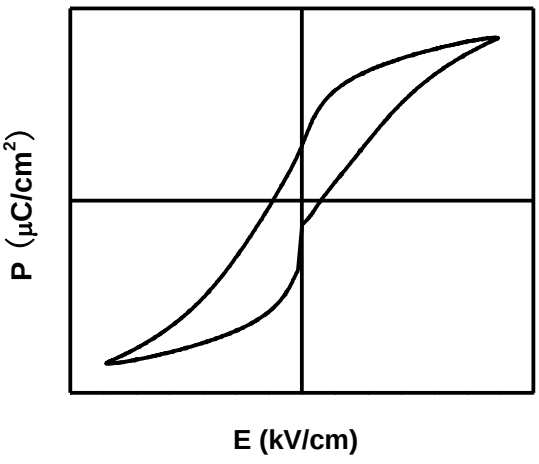

Fig. 2

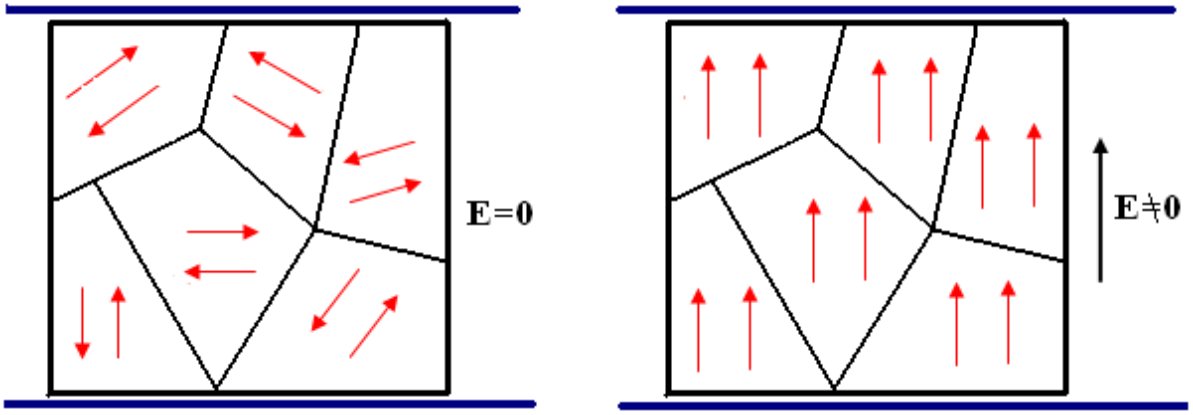

Before polarized

After polarized

Fig. 3

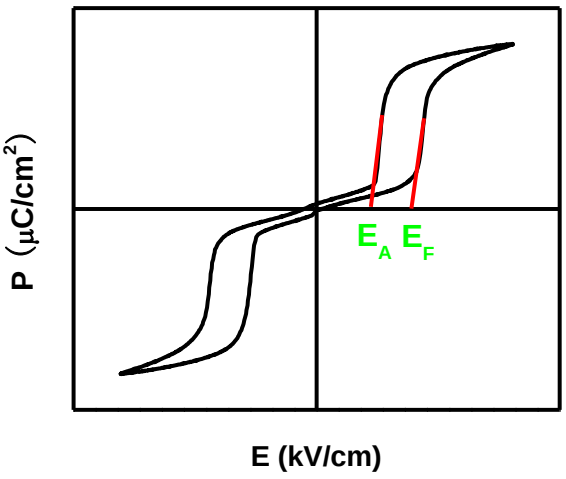

Fig. 4

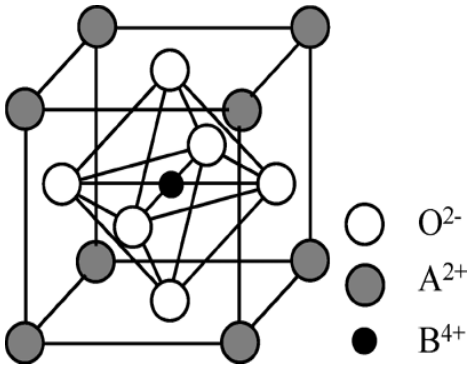

Fig. 5

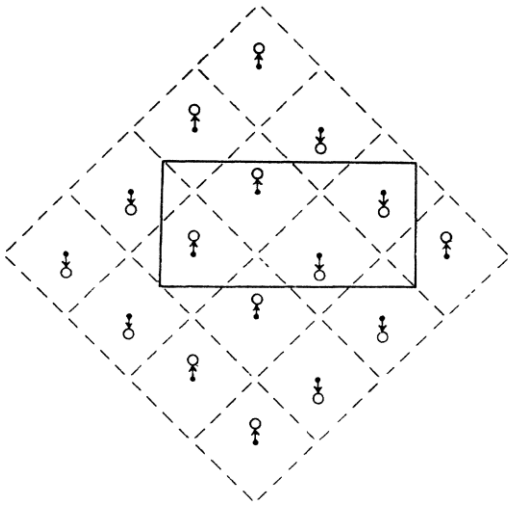

Fig. 6

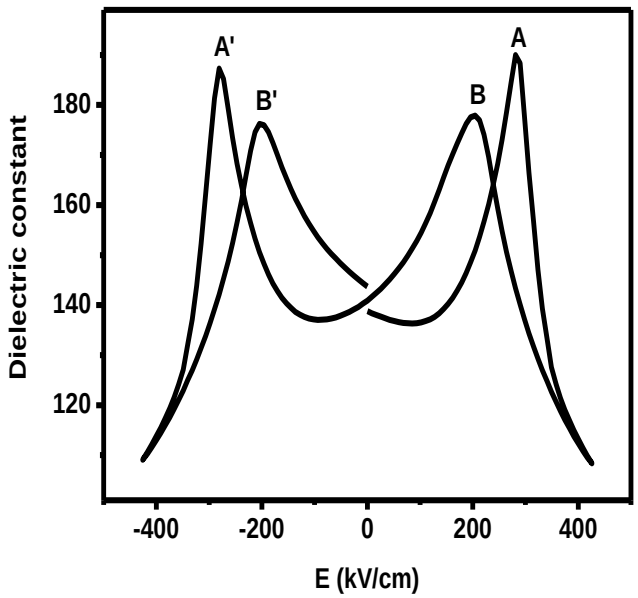
A'
B'
A
B
180
160
140
120
Dielectric constant
-400
-200
0
200
400
E (kV/cm)

Fig. 7

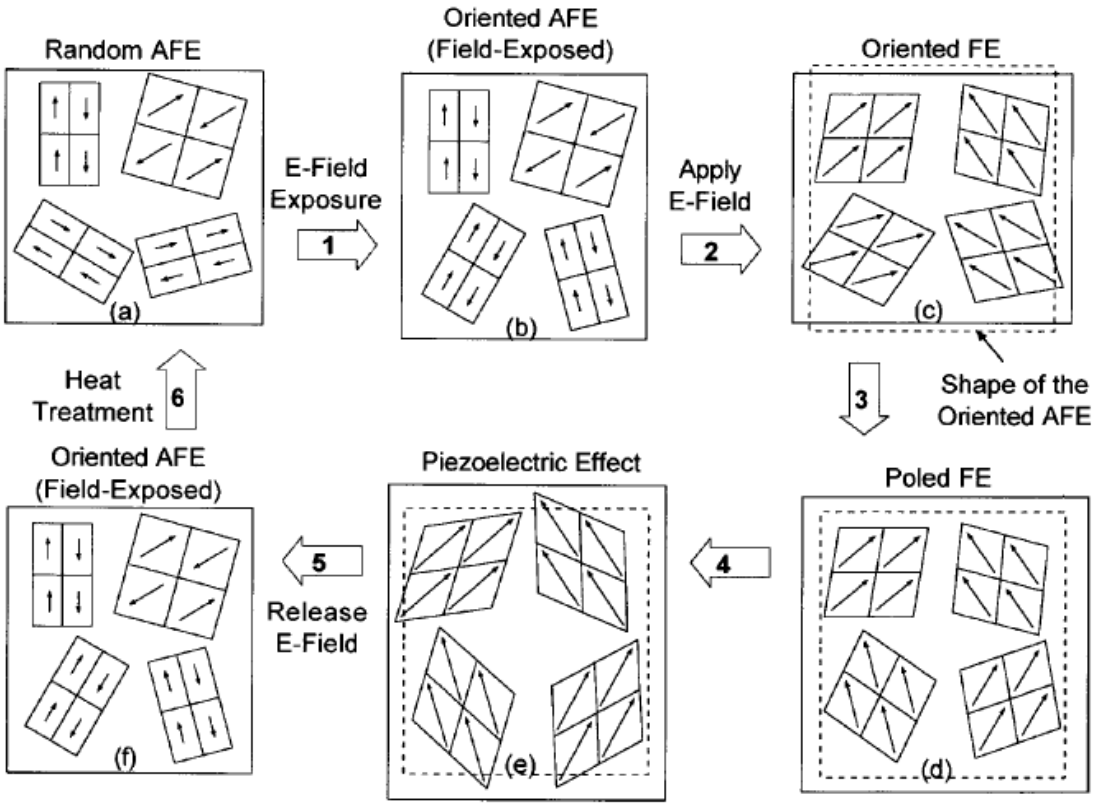
Random AFE
(a)
E-Field
Exposure
1
Oriented AFE
(Field-Exposed)
(b)
Apply
E-Field
2
Oriented FE
(c)
3
Shape of the
Oriented AFE
Poled FE
(d)
4
Piezoelectric Effect
(e)
5
Release
E-Field
Oriented AFE
(Field-Exposed)
(f)
Heat
Treatment
6

Fig. 8

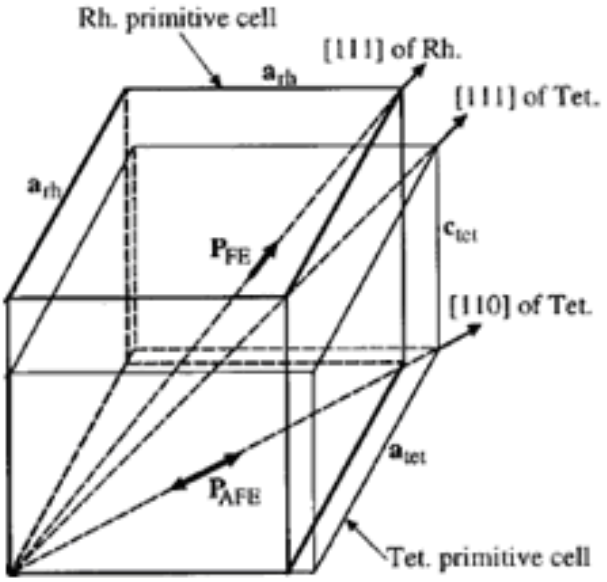
Rh. primitive cell
[111] of Rh.
a_{rh}
[111] of Tet.
a_{rh}
c_{tet}
P_{FE}
[110] of Tet.
a_{tet}
P_{AFE}
Tet. primitive cell

Fig. 9

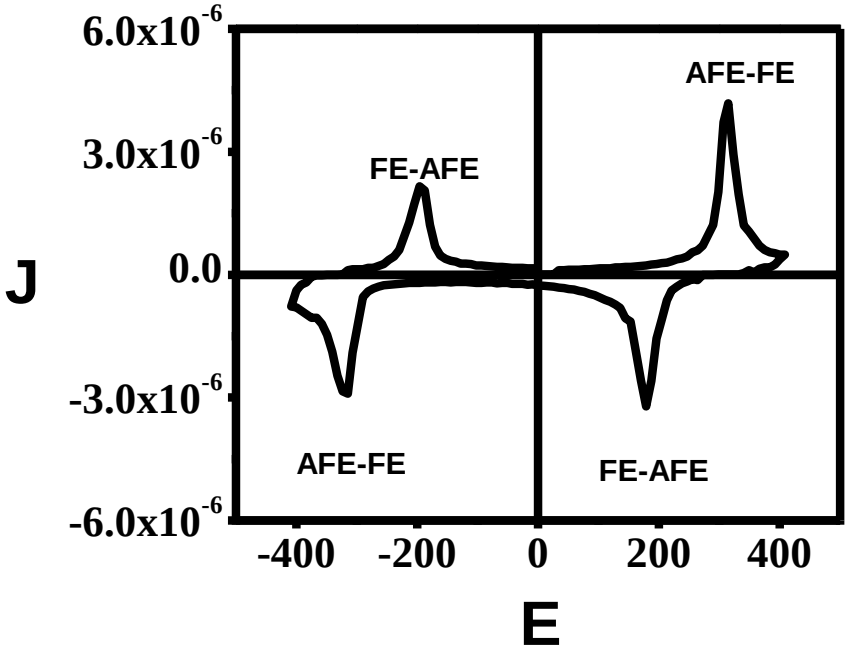
6.0x10-6
3.0x10-6
0.0
-3.0x10-6
-6.0x10-6
J
AFE-FE
FE-AFE
AFE-FE
FE-AFE
-400
-200
0
200
400
E

Fig. 10

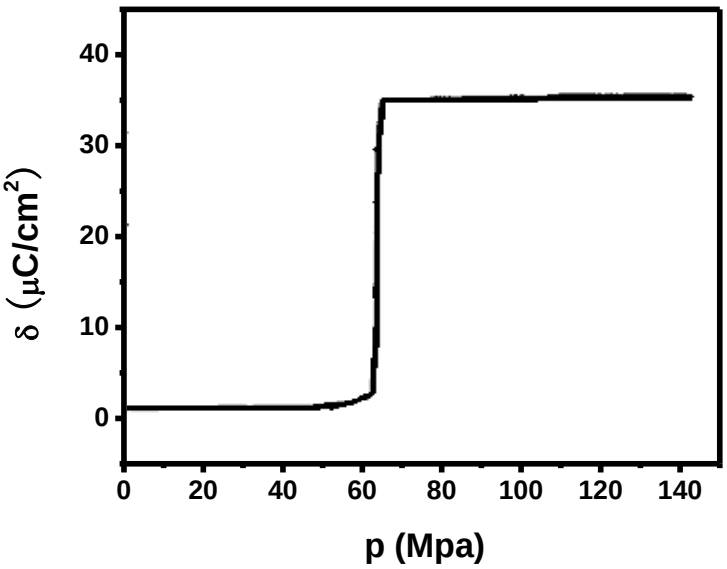

Fig. 11

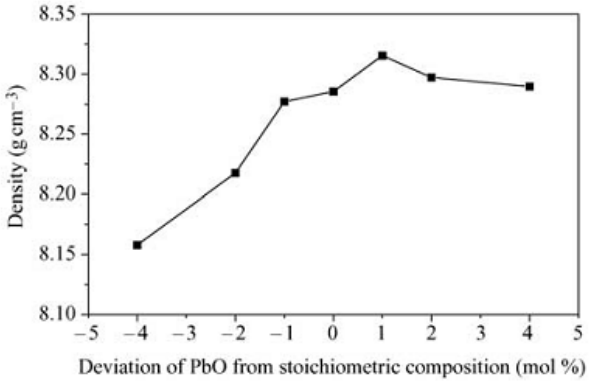

Fig. 12

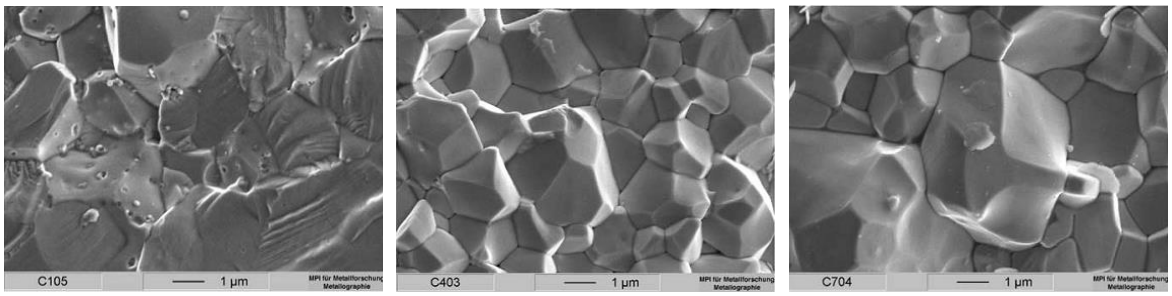

(a) 4 mol% PbO-deficient (b) Stoichiometric composition (c) 4 mol% PbO-excess

Fig. 13

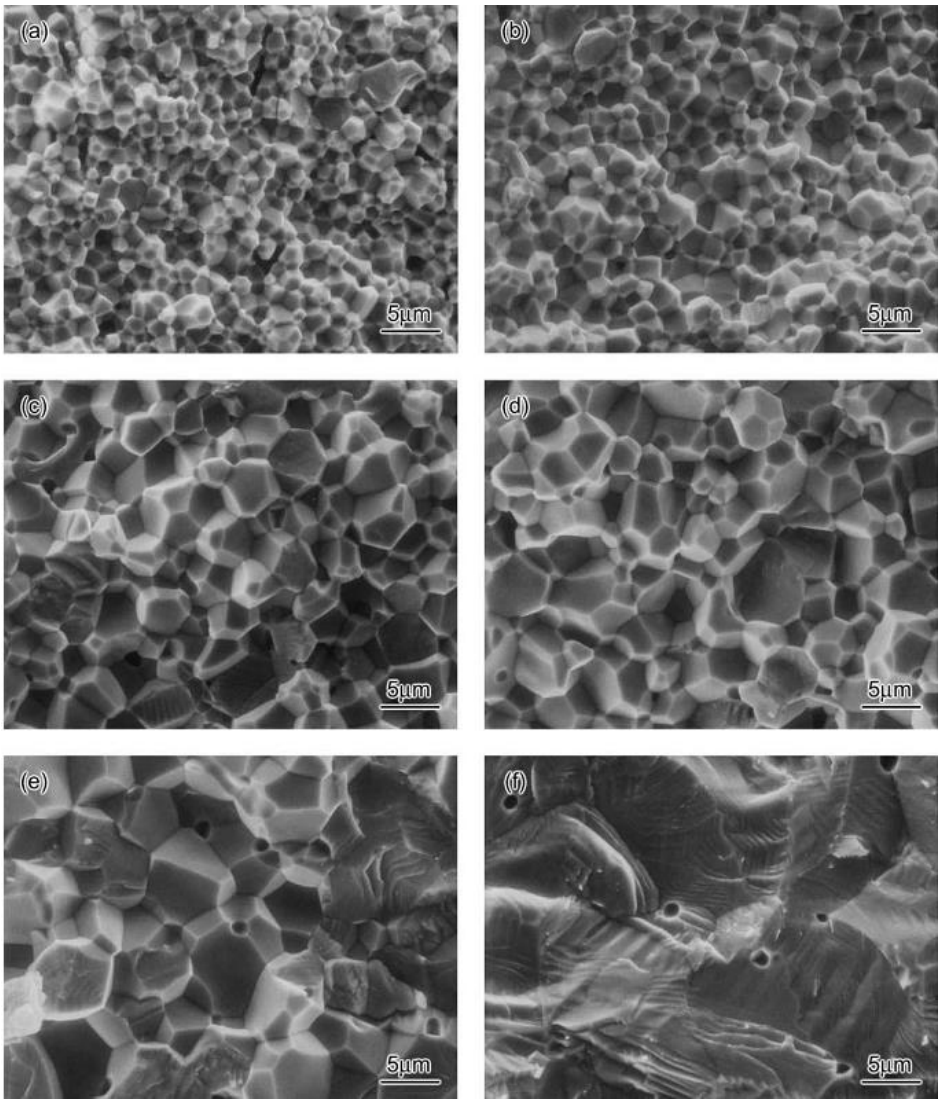
(a)
5μm
(b)
5μm
(c)
5μm
(d)
5μm
(e)
5μm
(f)
5μm

Fig. 14

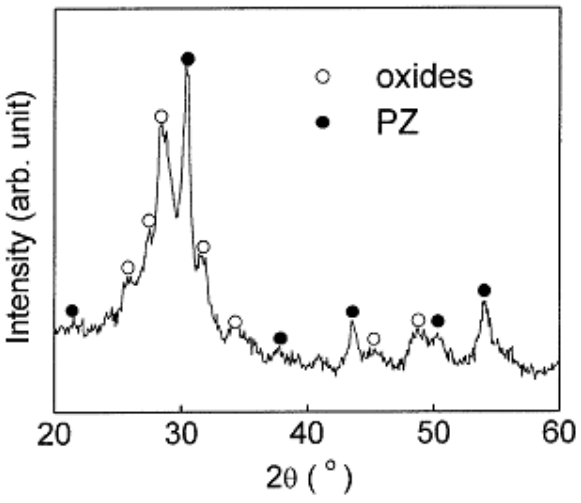
oxides
PZ
Intensity (arb. unit)
20
30
40
50
60
2θ (°)

Fig. 15

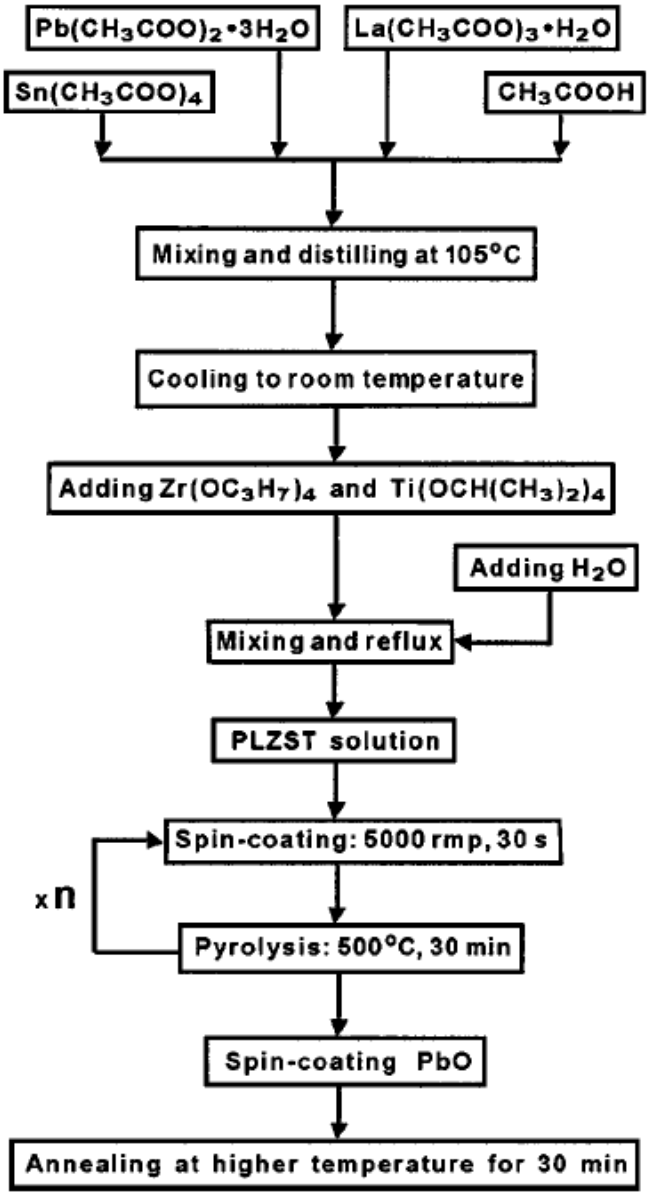
Pb(CH3COO)2•3H2O
La(CH3COO)3•H2O
Sn(CH3COO)4
CH3COOH
Mixing and distilling at 105°C
Cooling to room temperature
Adding Zr(OC3H7)4 and Ti(OCH(CH3)2)4
Adding H2O
Mixing and reflux
PLZST solution
Spin-coating: 5000 rmp, 30 s
x n
Pyrolysis: 500°C, 30 min
Spin-coating PbO
Annealing at higher temperature for 30 min

Fig. 16

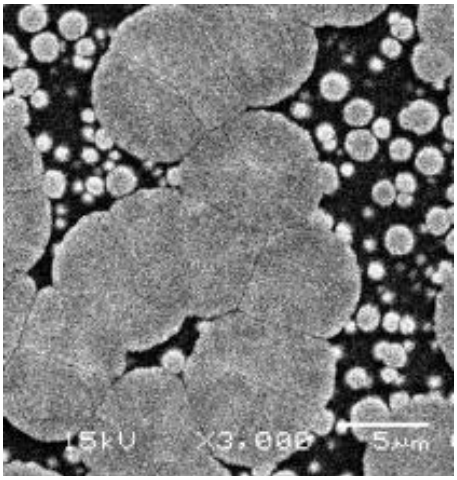
15kV X3,000 5μm

Fig. 17

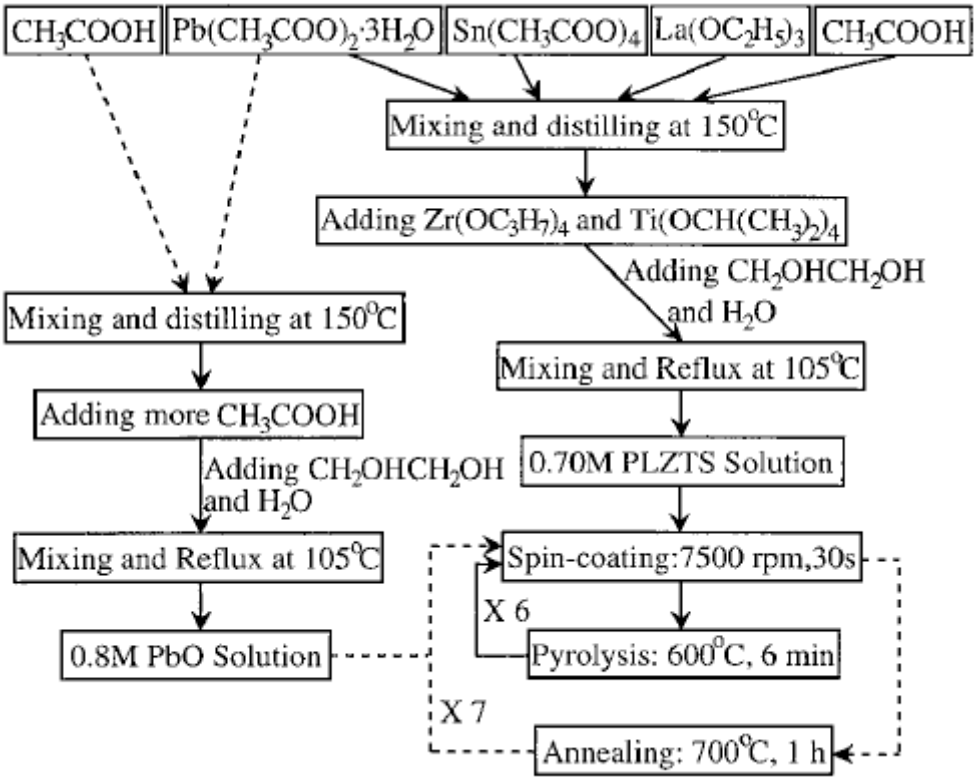
CH3COOH
Pb(CH3COO)2·3H2O
Sn(CH3COO)4
La(OC2H5)3
CH3COOH
Mixing and distilling at 150°C
Adding Zr(OC3H7)4 and Ti(OCH(CH3)2)4
Adding CH2OHCH2OH and H2O
Mixing and distilling at 150°C
Mixing and Reflux at 105°C
Adding more CH3COOH
0.70M PLZTS Solution
Adding CH2OHCH2OH and H2O
Mixing and Reflux at 105°C
Spin-coating:7500 rpm,30s
X 6
0.8M PbO Solution
Pyrolysis: 600°C, 6 min
X 7
Annealing: 700°C, 1 h

Fig. 18

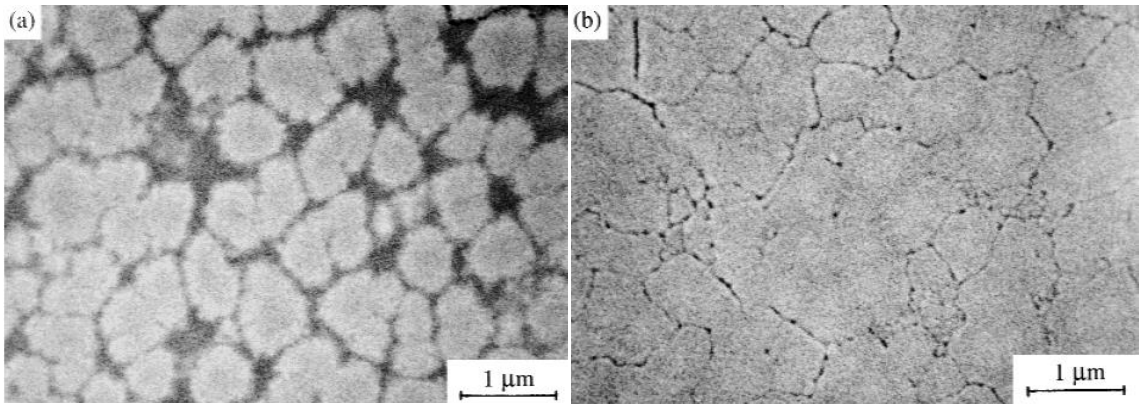
(a)
1 µm
(b)
1 µm

Fig. 19

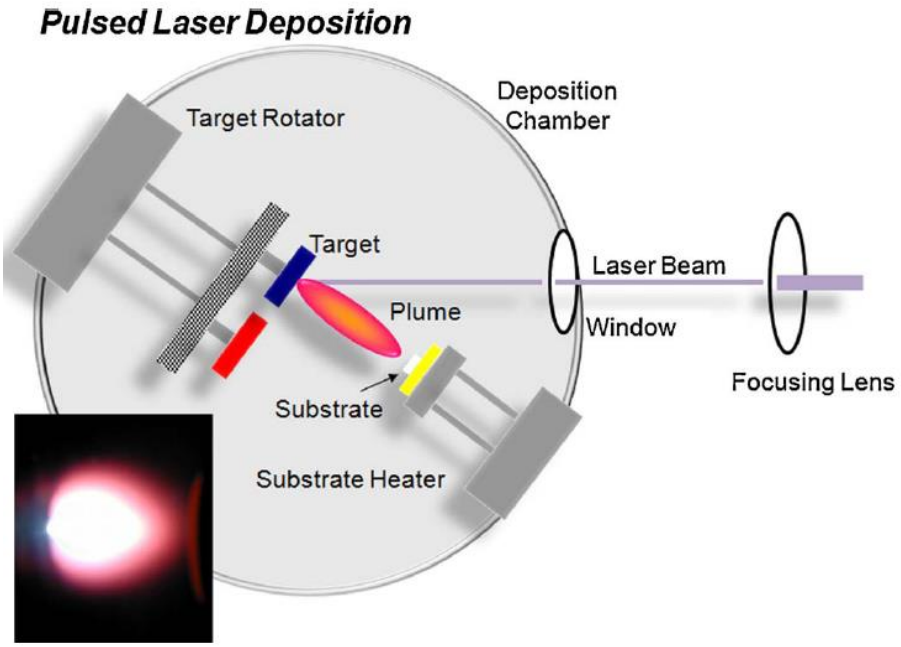
Pulsed Laser Deposition
Target Rotator
Deposition Chamber
Target
Laser Beam
Plume
Window
Focusing Lens
Substrate
Substrate Heater

Fig. 20

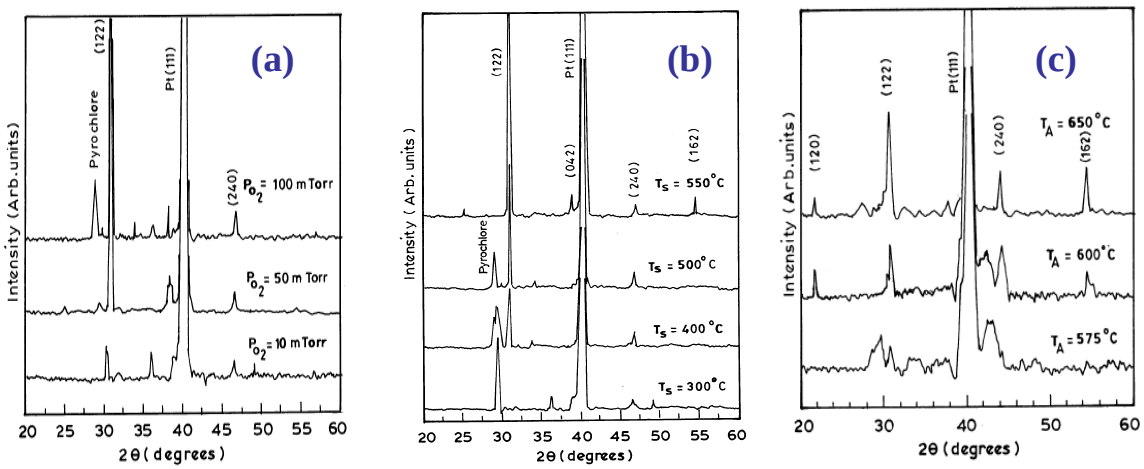
(a)
(b)
(c)
Intensity (Arb.units)
Pyrochlore
(122)
Pt(111)
(240)
(042)
(162)
(120)
P_{O_2} = 100 m Torr
P_{O_2} = 50 m Torr
P_{O_2} = 10 m Torr
T_s = 550°C
T_s = 500°C
T_s = 400°C
T_s = 300°C
T_A = 650°C
T_A = 600°C
T_A = 575°C
20 25 30 35 40 45 50 55 60
2θ (degrees)

Fig. 21

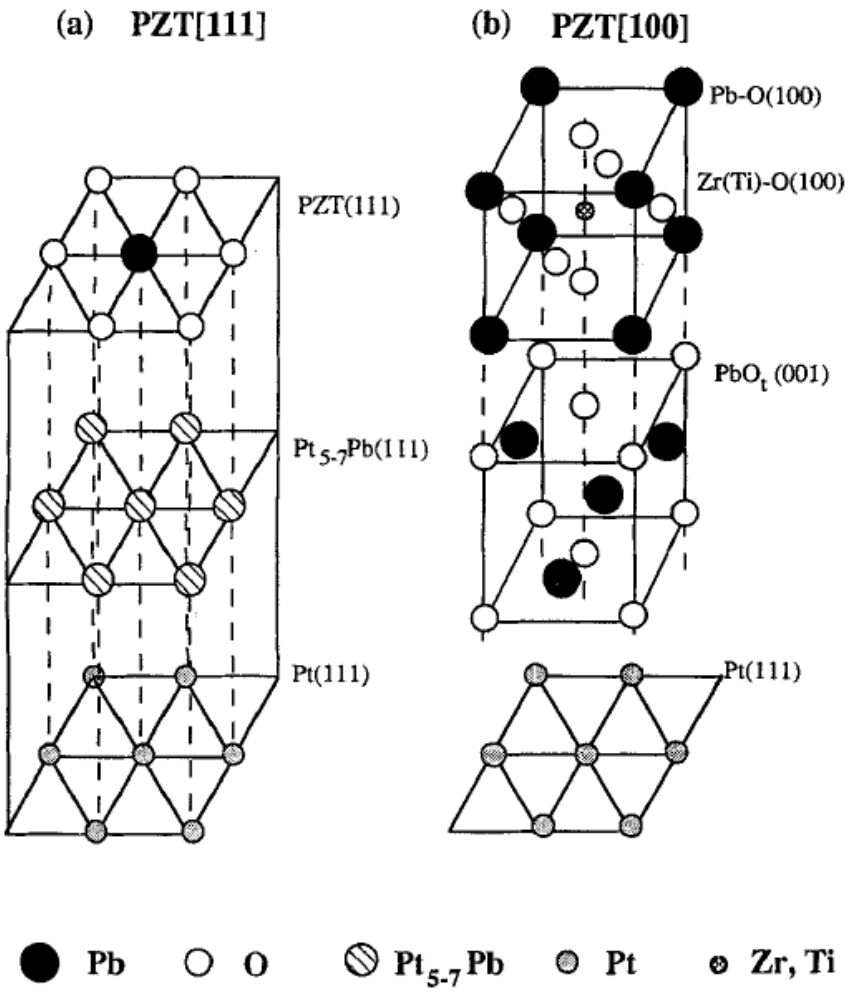
(a) PZT[111]
(b) PZT[100]
PZT(111)
$Pt_{5-7}Pb(111)$
Pt(111)
Pb-O(100)
Zr(Ti)-O(100)
PbO_t (001)
Pt(111)
Pb
O
$Pt_{5-7}Pb$
Pt
Zr, Ti

Fig. 22

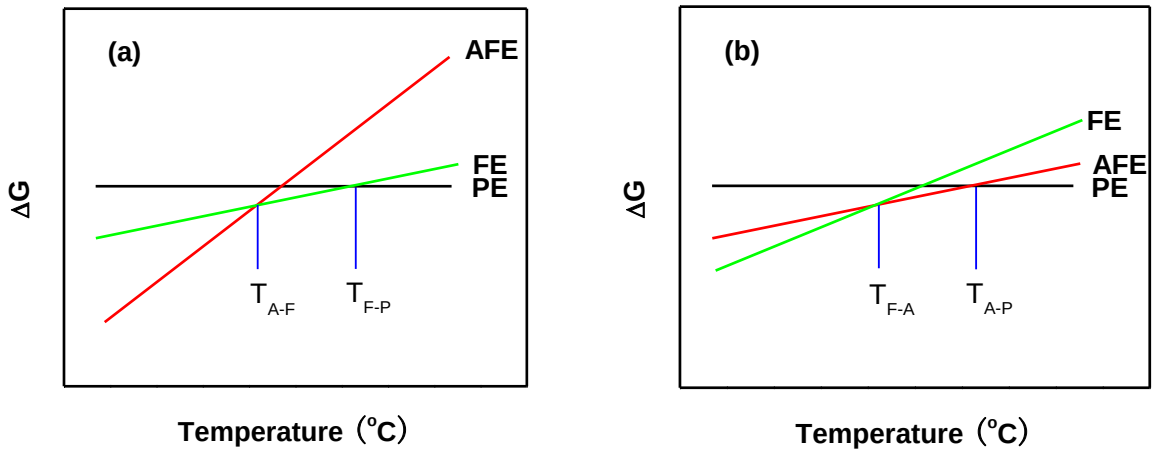
(a)
AFE
FE
PE
ΔG
T A-F
T F-P
Temperature（°C）
(b)
FE
AFE
PE
ΔG
T F-A
T A-P
Temperature（°C）

Fig. 23

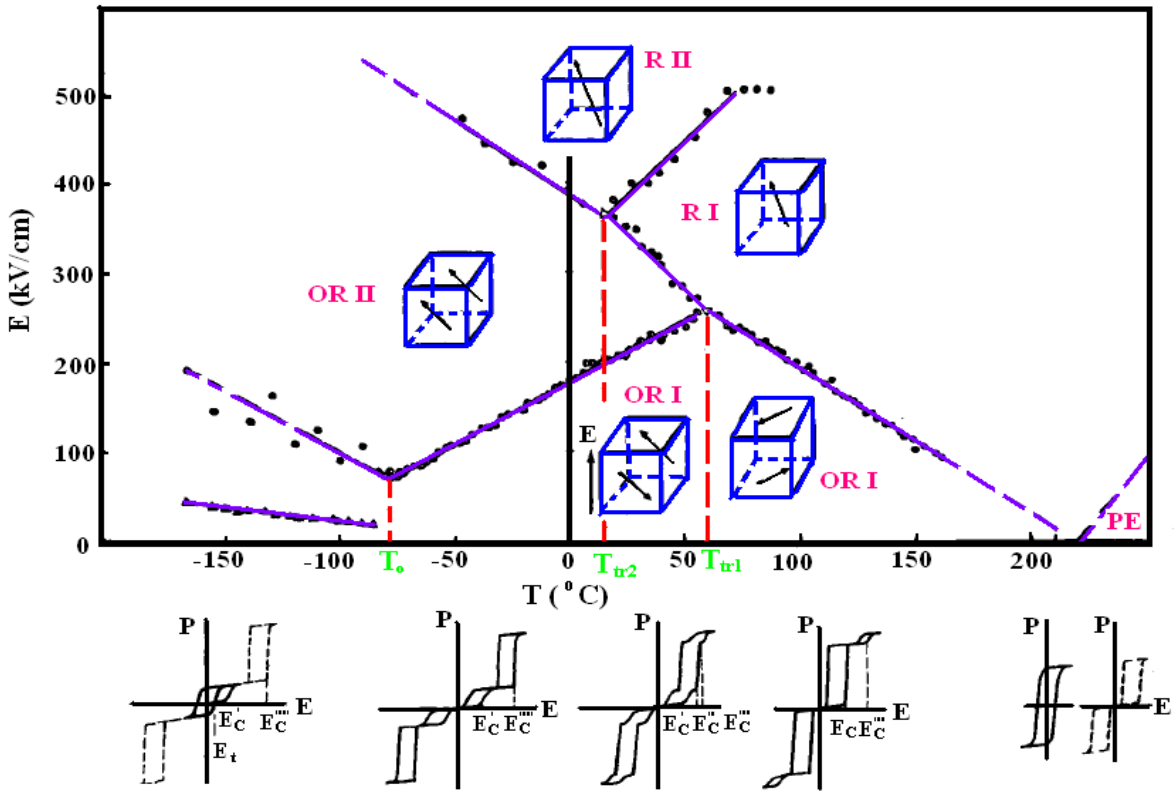
R II
R I
OR II
OR I
E
OR I
PE
E (kV/cm)
500
400
300
200
100
0
-150
-100
T₀
-50
0
T tr2
50
T tr1
100
150
200
T (°C)
P
E
E t

Fig. 24

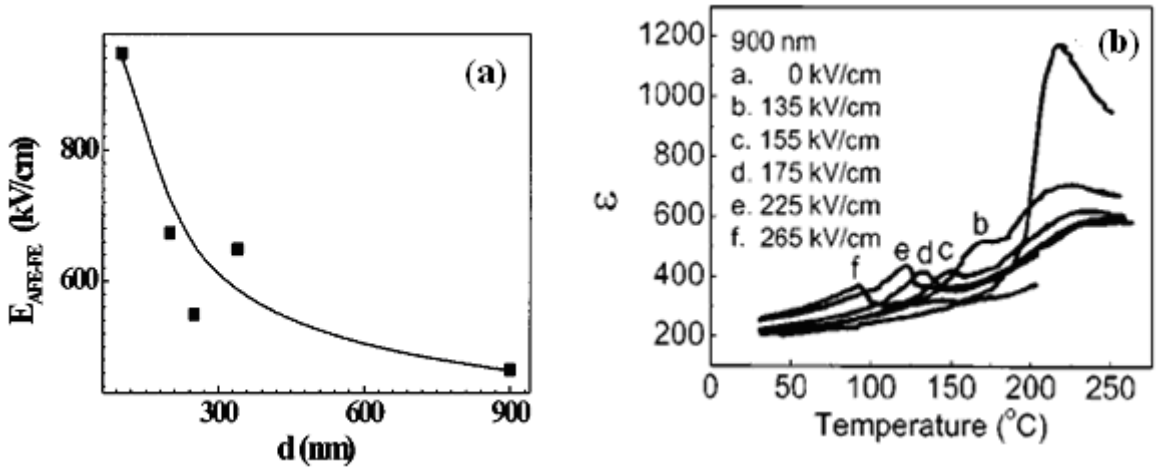
(a)
E_{AFE-FE} (kV/cm)
800
600
300
600
900
d (nm)
(b)
900 nm
a. 0 kV/cm
b. 135 kV/cm
c. 155 kV/cm
d. 175 kV/cm
e. 225 kV/cm
f. 265 kV/cm
ε
1200
1000
800
600
400
200
0
50
100
150
200
250
Temperature (°C)

Fig. 25

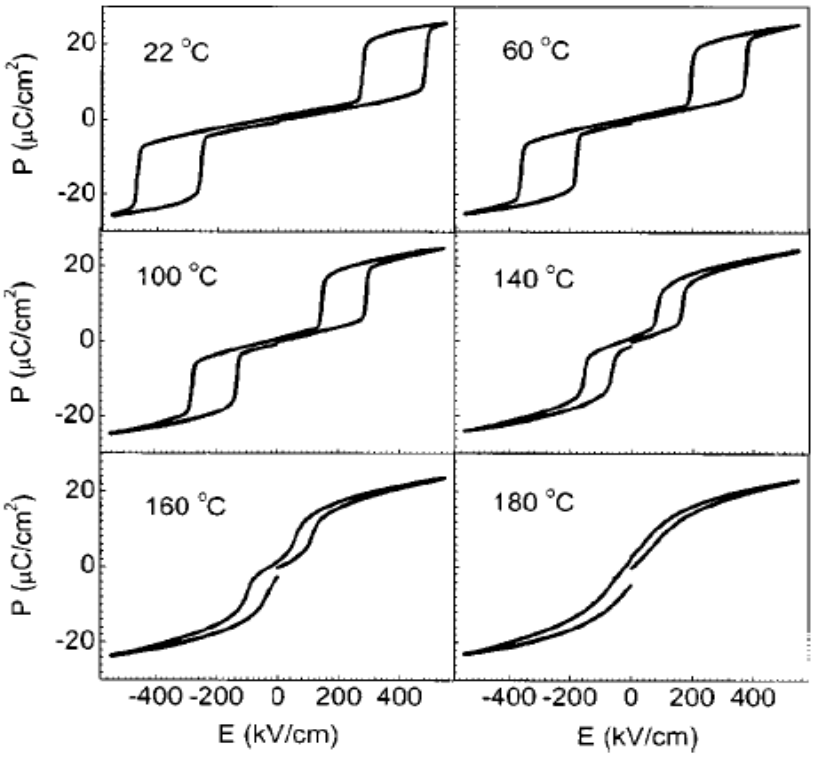
22 °C
60 °C
100 °C
140 °C
160 °C
180 °C
P (μC/cm²)
20
0
-20
-400 -200 0 200 400
E (kV/cm)

Fig. 26

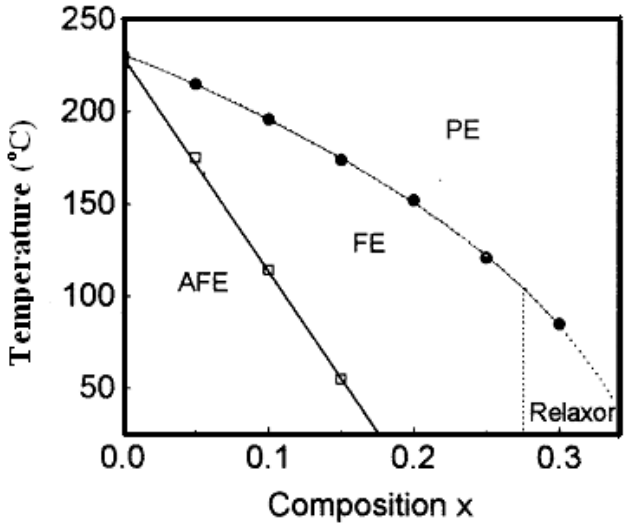
Temperature (°C)
250
200
150
100
50
0.0
0.1
0.2
0.3
Composition x
PE
FE
AFE
Relaxor

Fig. 27

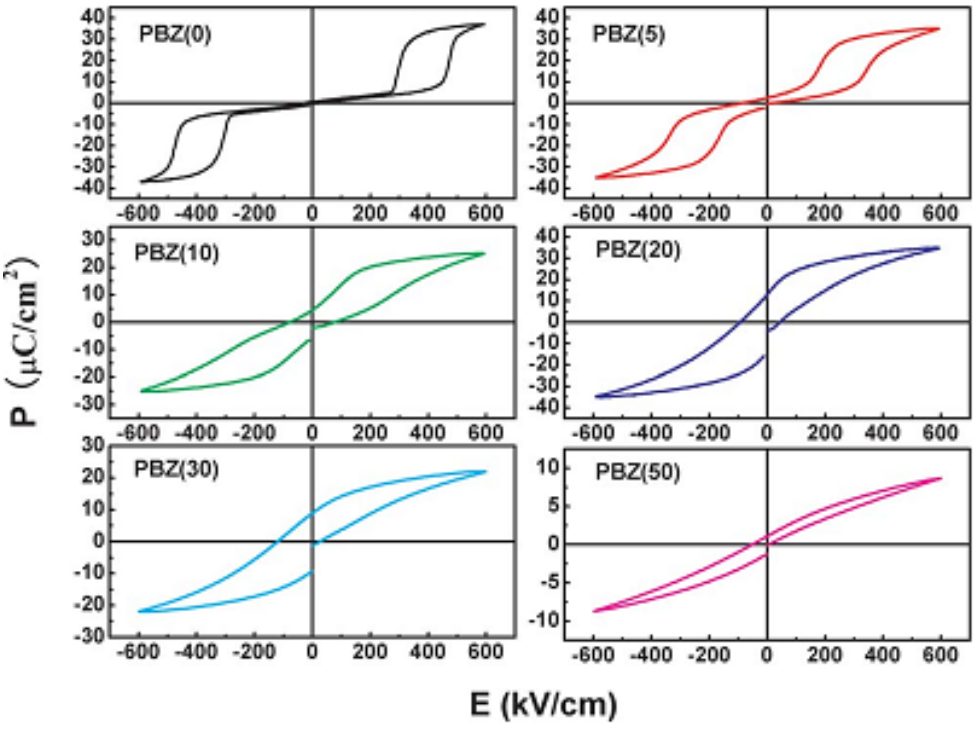
PBZ(0)
PBZ(5)
PBZ(10)
PBZ(20)
PBZ(30)
PBZ(50)
P (μC/cm²)
E (kV/cm)

Fig. 28

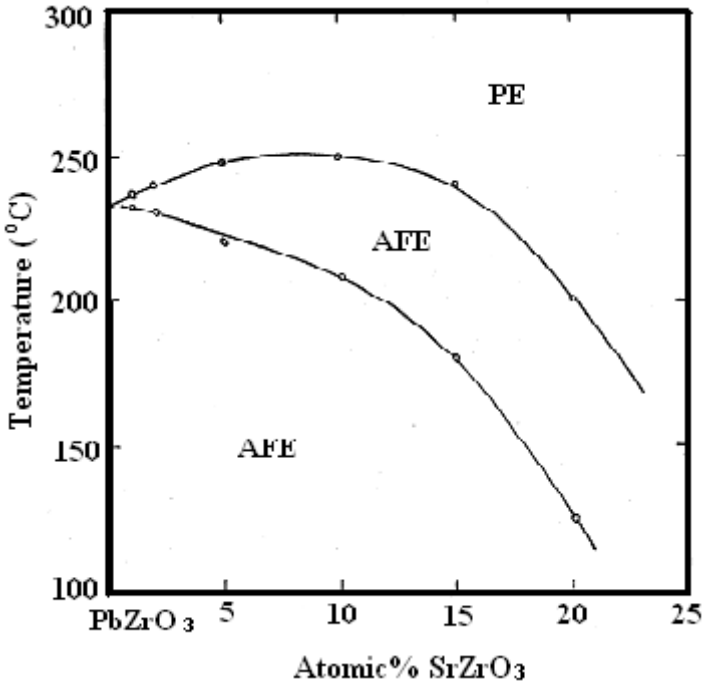
300
250
200
150
100
PE
AFE
AFE
Temperature (°C)
PbZrO3
5
10
15
20
25
Atomic% SrZrO3

Fig. 29

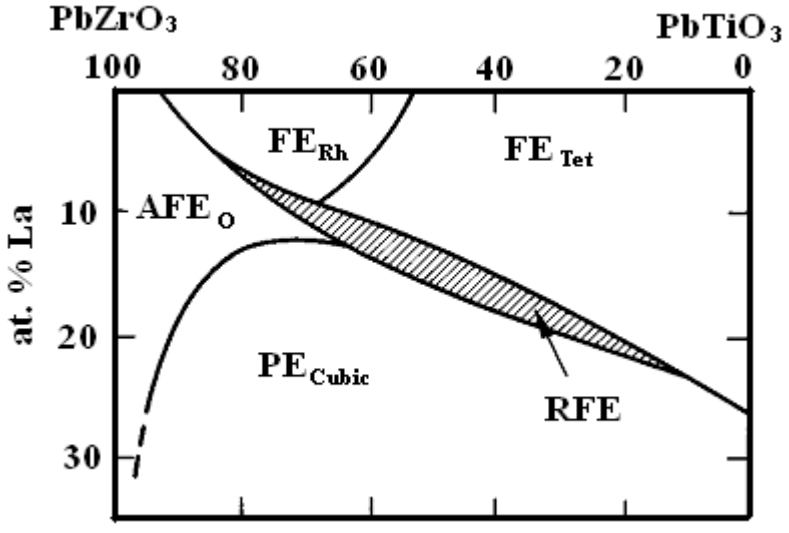
PbZrO3
PbTiO3
100
80
60
40
20
0
FERh
FETet
AFEO
10
20
30
at. % La
PECubic
RFE

Fig. 30

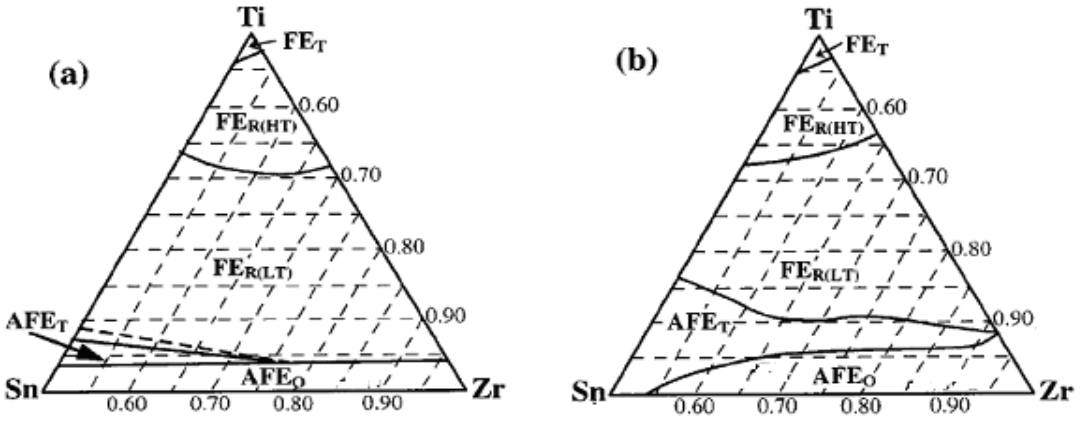
(a)
Ti
FE$_T$
0.60
FE$_{R(HT)}$
0.70
0.80
FE$_{R(LT)}$
AFE$_T$
0.90
Sn
AFE$_O$
Zr
0.60 0.70 0.80 0.90
(b)
Ti
FE$_T$
0.60
FE$_{R(HT)}$
0.70
0.80
FE$_{R(LT)}$
AFE$_T$
0.90
Sn
AFE$_O$
Zr
0.60 0.70 0.80 0.90

Fig. 31

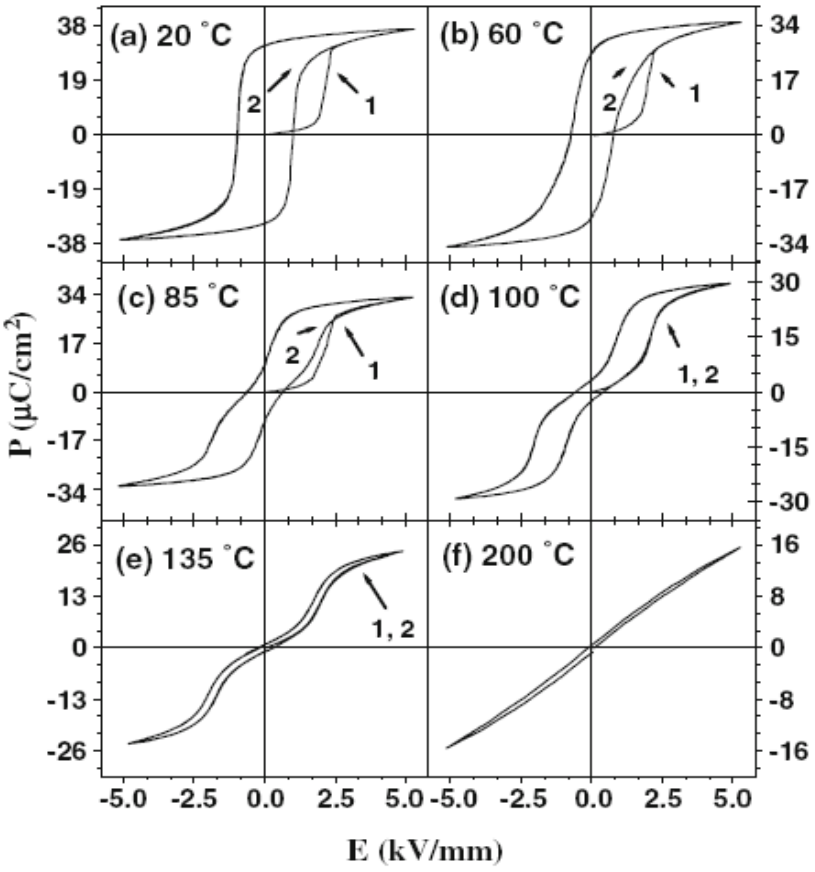
(a) 20 ˚C
(b) 60 ˚C
(c) 85 ˚C
(d) 100 ˚C
(e) 135 ˚C
(f) 200 ˚C
1
2
1, 2
P (μC/cm^2)
E (kV/mm)
38 19 0 -19 -38
34 17 0 -17 -34
34 17 0 -17 -34
30 15 0 -15 -30
26 13 0 -13 -26
16 8 0 -8 -16
-5.0 -2.5 0.0 2.5 5.0

Fig. 32

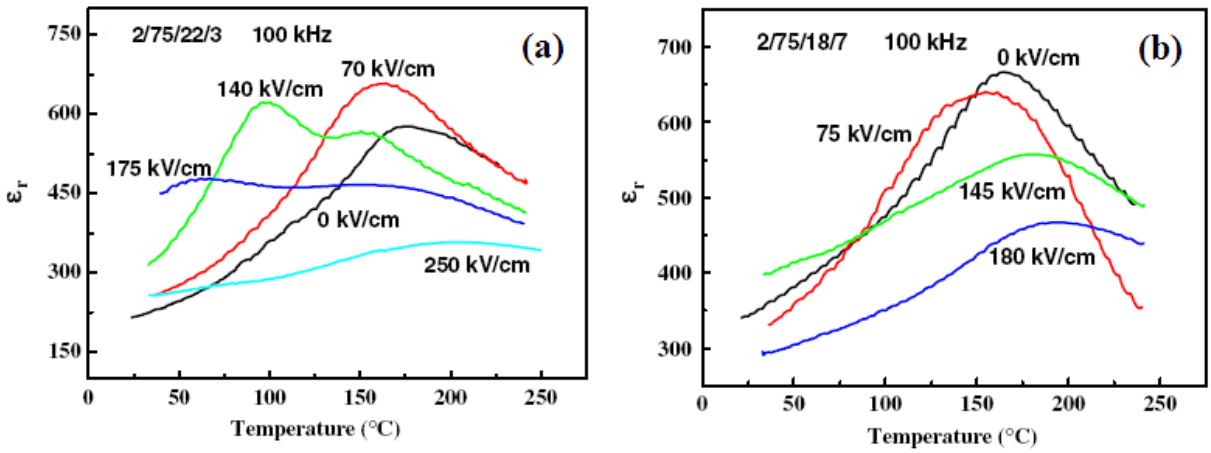
2/75/22/3 100 kHz
(a)
70 kV/cm
140 kV/cm
175 kV/cm
0 kV/cm
250 kV/cm
ε_r
Temperature (°C)
2/75/18/7 100 kHz
(b)
0 kV/cm
75 kV/cm
145 kV/cm
180 kV/cm
ε_r
Temperature (°C)

Fig. 33

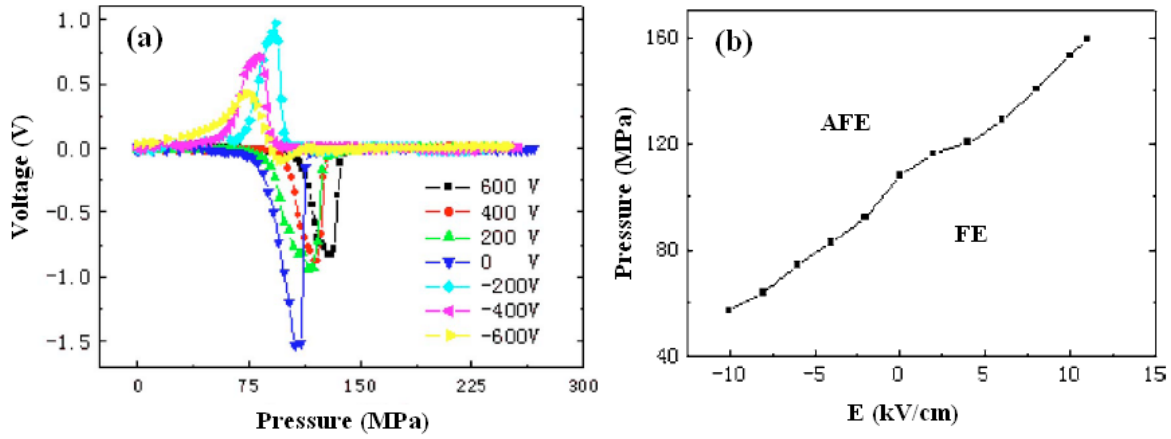
(a)
600 V
400 V
200 V
0 V
-200V
-400V
-600V
Voltage (V)
Pressure (MPa)
(b)
AFE
FE
Pressure (MPa)
E (kV/cm)

Fig. 34

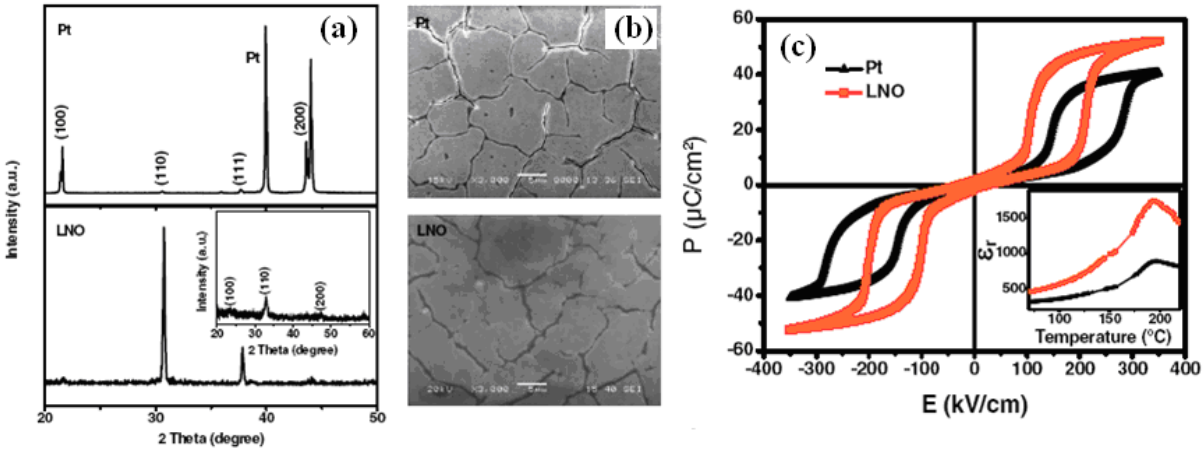
(a)
Pt
(100)
(110)
(111)
Pt
(200)
LNO
Intensity (a.u.)
2 Theta (degree)
(b)
Pt
LNO
(c)
Pt
LNO
P (μC/cm²)
E (kV/cm)
εr
Temperature (°C)

Fig. 35

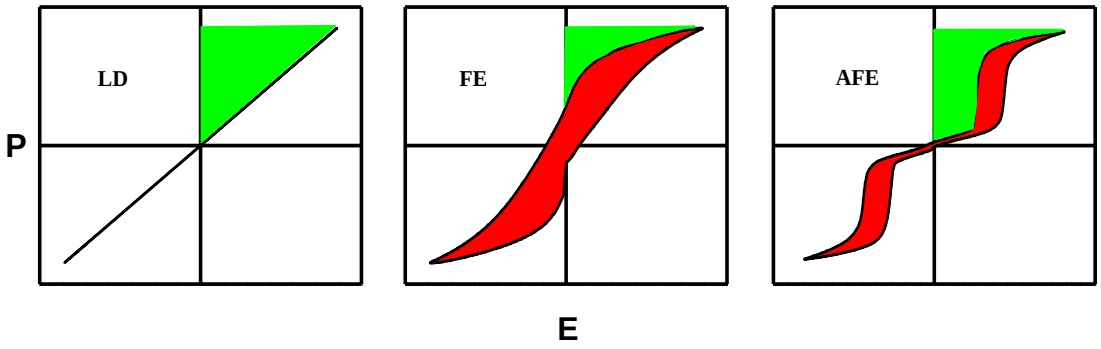
LD
FE
AFE
P
E

Fig. 36

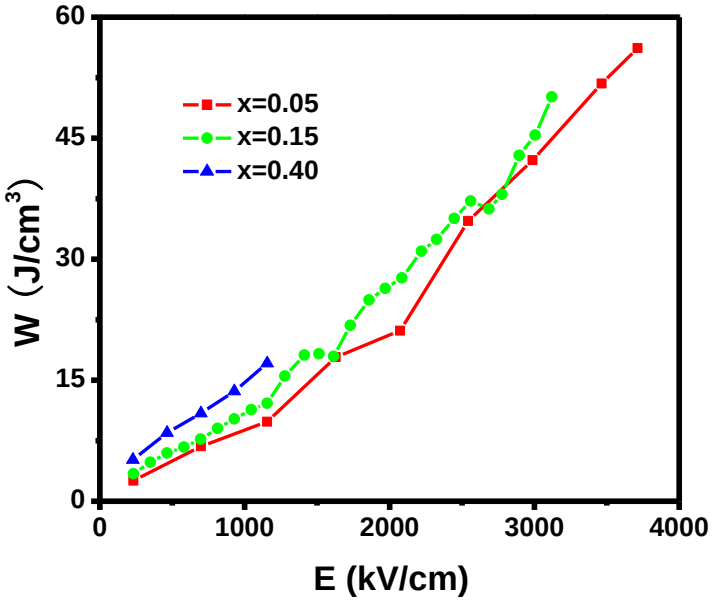
x=0.05
x=0.15
x=0.40
W (J/cm3)
E (kV/cm)
0
15
30
45
60
0
1000
2000
3000
4000

Fig. 37

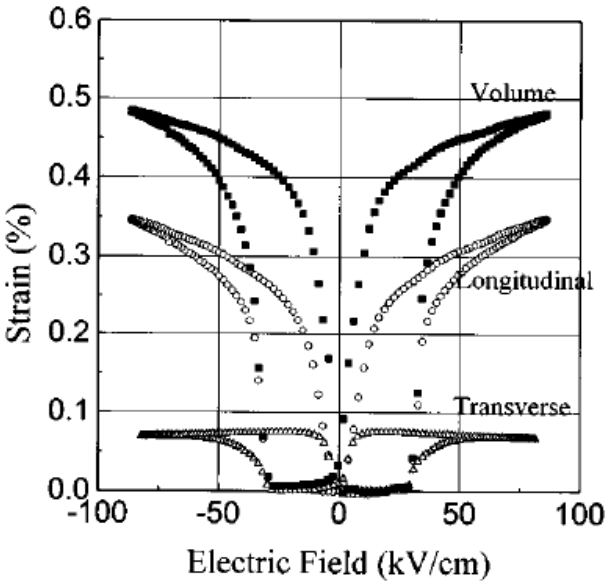
Volume
Longitudinal
Transverse
Strain (%)
Electric Field (kV/cm)
0.0
0.1
0.2
0.3
0.4
0.5
0.6
-100
-50
0
50
100

Fig. 38

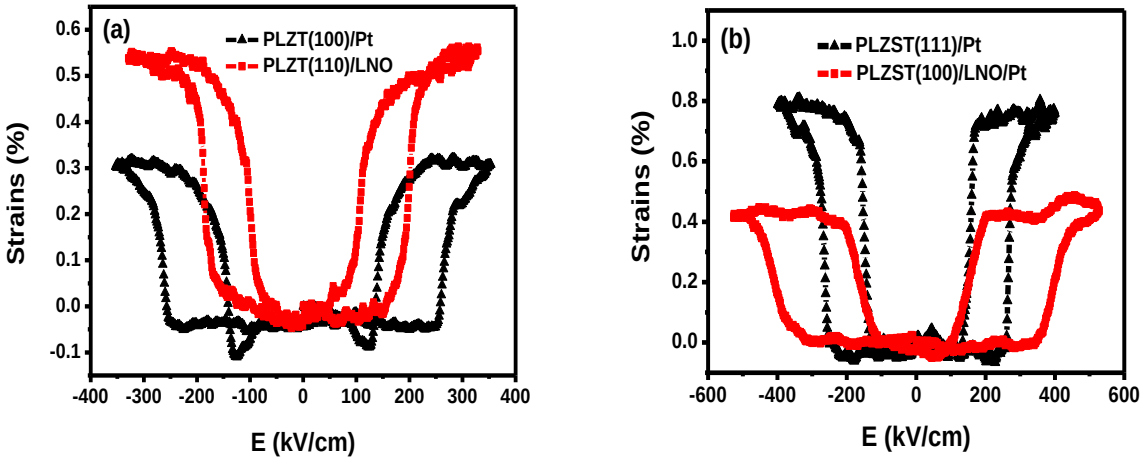
(a)
PLZT(100)/Pt
PLZT(110)/LNO
Strains (%)
E (kV/cm)
(b)
PLZST(111)/Pt
PLZST(100)/LNO/Pt
Strains (%)
E (kV/cm)

Fig. 39

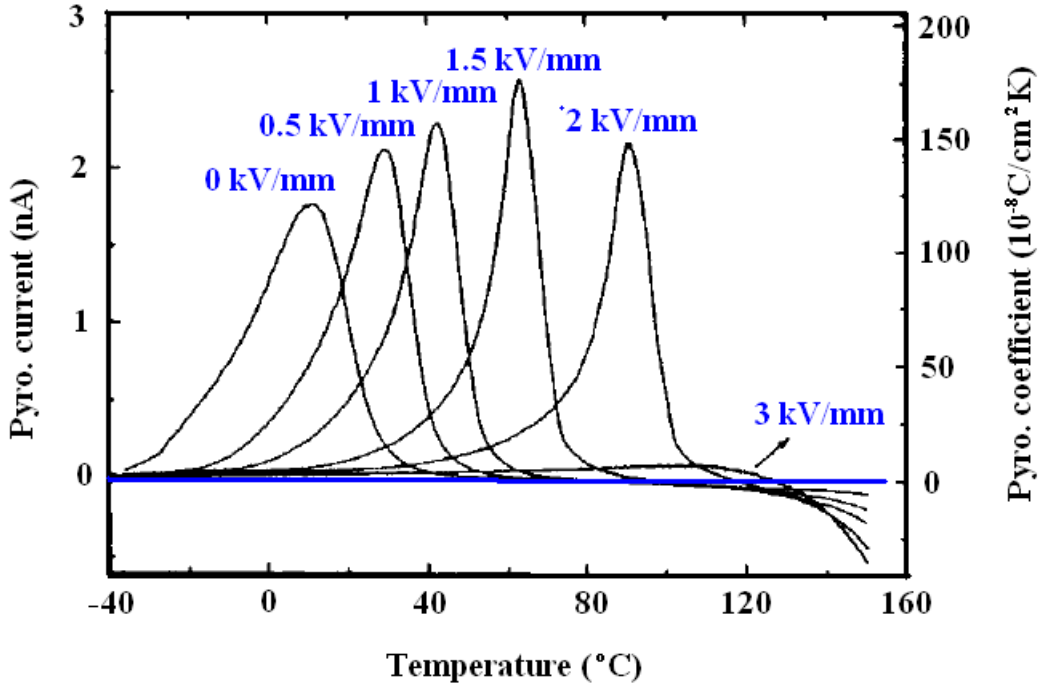
1.5 kV/mm
1 kV/mm
0.5 kV/mm
2 kV/mm
0 kV/mm
3 kV/mm
Pyro. current (nA)
Pyro. coefficient (10⁻⁸C/cm²K)
Temperature (°C)

Fig. 40

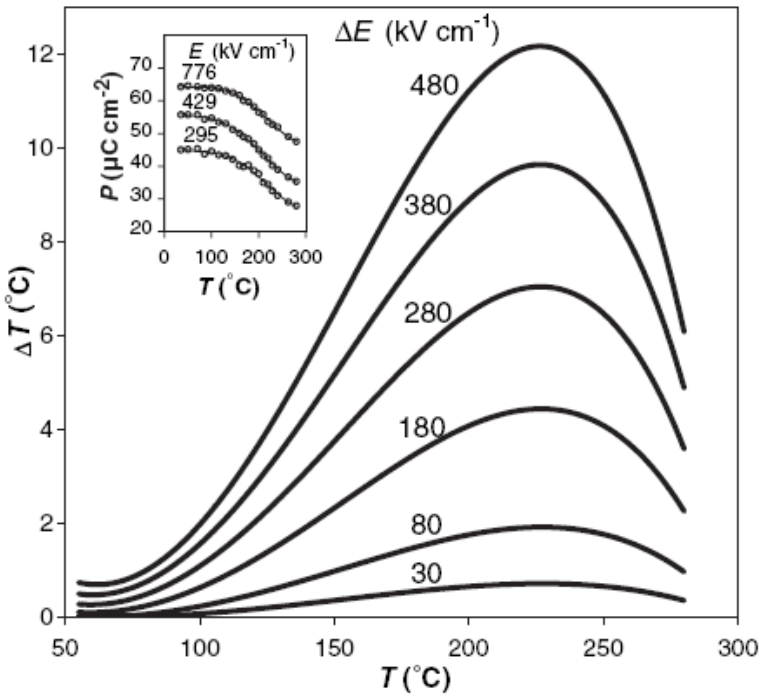
ΔE (kV cm-1)
480
380
280
180
80
30
ΔT (°C)
T (°C)
E (kV cm-1)
776
429
295
P (μC cm-2)
T (°C)

Fig. 41

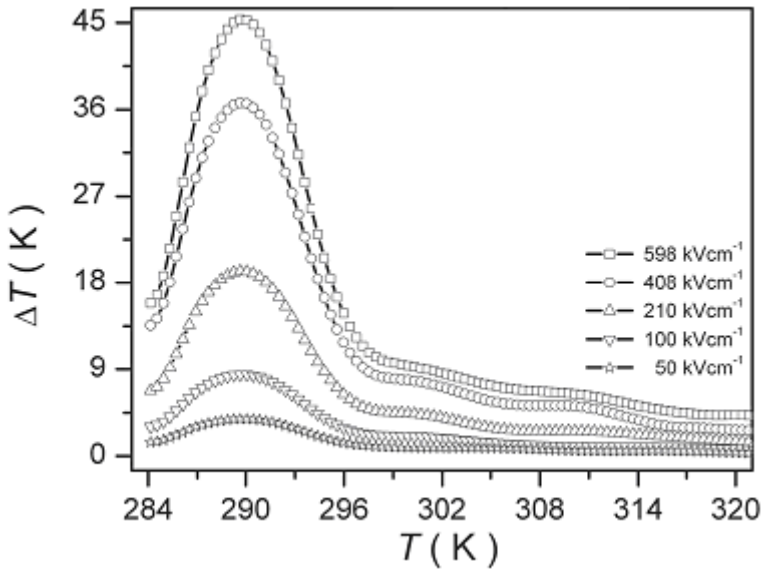
598 kVcm-1
408 kVcm-1
210 kVcm-1
100 kVcm-1
50 kVcm-1
ΔT (K)
T (K)

Fig. 42

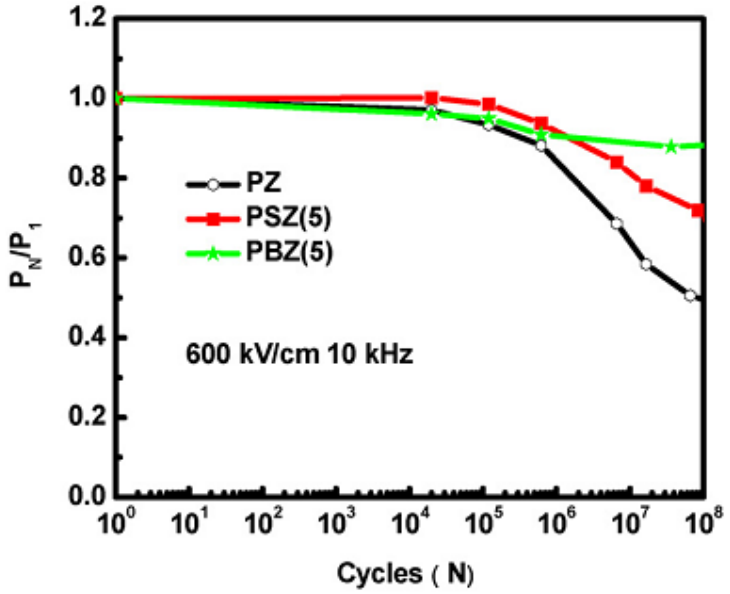

Fig. 43

Table 1

Composition	Phase	Thickness (nm)	**Determined from ε_r-E**			T_C (^oC)
			E_F (kV/cm)	E_A (kV/cm)	ΔE (kV/cm)	
$Pb_{0.97}La_{0.02}(Zr_{0.55}Sn_{0.40}Ti_{0.05})O_3$	AFE_T	550	142	130	12	132
$Pb_{0.97}La_{0.02}(Zr_{0.75}Sn_{0.20}Ti_{0.05})O_3$	AFE_O	505	157	127	30	171
$Pb_{0.97}La_{0.02}(Zr_{0.90}Sn_{0.05}Ti_{0.05})O_3$	AFE_O	584	180	133	47	195
$Pb_{0.97}La_{0.02}(Zr_{0.75}Sn_{0.22}Ti_{0.03})O_3$	AFE_O	556	221	171	50	175
$Pb_{0.97}La_{0.02}(Zr_{0.75}Sn_{0.18}Ti_{0.07})O_3$	AFE_T	548	108	81	27	163